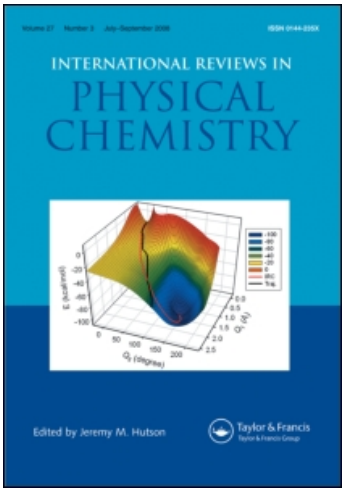

International Reviews in Physical Chemistry
Publication details, including instructions for authors and subscription information:
http://www.informaworld.com/smpp/title~content=t713724383

Infrared chemiluminescence from water-forming reactions: Characterization of dynamics and mechanisms

N. I. Butkovskaya[a]; D. W. Setser[b]
[a] Institute of Chemical Physics, Russian Academy of Sciences, Moscow, Russian Federation [b] Department of Chemistry, Kansas State University, Manhattan, KS, USA

Online publication date: 26 November 2010

To cite this Article Butkovskaya, N. I. and Setser, D. W.(2003) 'Infrared chemiluminescence from water-forming reactions: Characterization of dynamics and mechanisms', International Reviews in Physical Chemistry, 22: 1, 1 — 72
To link to this Article: DOI: 10.1080/0144235021000033381
URL: http://dx.doi.org/10.1080/0144235021000033381

INT. REVIEWS IN PHYSICAL CHEMISTRY, 2003
VOL. 22, NO. 1, 1–72

Taylor & Francis
Taylor & Francis Group

Infrared chemiluminescence from water-forming reactions: characterization of dynamics and mechanisms

N. I. BUTKOVSKAYA† and D. W. SETSER‡*

† Institute of Chemical Physics, Russian Academy of Sciences, 117334 Moscow, Russian Federation

‡ Department of Chemistry, Kansas State University, Manhattan, KS 66506, USA

The formation of water molecules via hydrogen atom abstraction by hydroxyl radicals and their formation via unimolecular elimination from vibrationally excited alcohols and organic acids are important processes in a variety of gas-phase chemical environments. The nascent vibrational distributions of the water molecules produced by such reactions have been obtained by analysis of the infrared chemiluminescence from H_2O, HOD and D_2O. The analysis required computer simulation of the spectra obtained by recording emission from a fast-flow reactor at 298 K with a low-resolution Fourier transform spectrometer. By combining the information deduced from simulation of the H_2O and HOD emission spectra from the reactions of OH and OD, the total vibrational energy released to the water molecule and the distribution between the stretch and bending modes have been assigned. The present report provides a summary of results from hydroxyl radicals reacting with inorganic hydride molecules, with the primary, secondary and tertiary bonds of hydrocarbons, and with oxygen- and sulphur-containing organic molecules. The overall fraction of the available energy released to water as vibrational energy is $\simeq 0.55$ for direct abstraction of hydrogen atoms by OH radicals. This fraction declines as the mechanism becomes less direct and reaches 0.15–0.20 for the unimolecular decomposition of vibrationally excited ethanol and acetic acid. The ratio of the energy in the bending mode to that in the stretch mode is sensitive to the dynamics of water-forming reactions. Macroscopic mechanisms, vibrational energy distributions and reaction dynamics are discussed.

Contents

* Corresponding author; Email: setserdw@ksu.edu

International Reviews in Physical Chemistry ISSN 0144–235X print/ISSN 1366–591X online
http://www.tandf.co.uk/journals
DOI: 10.1080/0144235021000033381

1. Introduction

The infrared chemiluminescence (IRCL) technique [1–3] was an important tool in the development of the field of state-resolved reaction kinetics [4]. For the atom + diatomic molecule type of bimolecular reaction, observation of the nascent rotational–vibrational distributions of the diatomic product molecule provided a complete map of the energy disposal. The principal experimental challenge of the IRCL technique was selecting conditions that eliminated rotational relaxation but still provided adequate infrared emission signal. Our laboratory at Kansas State University applied the IRCL technique to a tubular fast-flow reactor operating with ~ 0.5 Torr of Ar carrier gas. We gave up knowledge about the nascent rotational energy distributions in favour of the greater flexibility in choice of chemical systems that could be studied in a flow reactor [5–7]. The evolution of the IRCL technique in our laboratory has led to systematic studies of bimolecular and unimolecular reactions giving triatomic product molecules [8–11]. Elementary reactions giving water molecules proved to be ideal candidates for the IRCL technique, because strong emission could be observed from H_2O, HOD and D_2O under conditions of minimal vibrational relaxation and because anharmonic shifts permitted vibrational

distributions to be assigned [11,12] from computer simulation of the spectra. The simulation method has improved as better spectroscopic data for H_2O, HOD and D_2O were incorporated into the model. The results summarized here are based on current simulation models of water emission spectra, and they may differ slightly from the distributions given in the original papers [11–21].

Bimolecular and unimolecular gas-phase reactions that produce water molecules are important in both combustion and atmospheric chemistry [22,23]. Reactions of hydroxyl radicals provide the major removal pathway for most compounds in the troposphere, and they are important reactive species in the degradation of organic compounds in combustion processes. The systematic measurement of rate constants vs. temperature [24–26], and the development of state-of-the-art transition-state models [27–31] are currently active research areas for reactions of $OH(^2\Pi_{3/2,1/2})$ radicals. Recent theoretical developments include application of variational transition-state theory for reactions with small or no potential energy barriers and *ab initio* quantum mechanical calculations with extended basis sets to determine potential energy barriers for $OH(^2\Pi)$ reactions and to characterize the transition states [27–31]. The computation of reliable potential surfaces from the transition-state geometry to separated reaction products is a theoretical goal still to be attained for water-forming reactions. The experimental vibrational distributions of the water product provide information about the reaction dynamics after the trajectories leave the transition-state geometry. Such data can be inverted via trajectory calculations to obtain information about the potential surface [32]. The well-established kinematic constraints [33] associated with the transfer of a light atom between two heavy centres ($\boldsymbol{H'+L-H \rightarrow H'-L+H}$) should be remembered for water-forming reactions. The energy disposal pattern for reactions giving water can be compared with the bimolecular hydrogen atom abstraction of $F(^2P_J)$ and $O(^3P_J)$atoms with the same reagent and with unimolecular HF elimination reactions to learn more about the dynamics associated with the bending mode and the second stretching mode in water-forming reactions [34–38].

In this review, the vibrational distributions of H_2O and HOD molecules produced in the bimolecular hydrogen abstraction reactions by hydroxyl radicals will be presented for 30 reactants.

$$OH(^2\Pi) \text{ or } OD(^2\Pi) + HR \rightarrow H_2O(HOD) + R$$

The HR molecules can be placed in four classes: (i) inorganic hydrides with a range of exoergicity, (ii) hydrocarbons with primary, secondary and tertiary C–H bonds, (iii) representative oxygen-containing organic compounds and (iv) organic thiols and sulphides. The thermochemistry and rate constants for the individual reactions are given in table 2, *vide infra*. The information to be presented for classes (ii) and (iii) and for ethyl sulphide and ethyl thiol is based on new experiments. The available energies, $\langle E_{av} \rangle$, were obtained from the enthalpy changes, the Arrhenius activation energy and the thermal energy, $\langle E_{av} \rangle = -\Delta H_0^\circ + E_a + nRT$ ($n = 3.5$ for HR = diatomic molecule and $n = 4$ for all other reactants). The activation energies range from small negative values to ~ 2 kcal mol^{-1} (the negative values correspond to threshold energies that are essentially zero). The $\langle E_{av} \rangle$ range from 15 to 50 kcal mol^{-1}, which enables excitation of from 1 to 4 quanta in the OH stretch mode of H_2O or HOD. Although the activation energies are small, the room temperature rate constants are not so large, because the half-filled p orbital of the oxygen atom must be aligned with

the bond of the hydrogen atom (H′) to be abstracted, which also means that the HOH′ angle at the transition state is close to that of the H_2O product [27–31]. Thus, the potential energy surface for the abstraction reaction has a narrow entrance channel (or a significant steric factor in the language of collision theory). Reactions with rate constants smaller than 2×10^{-13} cm^3 molecule^{-1} s^{-1} at room temperature are difficult to study by the IRCL technique owing to weak emission from the water molecules.

Dehydration via four-centred elimination is a reaction pathway for the unimolecular decomposition of alcohols and organic acids, and the decomposition of ethanol [11, 13] and acetic acid [14] molecules with excitation energies of about 100 kcal mol^{-1}has been characterized by IRCL. These molecules were generated by the recombination reactions of H atoms with the radicals that were formed by fast iodide atom abstraction from ICH_2CH_2OH and ICH_2COOH. Unimolecular reactions of other molecules, such as those formed by reactions of formyl and acetyl radicals with OH and NO_2, also have been studied by IRCL [17, 21].

The only common feature of the vibrational distributions from the water-forming reactions is that they are non-statistical. The distributions from the direct H atom abstraction reactions extend to the thermochemical limit with inverted distributions in the stretching modes. Some OH radical reactions give distributions with decreasing populations in the stretching modes, which implies that weakly bound intermediates are important. The ratio of bend-to-stretch excitation varied from 0.20 to 1.5 for the abstraction reactions, and the bending mode of water must be included in models [32, 39–43] that attempt to describe the dynamics of these reactions. A similar conclusion seems to apply to HCN formation from H atom abstraction by CN radicals [8]. The unimolecular elimination reactions release only a small fraction of the available energy as H_2O vibrational energy, with distributions that decline monotonically with increasing E_v. The vibrational distributions from water-forming reactions thus encompass examples with direct abstraction over small barriers in the entrance channel, reactions with weak HO–RH bonding in the entrance channel followed by rearrangement, and unimolecular decomposition of stable molecules, which occur by passing over a large potential energy barrier.

State-resolved chemical reactions produce an enormous volume of data, and information theoretic analysis is a useful aid to organize and analyse such data [34,35]. The vibrational surprisal treatment developed by Bernstein and Levine [44] was extended to reactions giving triatomic molecular products [12,15]. Since the vibrational surprisal plots for water are linear, these plots provide estimates of populations in the dark states. The difference between the analysis for H_2O and HOD should be recognized at the outset. Because of collision-induced equilibration between ν_1 and ν_3 modes of H_2O, only the energy in the combined stretching modes and the distribution in the bending mode, ν_2, can be assigned. For HOD, a local mode molecule, the ν_1 and $2\nu_2$ levels equilibrate, and the distributions in the ν_3 mode and in the $\nu_1 + \nu_2$ modes can be assigned. By combining the two data sets, the energy in the new bond of HOD (ν_3) and the bending mode of H_2O (ν_2) can be identified separately. In the application of surprisal analysis, the distinction between a unique vs. a collisionally coupled set of vibrational levels of H_2O (or D_2O) and HOD must be remembered.

2. Experimental methods

2.1. *Chemical reactor*

The room temperature flow reactor was a 4 cm diameter Pyrex tube with Ar carrier gas to which reagents were added. The IRCL emanating from an NaCl window was collected with a short focal length CaF_2 lens and directed into the interferometer. The infrared emission spectra were recorded at 1 or 2 cm^{-1} resolution using a BIO-RAD Fourier transform (FT) infrared spectrometer (FTS-60). The spectrometer chamber and the tube connecting the observation window with the spectrometer were continuously flushed with dry air to remove water vapour and carbon dioxide. The response of the detection system, a liquid-N_2-cooled InSb detector, was calibrated with a standard black-body source. In some later experiments, a SPECTROGON SP 4300 nm filter was installed in front of the detector, which increased the sensitivity in the 2400–4000 cm^{-1} range. The flow reactor was pumped with a mechanical pump and rotary blower.

The bulk flow speed of the Ar carrier gas could be varied from 90 to 130 m s^{-1} with a throttling valve, and the pressure was varied by changing the Ar flow. The OH (OD) radicals were produced by the fast H (D) + $NO_2 \rightarrow$ OH (OD) + NO reaction ($k = 1.5 \times 10^{-10}$ cm^3 $molecule^{-1}$ s^{-1}) in the prereactor section of the flow tube. Excess NO_2 was used to convert all of the H/D atoms to OH or OD radicals. For typical NO_2 concentrations of $\approx 1 \times 10^{14}$ molecules cm^{-3}, the reaction was completed after ~ 0.2 ms. The H atoms were generated by a microwave discharge in a flowing H_2–Ar mixture. The degree of the dissociation of H_2 was 50% [45] and typical hydrogen atom concentrations were $(1–3) \times 10^{13}$ atoms cm^{-3}. Nitrogen dioxide was introduced together with the main Ar flow through a perforatd ring injector placed around the end of the discharge tube carrying the H_2–Ar mixture. For flow velocities of 90–130 m s^{-1}, the residence time in the prereactor was 1.5–2.2 ms, which ensured that the OH($^2\Pi_{3/2,1/2}$) radicals had reached thermal equilibrium before the reagent was added. Although the $2OH \rightarrow H_2O + H$ reaction ($k \cong 2\times\ 10^{-12}$ cm^3 $molecule^{-1}$ s^{-1} [25]) does occur to some extent in 2 ms, no H_2O emission was ever observed in the absence of added HR reagent.

The HR reagent diluted in Ar was introduced into the reactor through an injector located 20 cm downstream of the hydrogen and NO_2 inlets and 3.5 cm upstream of the centre of the NaCl observation window. A four-jet inlet arrangement was used to introduce the HR reagent into the carrier gas to provide better mixing. The HR concentrations were in the range $(0.1–10) \times 10^{13}$ molecules cm^{-3}. As a rule, the HR reactants were purified by several freeze–pump–thaw cycles and stored in glass vessels as 10% mixtures with Ar. When necessary, the flow lines and the reactor were heated to 55–65°C to prevent condensation of the reagent. Commercial tank grade Ar passed in succession through three traps filled with molecular sieves and cooled by acetone–dry ice mixture and liquid nitrogen was used to remove H_2O and CO_2 impurities. Tank grade H_2 and D_2 were used without purification.

2.2. *Primary and secondary reactions*

The flow velocity in the reactor was about 130 m s^{-1} at a working pressure of 0.5 Torr, corresponding to a mean reaction time for HR and OH of $\Delta t \sim 0.25$ ms. Such short reaction times makes the first-order differential rate law, $[H_2O]_{pri} = k_{pri}$ [HR] [OH] Δt, applicable, where k_{pri} is the rate constant of the primary OH + HR reaction. For typical conditions of $[OH] = 2 \times 10^{13}$ cm^3 $molecule^{-1}$ s^{-1} and $\Delta t = 0.25$ ms, the consumption of HR did not exceed a few per cent for

$k_{pri} < 2 \times 10^{11}$ cm^3 molecule^{-1} s^{-1}, as shown by the linear plots of the integrated spectral intensity vs. [HR].

Secondary reactions can be important for reagents containing more than one hydrogen atom. In such systems, the ratio of water concentrations produced in the secondary and primary steps at short reaction times may be expressed as $[H_2O]_{sec}/[H_2O]_{pri} = k_{sec}[OH]\Delta t/[2(1 - k_{pri}[OH]\Delta t/2)]$, where k_{sec} is the rate constant of the secondary OH + R reaction. Identification of a contribution from the secondary reaction is possible by changing Δt or [OH]. For typical conditions, the $[H_2O]_{sec}/[H_2O]_{pri}$ ratio will approach 0.1 only if $k_{sec} > 5 \times 10^{-11}$ cm^3 molecule^{-1} s^{-1}. Room temperature rate constants for OH reactions with hydrocarbon radicals are expected to be $\leq 5 \times 10^{-11}$ cm^3 molecule^{-1} s^{-1} [46]. To avoid interference from secondary reactions for $\Delta t \sim 0.2$ ms, the [OH] should be below 2×10^{13} molecules cm^{-3}. For normal operation $[NO_2] \gg [H]$, and secondary reactions of the R fragement with NO_2 with rate coefficients of the order of $(3–5) \times 10^{-11}$ cm^3 molecule^{-1} s^{-1} [47] will reduce [R] and suppress the secondary reaction with OH radicals. For the CH_2O and CH_3CHO systems, observation [18, 21] of the secondary reactions of OG with HCO and CH_3CO was possible only if $[NO_2] \cong [H_2]$. We frequently have used reactions of H atoms with iodo compounds to produce radicals which recombine with H atoms to yield vibrationally excited molecules that subsequently undergo unimolecular decomposition before being deactivated in 1 Torr of Ar [7, 11, 13]. For study of secondary reactions, a flow velocity of ≈ 90 m s^{-1}, corresponding to a reaction time of ~ 0.4 ms, and $[H_2] = 5 \times 10^{13}$ molecules cm^{-3} were typically used.

2.3. *Chemiluminescent spectra and vibrational relaxation*

Representative chemiluminescent spectra at 1 cm^{-1} resolution are shown in figure 1 from the reaction of OH(OD) with HBr (DBr); each spectrum is an average of 1024 scans of the spectrometer. The OH + HBr reaction gives emission in the 3200–3900 cm^{-1} range, which includes $\Delta v_1 = -1$ transitions (O–H symmetric stretch), $\Delta v_3 = -1$ transitions (O–H asymmetric stretch) and the first overtone of the bending mode, $\Delta v_2 = -2$ (see table 1 for band centre positions). The OD + HBr reaction gives HOD emission in the 3200–3900 cm^{-1} range from $\Delta v_3 = -1$ (OH stretch) and in the 2400–2900 cm^{-1} range; the latter includes $\Delta v_1 = -1$ (OD stretch) and $\Delta v_2 = -2$ transitions of the bending mode. Figure 1(*d*) shows the D_2O emission in the 2400–3000 cm^{-1} range, which, like H_2O, includes emission from $\Delta v_1 = 1$ (O–D symmetric stretch), $\Delta v_3 = -1$ (O–D asymmetric stretch) and the first overtone of the bending mode. The HOD emission in figure 1 (*d*) arises from a 6% contamination of HBr in the DBr sample.

To characterize the vibrational relaxation, spectra were systematically acquired with the OH + HBr reaction [12] from 0.5 Torr ($\Delta t \approx 0.2$ ms) to 2.0 Torr ($\Delta t \approx 1$ ms), which corresponds to a 20-fold change in the number of collisions of the water molecules during the residence time in the observation zone. Visual inspection of the spectra showed only small changes with pressure from 0.5 to 1.0 Torr, but a clear difference was noticeable between spectra at 1 and 2 Torr. Two conclusions are evident: (i) vibrational quenching is insignificant at pressures < 0.7 Torr and $\Delta t < 0.5$ ms; (ii) collisional equilibration between the resonant energy levels must already be achieved at 0.5 Torr [48–51]. The ν_1 and ν_3 levels equilibrate in a few collisions because of their similar energies, and the reservoir of ν_1, ν_3 levels will be denoted as $\nu_{1,3}$. Rate constants (in cm^3 molecule^{-1} s^{-1}) for the deactivation of the $\nu_{1,3}$

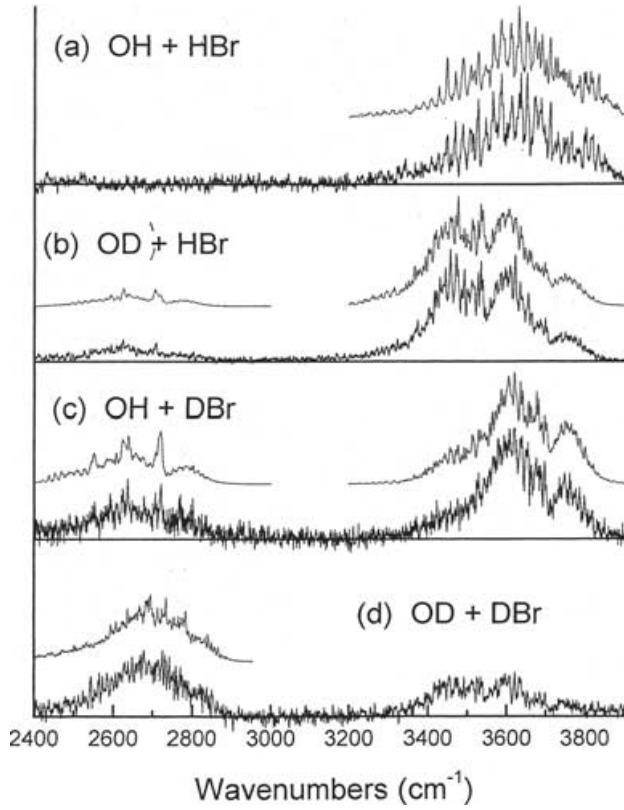

Figure 1. Chemiluminescent spectra from the flow reactor measured for 0.7 Torr of Ar and $[HBr] = 8 \times 10^{12}$ and $[DBr] = 2 \times 10^{13}$ molecules cm^{-3}: (*a*) H_2O from the OH + HBr reaction; (*b*) HOD from the OD + HBr reaction; (*c*) HOD from the OH + DBr reaction; (*d*) D_2O from the OD + DBr reaction; the emission in the 3400–3800 cm^{-1} region is mainly from a reaction with an HBr impurity. Each spectrum was normalized to the same maximum intensity. The simulated spectra are plotted directly above each experimental spectrum.

reservoir are 6.2×10^{-14} for Ar [48, 51], 8.0×10^{-13} for H_2 [50], 8.4×10^{-12} for HCl [50] and 3.0×10^{-11} for H_2O [49]. The dominant relaxation mechanism in Ar is transfer of populations from the $\nu_{1,3} = 1$ reservoir to $\nu_2 = 2$ followed by sequential loss of bending quanta in subsequent collisions. For molecular reagents, V–T, R energy transfer still dominates over intermolecular V–V processes [50]. To estimate relaxation times for the $v_{1,3} =$ level, we assume that the deactivation rate by OH does not exceed that by H_2O and that the deactivation rate by most HR is no larger than by HCl. For 0.5 Torr pressure, $[Ar] = 1.7 \times 10^{16}$, $[OH] = 1.2 \times 10^{13}$, $[HR] = 1 \times 10^{13}$ and $[H_2] = 6 \times 10^{12}$ molecules cm^{-3}, and the characteristic relaxation times are about $1.0, > 2.7, \sim 12$ and 200 ms respectively, confirming that relaxation of populations in the stretching levels for a residence time of ~ 0.2 ms is not important. Relaxation of the $2\nu_2$ levels is several times faster than for $\nu_{1,3}$ [48, 49, 51] with rate constants of 3.2×10^{-13} for Ar, 3×10^{-12} for H_2 and 5×10^{-11} cm^3 $molecule^{-1}$ s^{-1} for HCl, and Ar collisions could cause some change of ν_2 state populations for our experimental conditions. The combination levels, e.g. $\nu_1 + \nu_2$ and $\nu_3 + \nu_2$, are mixed by Coriolis and Fermi interactions with $3\nu_2$, and the rate

constant for relaxation of combination levels of the $\nu_{1,3}$ reservoir to the manifold of bending levels could be larger than the rate constant for relaxation of the $\nu_{1,3}$ stretching reservoir.

Fast collisional energy exchange between the O–D stretching and bending levels of HOD should take place owing to the similar energies of the ν_1 and $2\nu_2$ levels. Accordingly, all the (v_1, v_2)–$(v_1 - 1, v_2 + 2)$ states will be thermally equilibrated, similar to the (v_1, v_3)–$(v_1 + 1, v_3 - 1)$ equilibration in H_2O. This means that the population in the O–D vibrational levels of HOD could relax through the bending manifold, for which deactivation rate constants in Ar are expected to be of the same order or somewhat faster than for the H_2O molecule. The deactivation rates of the O–H stretching levels of HOD are expected to be similar to those of the $v_{1,3}$ levels of H_2O and vibrational relaxation should not be important.

The possibility of vibrational relaxation (beyond the coupling of ν_1 and ν_3 of H_2O and ν_1 and ν_2 of HOD) was investigated in more detail in experiments using the OH (OD) + GeH_4 reaction [15]. Because of the strong signal from this reaction, good spectra were obtained at 0.34, 0.46 and 0.71 Torr of Ar for $\Delta t = 0.35$ ms with the same [OH] and [GeH_4]; the spectra were identical, confirming that relaxation of H_2O or HOD by Ar was insignificant in this pressure range. Other possible quenching agents are OH radicals, NO, NO_2 and the HR molecules. For each reaction, we tested experimentally the range of HR concentrations for which the relative intensities of the prominent peaks in the spectra remained constant. For the inorganic hydrides, the upper limits were $[HBr] = [HI] = [H\tilde{2}S] \approx 3 \times 10^{13}$, $[GeH_4] \approx 1.5 \times 10^{13}$ molecules cm^{-3} for $\Delta t = 0.35$ ms. Using the OH + HBr reaction, no change in the relative intensities of the strongest peaks of the H_2O spectra was noted for $[OH] < 2.5 \times 10^{13}$ and $[NO_2] < 3 \times 10^{14}$ molecules cm^{-3} [12]. Tests for relaxation of D_2O or HOD formed by OD(OH) + DR reactions suggested that relaxation rates were more rapid for these cases; see section 4.1.1.

Before analysis, the measured spectra were corrected for the wavelength response function of the detector. The spectra presented in section 3 to demonstrate the fitting procedure were taken at 0.7 Torr, because the signal-to-noise ratios were good and the distributions were not seriously affected by collisional deactivation. For most reactions, the spectra that were used for analysis to obtain the H_2O and HOD distributions were obtained at 0.5 Torr and $\Delta t = 0.25$ ms.

3. Data analysis

3.1. *Spectral simulation*

3.1.1. *H_2O spectra*

The three normal mode frequencies are $\nu_1 = 3657.1, \nu_2 = 1594.7$ and $\nu_3 = 3755.9\,\text{cm}^{-1}$, and the fundamentals of the stretching modes, and the first overtone of the bending mode, $2\nu_2$, lie in the range of the observed emission. Although the rotational lines are partly resolved, direct assignment of individual transitions is complicated by overlapped transitions, centrifugal distortion and resonance effects [52]. Computer simulation was required to analyse a given spectrum and to assign the vibrational distribution.

The absorption intensities for the ν_1, $2\nu_2$ and ν_3 bands of H_2O in the HITRAN database [53] were used as the basis for modelling. The relative emission intensities for the individual rovibrational transitions $v_1v_2v_3JK_aK_c \rightarrow 000J'K_a'K_c'$ were obtained, according to the general relation between the Einstein transition probabilities

of absorption (B_{mn}) and spontaneous emission (A_{nm}) [52], where n and m denote the upper and lower states, ν_{nm} is the wavenumber of the transition,

$$A_{nm} = 8\pi hc\nu_{nm}^3(d_m/d_n)B_{mn}, \tag{E1}$$

d_n and d_m are the degeneracies of the states n and m, with $n = v_1v_2v_3JK_aK_c$, $m = 000J'K_a'K_c'$, $d_n = 2J + 1$ and $d_m = 2J' + 1$. On the basis of observations of many HF and HCl distributions in our reactor [7, 34, 35], a room temperature Boltzmann distribution of rotational states is expected for H_2O and HOD. Although rotational levels up to $J = 12$ are populated at 298 K, the 196 transitions from the $J \leq 8$ levels constitute 99.3% of the intensity of the 001–000 band. The most intense lines are from the $J = 2$ and 3 levels, for example, $JK_aK_c \rightarrow J'K_a'K_c' = 303 \rightarrow 202$ at 3688.5, $221 \rightarrow 220$ at 3752.2 or $303 \rightarrow 404$ at 3837.9 cm^{-1}. With addition of the most intense lines from $J = 9$ and 10, a total of 228 rotational lines were included in the model. Since the populations in the rotational levels of H_2O obey Fermi–Dirac statistics, the weights of *eo* and *oe* levels are three times larger than those of *ee* and *oo* levels. Since the 001–000 band is a pure *a*-branch (i.e. the transition dipole moment changes along the molecular axis with the smaller moment of inertia) in which only transitions between the rotational levels of different symmetry *ee* ↔ *eo* and *oo* ↔ *oe* are allowed, the statistical weights of the same transition in absorption and emission were interchanged. The (100) and (020) transitions are *b*-branches and no change of symmetry occurs during the transition. Finally, a conversion expression may be written as

$$I_{em} = \text{const} \times I_{abs}\nu_{nm}^3(g_n/g_m)\exp[(\nu_o - \nu_{nm})/kT], \tag{E2}$$

where ν_o is the band centre and g_n and g_m are the nuclear spin statistical weights of the upper and lower states. Lorentzian lineshapes were assumed with a half-width given by the resolution of the spectrometer (2 or 1 cm^{-1}). The band-sum intensities, S_v^0, defined as the sum of the intensities of all lines belonging to a given band, are presented in table 1. The ratios of the band emission intensities are $\nu_3 : \nu_1 : 2\nu_2 = 100 : 8.9 : 1.3$ and, hence, the $2\nu_2$ band was neglected. Although the $\Delta\nu_1 = -1$ bands were included in the analysis, the $\Delta\nu_3 = -1$ transitions dominate the emission spectrum.

In our first model [11, 14], the line positions of the $(v_1v_2v_3) \rightarrow (v_1v_2v_3 - 1)$ bands were calculated by red-shifting the band centre of the fundamental ν_3 band by $\Delta\nu = \nu_0' - \nu_0$, where $\nu_0' = G(v_1v_2v_3) - G(v_1'v_2'v_3')$, $\nu_0 = G(001) - G(000)$, and $G(v_1v_2v_3)$ is given by the conventional expression for the vibrational energy levels of a non-linear triatomic molecule:

$$G(v_1v_2v_3) = \sum \omega_i(v_i + 1/2) + \sum\sum x_{ik}(v_i + 1/2)(v_k + 1/2). \tag{E3}$$

The ω_i values and anharmonicity coefficients, see table 1, were taken from Benedict *et al.* [55]. The same method was applied to estimate the positions of the $(v_1v_sv_3) \rightarrow (v_1 - 1v_2v_3)$ combination and hot bands. Obviously, the shifts for the combination $(0v_21) \rightarrow (0v_20)$ or $(v_a01) \rightarrow (v_100)$ bands depend on the anharmonic coefficients x_{23} or x_{13}, while that for the hot bands, $(00v_3) \rightarrow (00v_3 - 1)$, depends only on x_{33}. The individual shifts are $\Delta\nu = v_2x_{23}v_1x_{13}$ and $2(v_3 - 1)x_{33}$ which give, for example, a shift of $\Delta\nu = |x_{23}| = 20.3\,cm^{-1}$ for the $(011) \rightarrow (010)$ band, $\Delta\nu = |x_{13}| = 165.8\,cm^{-1}$ for the $(101) \rightarrow (100)$ band, and $\Delta\nu = 2|x_{33}| = 95.2\,cm^{-1}$ for the $(002) \rightarrow (001)$ band. The large anhar-

Table 1. Spectroscopic information for H_2O, HOD and D_2O.

Molecule	v_1[a]	$2v_2$[a]	v_3[a]	$-x_{11}$[d] $-x_{12}$[d]	$-x_{22}$[d] $-x_{13}$[d]	$-x_{33}$[d] $-x_{23}$[d]	$\alpha(v_i)$[e]			
	$S_v^0(\nu_i)$[b] (10^{-19} cm^{-1}/(molecule cm^{-2})) $S'_v(\nu_i)/S'_v(\nu_3, H_2O)$ in emission[c]									
H_2O	3657.1	3151.6	3755.9	42.58	16.81	47.57	$v_{1,3} = 1$	$v_{1,3} = 2$	$v_{1,3} = 3$	$v_{1,3} = 4$
	4.96	0.757	72.0							
	0.089	0.013	1.00	15.93	165.8	20.33	0.44	0.77	0.93	1.17
HDO	2723.7	2782.0	3707.5	43.36	11.77	82.88	$v_3 = 1$	$v_3 = 2$	$v_3 = 3$	$v_3 = 4$
	42.2	5.64	94.5							
	0.23	0.031	1.32	8.60	13.14	20.08	1.0	1.75	2.28	2.58
D_2O	2671.6	2336.8	2787.7	22.58	9.18	26.15	$v_{1,3} = 1$	$v_{1,3} = 2$	$v_{1,3} = 3$	$v_{1,3} = 4$
	4.7	0.52	38.5							
	0.039	0.0043	0.29	7.58	87.15	10.61	0.45	0.82	1.11	1.08

[a] Band centres of the indicated transitions; the information for H_2O and HOD is from [53] and that for D_2O is from [54]. The $H_2O(011\rightarrow000)$ and $HOD(011\rightarrow000)$ emission bands are discussed in [15].

[b] The band-sum intensities, $S_v^0(\nu_i)$, were taken from [53] for H_2O and HOD; the $S_v^0(v_3)$ and $S_v^0(v_1)$ values for D_2O were calculated [20] and $S_v^0(2v_2)$ was taken from [67].

[c] Ratio of the band-sum intensity in emission to that for ν_3 of H_2O. The $S'_v(\nu_i)$ values for H_2O, $S_v^1(v_3)$ for HOD and $S_v^1(v_1)$ and $S_v^1(v_3)$ for D_2O are based on calculations using equation (2) [20]. The ratios for $S'_v(2v_2, D_2O)$, $S'_v(2v_2, HOD)$ and $S'_v(v_1, HOD)$ were obtained from scaling the $S_v^0(v_i)/S_v^0(v_3)$ ratios by the ratio of ν^3 factors.

[d] The anharmonicity coefficients are from [55].

[e] The intensities from the thermally equilibrated $\nu_{1,3}$ levels of H_2O (or D_2O), relative to that of $v_3 = 1$ of H_2O (or D_2O), and the intensities from the thermally equilibrated levels of HOD relative to that of $v_3 = 1$. To compare intensitiesfrom H_2O to HOD or D_2O, the relative emission probabilities for $v_3 = 1$ must be added to the $\alpha(v_i)$ values; see section 3.2 for a description.

monic shifts lead to a significant difference in spectra for different populations in ν_1, ν_2 and ν_3 and permit contributions of the individual bands to be identified from the experimental spectrum. Although equation (E3) (even including the third-order terms with anharmonicity constants y_{ijk}) is not sufficiently accurate for levels higher than $v_2 > 2$ and $v_3 > 2$, the band shifts given by the anharmonicity coefficients show how a vibrational distribution can be assigned from fitting an H_2O spectrum.

Experimental values for the band centres for the $v_{1,3} \leq 3$, $v_2 \leq 3$ bands from the HITRAN database were used in later work [12, 15]. This database gives, for example, 163.1 and 66.7 cm^{-1} for the shifts of the $(101) \rightarrow (100)$ and $(002) \rightarrow (001)$ bands relative to the $(001) \rightarrow (000)$ fundamental. The shifts for the bending levels also are significant with $\Delta v = 19.4$, 36.0 and 48.9 cm^{-1} for the $(011) \rightarrow (010)$, $(021) \rightarrow (020)$ and $(031) \rightarrow (030)$ transitions respectively. Experimental values [57] were taken from some high v_2 states (e.g. (151) and (042)); others were from variational calculations [58, 59]. Corrections for line positions of H_2O bands with $v_2 = 5$ and 6 were made in [18] using the band origins determined from spectra of water from the sun [60].

Using the shifts of the fundamental bands to model spectra emission from higher vibrational levels implies that the rotational energy levels are the same for each $(v_1 v_2 v_3)$ vibrational level. However, perturbations between rotational levels can lead to dramatic displacements of line positions. The discrepancy increases with rotational quantum number and may be hundreds of cm^{-1} for certain transitions from $J > 6$. In the final modification of the simulation program, line positions for all the $(v_1, v_2, v_3) \rightarrow (v_1, v_2, v_3 - 1)$ and $(v_1, v_2, v_3) \rightarrow (v_1 - 1, v_2, v_3)$ bands of H_2O were obtained as a difference of the rovibrational energy levels of the corresponding transitions. Since the energy available for some reactions is sufficient to excite up to four H_2O stretching quanta, bands with $v_1 + v_3 = 4$, $v_2 \leq 2$; $v_1 + v_3 = 3$, $v_2 \leq 4$; $v_1 + v_3 = 2$, $v_2 \leq 6$ and $v_1 + v_3 = 1$, $v_2 \leq 6$ were considered. Since the $v_2 \geq 7$ levels are above the inversion barrier, $v_2 = 6$ was the highest bending level included in the model. Transitions between rotational levels with $J \leq 7$ (all K_a, K_c), $J = 8(K_a - K_c < 2)$, $J = 9(K_a - K_c < -5)$ and $J = 10(K_a - K_c < -6)$ were included. Fortunately, many H_2O bands in the 0–17 000 cm^{-1} range have been examined in absorption, and most of the rovibrational energy levels for $v_1, v_3 \leq 4$, $v_2 \leq 2$ and $J \leq 8$ states are known [15]. Missing levels were calculated using expressions for rotational energy derived by Kwan [61], neglecting J- and K-dependent terms for Fermi and Darling–Dennison interactions. The energy levels for the states with $v_2 = 5$ and 6, with poor convergence for $J \geq 6$, were calculated [61] using a polynomial extrapolation of the rotational levels of $v_2 = 0$–4 states.

In the early studies [11–14], the intensities of the rotational transitions, JK_aK_c–$J'K'_aK'_c$, in combination bands were taken as equal to the intensities of the same transitions in the basic (001)–(000) band. The harmonic oscillator approximation [56] with a cubed frequency adjustment was used to calculate the intensity of the $\Delta v_3 = -1$ and $\Delta v_1 = -1$ bands from higher v_3 and $v_2 \geq 2$ levels. A centrifugal correction to the line intensities of the $\Delta v_3 = -1$ combination bands was made in more recent work with the help of F–factors, which were calculated according to the first-order intensity perturbations for the vibration–rotation lines of asymmetric rotors for fundamental bands [62]. The theory was extended [15] to give F factors for combination and hot bands. No allowance, except for the v^3 adjustment, was made for the influence of v_2 or v_1 on the transition probabilities of $\Delta v_3 = -1$ combination bands.

After an initial rapid eqiuilibration, the $v_1 = 1$ and $v_3 = 1$ levels of H_2O will relax as a single reservoir ($v_{1,3} = 1$). We presumed this to be true for all levels with the same number of stretching quanta $v_{1,3} = v_1 + v_3$. Accordingly, a Boltzmann weighting of ν_1 and ν_3 levels within each group of $(v_{1,3}, v_2)$ states was adopted and the simulated spectra for H_2O were calculated as a superposition of the 'equilibrated' $(v_{1,3}, v_2)$ bands. The weights of each band is denoted as $P(v_{1,3}v_2)$ and when normalized, $\sum_{v_{1,3}} \sum_{v_2} P(v_{1,3}, v_2) = 100$, the weights become the relative population of each $(v_{1,3}, v_2)$ state. Omitting levels with a negligible 298 K Boltzmann weight gives the following $(v_{1,3}, v_2)$ groups:

$$(1, v_2) = 0.384(0, v_2, 1) + 0.616(1, v_2, 0),$$

$$(2, v_2) = 0.15(0, v_2, 2) + 0.38(1, v_2, 1) + 0.47(2, v_2, 0),$$

$$(3, v_2) = 0.054(0, v_2, 3) + 0.119(1, v_2, 2) + 0.400(2, v_2, 1) + 0.427(3, v_2, 0),$$

$$(4, v_2) = 0.043(1, v_2, 3) + 0.440(2, v_2, 2) + 0.434(3, v_2, 1). \quad \text{(E4)}$$

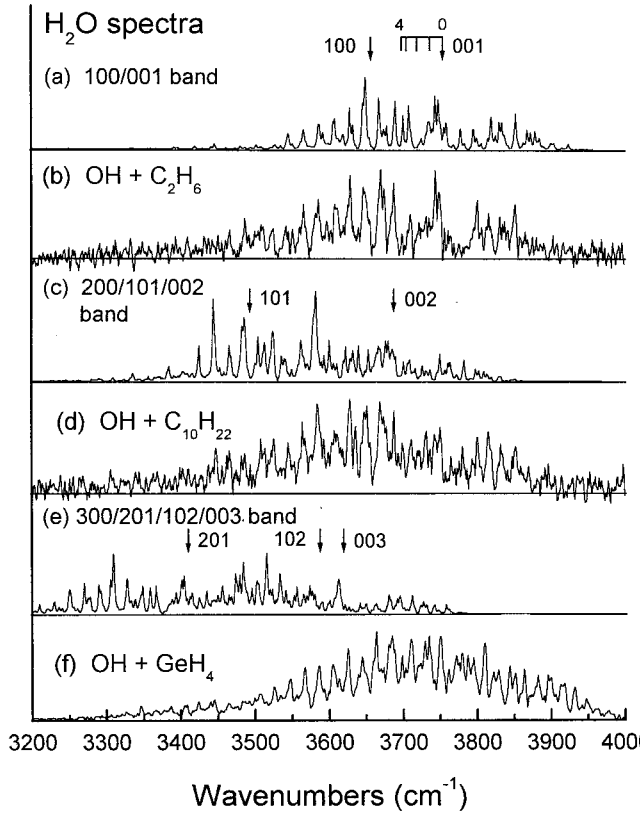

Figure 2. Demonstration for modelling H_2O spectra: (*a*) calculated spectrum from $\nu_3 + \nu_1$ fundamental bands with relative intensities of 100:8.9, (*b*) emission from the $OH + C_2H_6$ reaction; (*c*) calculated spectrum from equilibrated $2\nu_3 + \nu_1\nu_3 + 2\nu_1$ levels; (*d*) emission from the $OH + C_{10}H_{22}$ reaction; (*e*) calculated spectrum from equilibrated $\nu_3 + \nu_1 2\nu_3 + 2\nu_1\nu_3 + 3\nu_1$ levels; (*f*) emission from the $OH + GeH_4$ reaction. Arrows indicate band centres; vertical ticks correspond to the shifts from excitation of the bending levels in the 001 band; the calculated spectra in (*c*) and (*e*) have no population in ν_2 levels.

Figure 2 shows calculated bands from $v_{1,3} = 1, 2$ and 3 for $v_2 = 0$ with comparison with experimental spectra. The (1,0) band, which is a combination of (001) and (100) fundamental bands, is shown in figure 2 (*a*) and the (2, 0) band is shown in figure 2 (*c*). The spectrum in figure 2 (*b*) from the $OH + C_2H_6$ reaction required a low bending excitation of $P(1,0) = 44$, $P(1,1) = 18$ and $P(1,2) = 3$ plus $P(2,0) = 14$ for simulation. The best fit to the spectrum from the *n*-decane reaction was $P(1,0) = 26$, $P(1,1) = 19$, $P(1,2) = 9$ and $P(1,3) = 1$ plus $P(2,0) = 16$ and $P(2,1) = 12$; the contribution from the $v_{1,3} = 2$ states is twice that from the ethane spectrum. Figures 2 (*e*) and 2 (*f*) display the equilibrated (3,0) band and the H_2O spectrum from the OH reaction with GeH_4, see table 3 for the distribution. Since the band centres of the $v_{1,3} = 1$–4 transitions are separated by $\sim 90\,cm^{-1}$, the v_2 distribution of each $v_{1,3}$ level can be assigned.

The best fit to an experimental spectrum was selected using a least-squares procedure. Every $(v_{1,3}, v_2)$ emission band was considered as a vector with $N = 1452$ elements, which corresponds to the number of points in a 3200–3900 cm^{-1} spectrum at 1 cm^{-1} resolution. For measurements of equal accuracy, the least-squares method requires a minimization of the value of the estimator $Q = \sum(s_i - \sum P_j b_{ij})^2$, where s_i is the *i*th measurement in the experimental spectrum (intensity), b_{ij} is the *i*th element of the *j*th basis band and P_j are the populations of the corresponding vibrational states. The inner summation is made over the basis vectors, and the outer one is a summation over all the spectral points. The parameters, P_j, were found in a circular search with a step-by-step inclusion of additional bands. Thus, for the spectrum in figure 1 (*a*) the best fit was obtained with 12 bands extending to (1, 5), (2, 3) and (3, 1) as given in table 3. The standard deviation [63] of the populations, $\sigma(P_j)$, was estimated from $\sigma(P_i) = [(G)_{ii}^{-1} Q/N]^{1/2}$, where $(G)_{ii}^{-1}$ is the diagonal element of the reciprocal Gram's matrix of the basis vectors $\mathbf{b}_i = (b_{1i}\, b_{2i} \ldots b_{Ni})$, i.e. $C_{kl} = \mathbf{b}_k^{\mathrm{T}} \mathbf{b}_l$. For the fit of figure 1 (*a*) with $Q = 1.68 \times 10^6$, the calculated values of $(G)_{ii}^{-1}$ vary from 3.5×10^{-6} to 4.4×10^{-6} with the largest $\sigma(P_j)$ having a magnitude of 13%. This value corresponds only to the uncertainty associated with the least-squares fitting and does not include experimental errors or errors in the basis vectors. The main uncertainty in the assigned distributions is the population in the 'dark' vibrational states, namely the $0v_20$ states ($v_{1,3} = 0$) of H_2O or D_2O, and 001 and 011 states of HOD.

The total population in a given $v_{1,3}$ level was obtained by summation over the v_2 distribution: $P_{1,3}(v_{1,3}) = \sum_{v_2}(P_{v_{1,3},v_2})$. Similarly, $P_2(v_2) = \sum_{v_{1,3}}(P_{v_{1,3},v_2})$, is the weight of the states with a particular bending vibrational number, v_2. Three $P_{1,3}(v_{1,3})$ distributions are presented in tables 3–8 for different assignments of the $P_{1,3}(0)$ population: (a) $P_{1,3}(0)$ is not considered, (b) $P_{1,3}(0)$ as obtained from linear surprisal plots and (c) the calculated statistical distribution, $P^0_{1,3}(v_{1,3})$. The mean fraction of vibrational energy was calculated as $\langle f_v(H_2O)\rangle = [\sum_v P_v \cdot E_v]/\langle E_{av}\rangle$, where the energy $E_v = E(v_{1,3}, v_2)$ is the sum of the Boltzmann-weighted energies of $(n, v_2, v_{1,3} - n)$ states with $n = 0, \ldots, v_{1,3}$. The energy in bending vibrations was calculated as $\langle E_{v_2}\rangle = \sum_v P_v[E(v_{1,3}, v_2) - (E(v_{1,3}, 0)]$; the fractional contribution from bending to the total vibrational energy is $\langle f_{v_2}\rangle = \langle E_{v_2}\rangle/\langle E_{vib}\rangle$. Since the $v_3 = 0$ population of HOD could be experimentally measured, the $P_{1,3}(0)$ value deduced from the linear surprisal could be verified. The bending distribution in $v_{1,3} = 0$ was assumed to be similar either to that of $v_{1,3} = 1$ or to the statistical bending distribution; the latter was preferred if $\langle E_{av}\rangle \leq 30\,kcal\,mol^{-1}$. Both estimates are probably lower limits to the bending excitation.

3.1.2. *HOD spectra*

The normal mode frequencies are $\nu_1 = 2723.7$ (O–D stretching), $\nu_2 = 1403.5$ (bending) and $\nu_3 = 3707.5\,\text{cm}^{-1}$ (O–H stretching). Simulations were carried out separately for the $\Delta\nu_3 = -1$ emission in the 3200–3900 cm^{-1} range and for the $\Delta\nu_1 = -1$ and $\Delta\nu_2 = -2$ emissions in the 2400–2900 cm^{-1} range (see figures 1 (*b*) and 1 (*c*)). A method similar to the one described above for H_2O was used to simulate the emission spectra for HOD. The fundamental (001), (100) and (020) absorption bands and the band-sum intensities were taken from the HITRAN database; see table 1. The relative emission intensities for $v_3 : v_1 : 2v_2$ are 100:18:2.5 and the O–H transitions are 5.5 times stronger than O–D transitions. Although the $\Delta\nu_2 = -2$ contribution is much less than from $\Delta\nu_3 = -1$, the $\Delta\nu_2 = -2$ transitions were included in the simulation of the 2400–2900 cm^{-1} band. The calculated (001) and (100) plus (020) emission spectra, with half-widths of 1 cm^{-1} for each line, are shown in figure 3 (*a*).

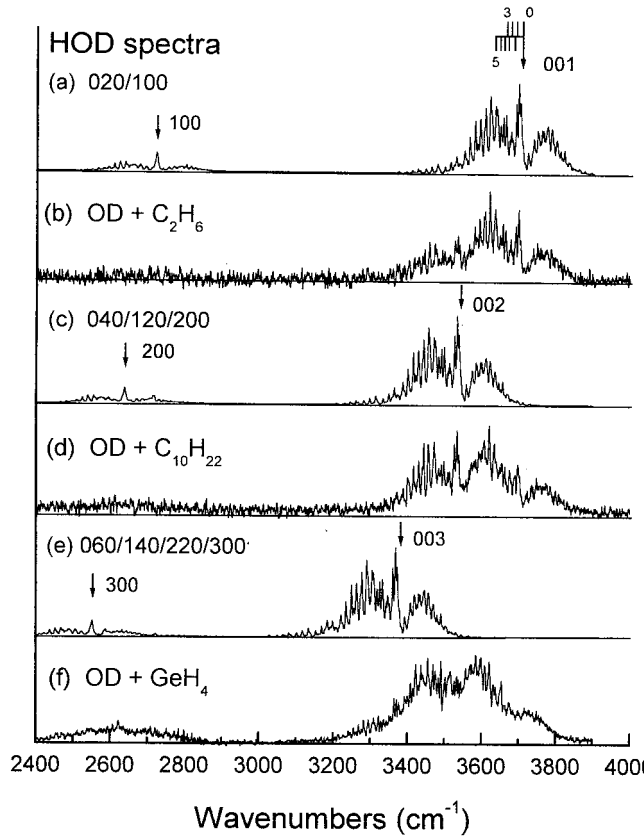

Figure 3. Demonstration for modelling of HOD spectra: (*a*) calculated ν_3 and ν_1 fundamental bands; (*b*) emission from the $OD + C_2H_6$ reaction; (*c*) calculated $2\nu_3$ and equilibrated $2\nu_1 + \nu_1 2\nu_2 + 4\nu_2$ bands; (*d*) emission from the $OD + C_{10}H_{22}$ reaction; (*e*) calculated $3\nu_3$ and equilibrated $3\nu_1 + 2\nu_1 2\nu_2 + \nu_1 4\nu_2 + 6\nu_2$ bands; (*f*) emission from the $OD + GeH_4$ reaction. Arrows indicate the band centres; the downward vertical ticks in (*a*) identify the shifts owing to bending excitation, the upward ones correspond to shifts from excitation of ν_1 levels.

The spectroscopic database for HOD is more limited than for H_2O; hence, the positions of the HOD bands from high levels were approximated by red-shifting the origins of the fundamental bands. The magnitude of the shift was calculated as a difference of band centres, which were taken from the HITRAN database, calculations [64] or recent spectroscopic studies [65]. Band centres for transitions that were not previously reported were calculated using equation (3) with anharmonic and Fermi-resonance constants from [64]. The (002) → (001) and (003) → (002) emission bands are shown in figures 3 (*c*) and 3 (*e*). The simulation model included v_3 and v_1 levels to ≤ 4 and $v_2 \leq 7$. The simulation of the HOD spectrum from $OD + C_2H_6$ shown in figure 3 (*b*) is illustrative. The blue side of the HOD spectrum is described by the (001) emission with low v_2 excitation, but the red side of the spectrum obviously has a contribution (21%) from the (002) → (001) band.

To obtain a more complete picture of the HOD vibrational distribution, the 2400–2900 cm^{-1} spectrum was simulated. This intensity is much weaker and the signal-to-noise ratio is poorer than for O–H emission (see figure 3), but a good estimate for the $(v_1 v_2 0)$ populations can be obtained. The near energy match between (100) and (020) vibrational states was assumed to give a thermal equilibrium between all the vibrational states in a $(v_1 + n, v_2 - 2n, v_3)$ series, where $n = 0, 1, \ldots, v_2/2$ for even v_2 and $n = (v_2 - 1)/2$ for odd v_2. For example, the $(4, v_3)$ level is composed of three states: $a_1(0, 4, v_3) + a_2(1, 2, v_3) + a_3(2, 0, v_3)$, where the 298 K Boltzmann weights are $a_1 = 0.333$, $a_2 = 0.253$ and $a_3 = 0.414$ for $v_3 = 1$, $a_1 = 0.364$, $a_2 = 0.260$ and $a_3 = 0.376$ for $v_3 = 2$, etc. Accounting for these equilibrated levels affects the simulation of both the O–H and the O–D bands. For example, the 021/101, 031/111, 041/121/201, ... groups for $v_3 = 1$ and 022/102, 032/112, ... groups for $v_3 = 2$ give emission in the O–H and O–D ranges, while the 020/100, 040/120/200, 060/140/220/300, etc. groups give emission only in the O–D range. Transitions from the last group are shown in figures 3 (*a*), 3 (*c*) and 3 (*e*) respectively. Having the $P(v_{1,2}, v_3)$ distributions, we can sum over the $\nu_{1,2}$ states for each v_3 level, and obtain the total relative population $P_3(v_3) = \sum_{v_{1,2}}(P_v)$, where $v = (v_{1,2}, v_3)$, for a given v_3 state. The total populations in a given $v_{1,2}$ state are obtained by summation over the v_3 number. The $P_3(v_3)$ distributions are presented in tables 3–8 for three assignments of the $P_3(0)$ population: (a) $P_3(0)$ was not considered; (b) $P_3(0)$ was obtained from linear surprisal plots; (c) $P_3(0)$ was estimated from the 2400–2900 cm^{-1} spectrum. The two dark states, 000 and 010, which contribute to the overall $P_3(0)$ population were assigned either by analogy to the statistical distribution (for low $\langle E_{av} \rangle$ reactions) or by analogy to the $v_{1,2}$ distribution in the $v_3 = 1$ manifold for cases with larger $\langle E_{av} \rangle$.

Figure 3 (*d*) demonstrates a simulation of the $\Delta v_3 = -1$ HOD spectrum from the *n*-decane reaction using five states, 01, 11, 21, 02 and 12, with weights of 53, 6, 3, 36 and 2 (see table 4). Fitting the more complex spectrum from $OD + GeH_4$, see figure 3 (*f*), required 19 bands extending to $(v_{1,2}, v_3) = (7, 1)$, (5,2) and (1,3). Fitting the 2400–2800 cm^{-1} region of figure 3 (*f*) established a 44% contribution from $P_3(0)$ with a broad distribution in $v_{1,2}$ (see table 3). As in the case of H_2O, the fitting for HOD spectra was made by a least-squares method. The values of the least-squares estimators Q were approximately two times smaller for HOD than those for the H_2O spectra, with fitting errors usually less than 10%. The better fitting is explained by the intrinsically stronger signal and the simpler $\Delta v_3 = -1$ emission band of HOD. The mean fraction of vibrational energy of HOD was calculated as $\langle f_v(\text{HOD}) \rangle = (\sum_v P_v E_v)/\langle E_{av} \rangle$, where the energy $E_v = E(v_{1,2}, v_3)$ is the sum of the

Boltzmann-weighted energies of $(v_1 + n, v_2 - 2n, v_3)$ states. The energy in ν_3 was calculated as $\langle E_{v_3}\rangle = \sum_v P_v[E(v_{1,2}, v_3) - E(v_{1,2}0)]$. The fraction of the excitation in the newly formed O–H bond is $\langle f_{v_3}\rangle = \langle E_{v_3}\rangle/\langle E_{\text{vib}}\rangle$. The ratio of $\langle E_2\rangle$ from H_2O to $\langle E_3\rangle$ from HOD was used as the index for the bend-to-stretch excitation for a given reaction.

The reader must remember the difference between the $P_{1,3}(v_{1,3})$ and $P_3(v_3)$ distributions. The $P_3(v_3)$ distribution is a sum over all v_1 and v_2 numbers for a given v_3 number of HOD, while $P_{1,3}(v_{1,3})$ is a sum over v_2 for a given $v_1 + v_3$ quantum number of H_2O. For example, consider a hypothetical stretching distribution $\{P(v_1 = 0, v_3 = 0) = a,\ \ P(v_1 = 1, v_3 = 0) = b,\ \ P(v_1 = 0, v_3 = 1) = c, P(v_1 = 1, v_3 = 1) = d\}$; we have $P_3(0\text{–}2) = (a + b) : (c + d) : 0$ and $P_{1,3}(0\text{–}2) = a : (b + c) : d$. Consider a more descriptive example; the local O–H and O–D modes for HOD nearly correspond to the normal modes, while for H_2O and D_2O the symmetric (ν_1) and antisymmetric (ν_3) normal modes are linear combinations of local modes [66]. Thus, excitation of the H_2O local mode would result in equal probabilities for excitation in the ν_1 and ν_3 states. Let p_n^v and p_o^v denote the probabilities of the excitation of the vth vibrational level in the local mode corresponding to the new and old O–H bonds, respectively. Then, the probability to find the H_2O molecule in the ground stretching state $v_{1,3} = v_1 + v_3 = 0$ is $P_{1,3}(0) = p_n^0 p_o^0$. The probability for the $v_{1,3} = 1$ state is $P_{1,3}(1) = p_n^1 p_o^0 + p_n^0 p_o^1$, for the $v_{1,3} = 2$ state is $P_{1,3}(2) = p_n^2 p_o^0 + p_n^0 p_o^2 + p_n^1 p_o^1$, and so on. For the HOD molecule, the $P_3(v_3)$ distribution coincides with p_n^v probabilities and $P_3(0) = p_n^0$. Even if the release of energy to the newly formed O–H bond is identical in OH and OD reactions, in general $P_3(0) \geq P_{1,3}(0)$ because equality of $P_3(0)$ and $P_{1,3}(0)$ can be achieved only when $p_o^0 = 0$, i.e. the old bond does not receive any energy and it acts as a spectator. Inspection of the statistical distributions, $P_{1,3}^0(v_{1,3})$ and $P_3^0(v_3)$, presented in tables 3–7, also illustrates the difference in the $v_{1,3}$ and v_3 distributions.

3.1.3. *D_2O spectra*

Emission occurs in the 2400–2900 cm^{-1} range (figure 1 (*d*)), and the fundamentals of the ν_1 and the ν_3 modes lie in the range of the observed emission (see table 1). The first overtone of the bending mode, $2\nu_2 = 2336.8\,\text{cm}^{-1}$, is close to the red side of this range. The wavelengths of the (100), (020) and (001) bands could not be taken from absorption spectra, since the only published D_2O (001)–(000) absorption spectrum [55] does not contain a complete assignment of rotational lines, and the complete list of lines [67] includes saturated intensities for the most important transitions. Account of the nuclear spin statistics of the rotational levels must be made for the (001) band; in this case the ratio of the statistical weights of *ee* and *oo* levels to that of *eo* and *oe* levels is 2:1. Calculation of the fundamental ν_1 and ν_3 emission bands of D_2O, which was described in the appendix of [20], included the 443 most intense lines of ν_3 and 424 lines of ν_1 bands from Papineau *et al.* [67]. The transition intensities were calculated using the expansion of the transformed dipole moment [68] with account of the interactions between the close rotational levels of (100) and (001) states. The calculated ν_1 and ν_3 bands are presented in figure 4 (*a*).

The ratios of the integrated emission intensities for the (001):(100):(020) bands are 100:13:1.5, and emission from the overtone levels of ν_2 can be neglected. As in the case of H_2O, the energy levels of the ν_1 and ν_3 modes were assumed to have equilibrium populations; the 298 K Boltzmann weights are given by

$$(1, v_2) = 0.365(0, v_2, 1) + 0.635(1, v_2, 0),$$

$$(2, v_2) = 0.163(0, v_2, 2) + 0.337(1, v_2, 1) + 0.50(2, v_2, 0),$$

$$(3, v_2) = 0.075(0, v_2, 3) + 0.164(1, v_2, 2) + 0.338(2, v_2, 1) + 0.43(3, v_2, 0),$$

$$(4, v_2) = 0.018(0, v_2, 4) + 0.036(1, v_2, 3) + 0.078(2, v_2, 2) + 0.241(3, v_2, 1) + 0.626(4, v_2, 0). \quad \text{(E5)}$$

The modelling of the D_2O spectra was done by red-shifting the fundamentals using the experimental band centres of Bykov *et al.* [69]. The centres for unknown bands were taken from calculations [58, 70]. The band centres for $v_2 \geq 5$ were estimated by extrapolation. Figure 4 (*a*) shows that the emission from $(1, v_2)$ with $v_2 > 4$ overlaps the emission from the (2,0) and (2,1) states. Figure 4 (*b*) shows the D_2O spectrum from the OD + DCl reaction; the shape of the weak spectrum coincides with the $\nu_{1,3} = 1$ band. Emissions from higher levels, including $v_{1,3} = 2, 3$ and 4, are needed to simulate the spectrum from the OD + DBr reaction, figure 4 (*c*), and least-squares fitting gave $P_{1,3}(1\text{–}4) = 51 : 40 : 7 : 2$ with bending excitation up to $v_2 = 6$. The

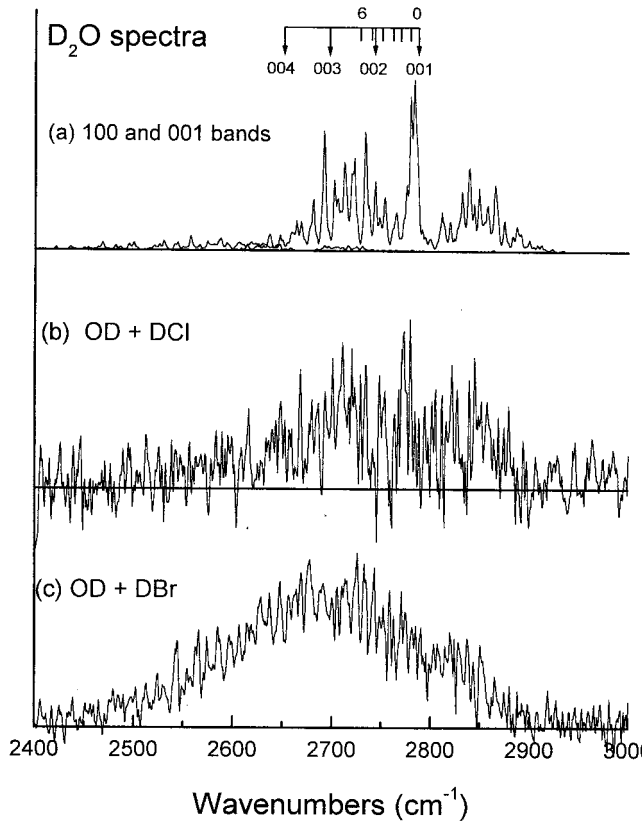

Figure 4. Demonstration for modelling of D_2O spectra: (*a*) calculated $\nu_3 + \nu_1$ fundamental bands with relative intensities of 100:12; (*b*) emission from the OD + DCl reaction; (*c*) emission from the OD + DBr reaction. The arrows in (*a*) indicate the $n\nu_3$ ($n = 1$–5) band centres; vertical ticks correspond to band shifts owing to bending excitation.

populations for $v_2 > 4$ were assigned according to a geometrical progression, rather than by least-squares fitting, because of overlap of emission from the next higher ν_3 level.

3.2. *Integrated relative intensity data*

Integrated relative intensities can be employed to evaluate relative rate constants. For example, the rate constant of $OH + GeH_4$ was measured using $OH + HBr$ as a reference reaction. From measurements of the intensity, $I(H_2O)$, as a function of both reagent concentrations for the same [OH], the relative reaction rate constants can be determined as

$$k/k_{\text{ref}} = \gamma\beta_{\text{ref}}(H_2O)/\gamma_{\text{ref}}\beta(H_2O), \tag{E6}$$

where γ and γ_{ref} are the slopes of $I(H_2O)$ vs. [HR] plots for the studied and reference reaction respectively and the β factors are determined as follows. The ratio of the H_2O fundamental band-sum intensities in emission, $S'_v(\nu_1, H_2O)/S'_v(\nu_3, H_2O)$, is equal to 0.089. From this ratio, equations (E4) and the scaled harmonic-oscillator approximation, the band-strength coefficients of the equilibrated $\nu_{1,3}$ bands given in table 1 are obtained. For example, the $(2, v_2)$ band consists of two $\Delta v_3 = -1$ bands from $(0, v_2, 2)$ and $(1, v_2, 1)$ states and two $\Delta v_1 = -1$ bands from $(1, v_2, 1)$ and $(2, v_2, 0)$ states. The Boltzmann weights are determined by equations (E4), and vibrational band strengths are equal to $1.89S'_v(\nu_3, H_2O)$ and $1.0S'_v(\nu_3, H_2O)$ respectively for the two $\Delta v_3 = -1$ bands and $1.0S'_v(\nu_1, H_2O)$ and $1.82S'_v(\nu_1, H_2O)$ respectively for the two $\Delta v_1 = -1$ bands. Taking into account that $S'_v(\nu_1, H_2O) = 0.89S'_v(\nu_3, H_2O)$, the emission strength for $(2, v_2)$ is $0.15[1.89S'_v(\nu_3)] + 0.38[1.0S'_v(\nu_3)] + [0.089S'_v(\nu_3)] + 0.47[1.82 \times 0.089S'_v(\nu_3)] = 0.77S'_v(\nu_3) = \alpha_2 S'_v(\nu_3, H_2O)$. In the same manner, the band-strength coefficients for the $(1, v_2)$ and $(3, v_2)$ bands are calculated as $\alpha_1 = 0.44$ and $\alpha_3 = 0.93$. For a given $P_{1,3}(v_{1,3})$ distribution, the H_2O emission strength from a certain reaction at unit water concentration, $I(H_2O)$, is equal to $\sum \alpha_i P_{1,3}(i) S'_v(\nu_3, H_2O) = \beta S'_v(\nu_3, H_2O)$. On average, the H_2O emission from GeH_4 was 5.8 times stronger than that from HBr. From the distributions presented in table 3, $\beta_{\text{ref}}(H_2O) = 0.54$(HBr) and $\beta(H_2O) = 0.39(GeH_4)$ and $k_3/k_1 = 8.0 \pm 0.9$. Taking $k_1 = 1.1 \times 10^{-11}$ gives $k_3 = (8.8 \pm 1.4) \times 10^{-11}\,\text{cm}^3\,\text{molecule}^{-1}\,\text{s}^{-1}$.

The secondary kinetic-isotope effect, k_{OH}/k_{OD}, can be determined from the $P_{1,3}(v_{1,3})$ and $P_3(v_3)$ distributions for a pair of OH and OD reactions.

$$k_{OH}/k_{OD} = [I(H_2O)\beta(HOD)S'_v(\nu_3, HOD)]/[I(HOD)\beta(H_2O)S'_v(\nu_3, H_2O)]. \tag{E7}$$

$I(H_2O)$ and $I(HOD)$ are the integrated emission intensities from the OH and OD reactions measured at the same [HR]. For such experiments, the H_2 flow is substituted by an equivalent D_2 flow, and the assumption is made that [OH] = [OD]. The procedure is similar to that in the paragraph above, but the band-sum intensity ratio for the H_2O and HOD bands, $S'_v(\nu_3, H_2O)/S'_v(\nu_3, HOD) = 0.76$, must be included. The normalized HOD emission strength is equal to $\sum \alpha_i P_3(i) S'_v(\nu_3, HOD) = \beta S'_v(\nu_3, HOD)$. The band-strength coefficients α_{ν_3} for $(v_{1,2}, v_3)$ bands in the 3200–3900 cm^{-1} range were calculated as $[\nu(v_3)/\nu(1)]^3 v_3 S'_v(v_3)$, where $\nu(\nu_3)$ is the centre of the $(00v_3)$–$(00v_3 - 1)$ band; this gives $\alpha_1 = 1.0$, $\alpha_2 - 1.75$ and $\alpha_3 = 2.28$. The intensity ratios $I(H_2O)/I(HOD) = 0.43 \pm 0.05$, 0.49 ± 0.10 and 0.52 ± 0.04 from experiments with HBr (re-evaluated data), HI and GeH_4 [15] respectively give $k_{OH}/k_{OD} = 1.2 \pm 0.2$, 1.1 ± 0.2 and 1.4 ± 0.1. Similar experiments gave $k_{OH}/k_{OD} = 1.1 \pm 0.3$ and 1.0 ± 0.2 for cyclohex-

ane and *n*-butane respectively [16]. Most direct measurements, as well as most transition-state models, report small inverse kinetic-isotope effects for OH vs. OD hydrogen atom abstraction reactions. Given the experimental assumption that [OH] = [OD] and the sensitivity of the calculations to the $v_{1,3} = 0$ and $v_3 = 0$ populations and to the $\alpha(v_3)$ and $\alpha(v_{1,3})$ terms, the reasonable values for k_{OH}/k_{OD} are regarded as support for the simulation model, rather than as measurements of kinetic-isotope effects.

Integrated emission intensities can be used to determine branching ratios of multichannel reactions, if deuterium-labelled reagents are used. For example, consider the reactions with 2-butanone. The reactions of OD with 2-butanone-1,1,1,3,3-d_5 give different products depending on the site of attack:

$$OD + CH_3C(O)CH_2CH_3 \rightarrow HOD + CH_3C(O)CHCH_3 \qquad (22Da)$$

$$\rightarrow HOD + CH_3C(O)CH_2CH_2 \qquad (22Db)$$

$$OD + CD_3C(O)CD_2CH_3 \rightarrow D_2O + CD_3C(O)CDCH_3 \qquad (22'Da)$$

$$\rightarrow HOD + CD_3C(O)CD_2CH_2 \qquad (22'Db)$$

The emission spectra shown in figure 5, which were measured at 0.6 Torr, display comparable emission intensities in the 2400–3000 and 3200–3900 cm^{-1} ranges for

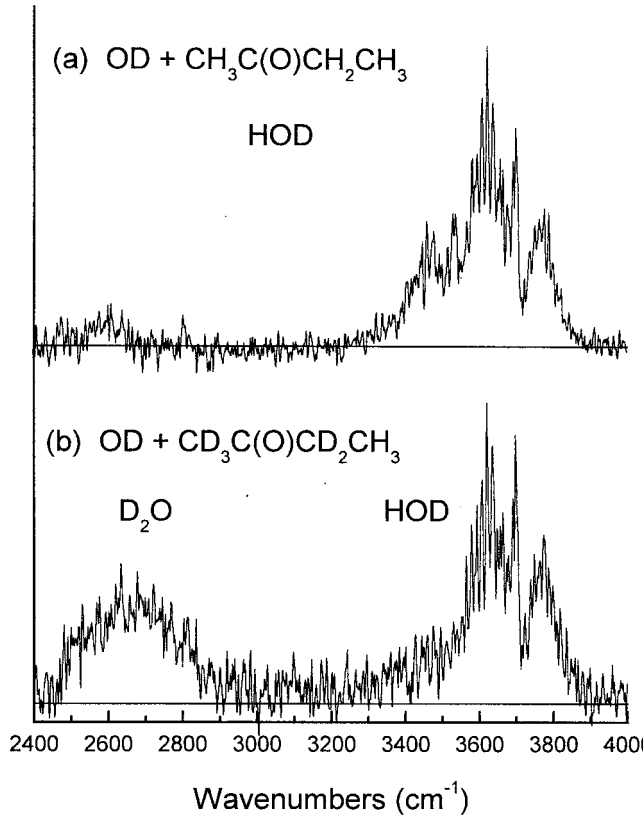

Figure 5. Chemiluminescenct spectra from (*a*) the OD + 2-butanone reaction and (*b*) the OD + 2-butanone-d_5 reaction.

reactions (22), and both (*a*) and (*b*) channels are important (abstraction from the α-CH_3 group is negligible). The branching ratio was determined by comparison of the intensity, I_{D_2O}, of D_2O from channel (*a*) in the 2400–3000 cm^{-1} range and the intensity, I_{HOD}, of HOD from channel (*b*) in the 3200–3900 cm^{-1} range. The intensity ratio, $I_{D_2O}/I_{HOD} = 0.37 \pm 0.06$, was converted to the ratio of HOD to D_2O yields, using

$$\frac{[HOD]}{[D_2O]} = \frac{I_{HOD}\beta(D_2O)S'_v(\nu_3, D_2O)}{I_{D_2O}\beta(HOD)S'_v(\nu_3, HOD)}. \tag{E8}$$

The $\beta(D_2O) = \sum_i \alpha_i P_{1,3}(v_i)$ coefficient is defined in the same way as for H_2O, and $\beta(HOD) = \sum_i \alpha_i P_3(v_i)$ was defined above. The estimation of the band strength for D_2O was made using equation (E5) and the relation $S'_v(\nu_1)/S'_v(\nu_3) = 0.134$; the equilibrated $(1, v_2)$, $(2, v_2)$, $(3, v_2)$ and $(4, v_2)$ band strengths are 0.45, 0.82, 1.11 and 1.27 respectively. The $P_{1,3}(1\text{–}3)$ distributions are 49 : 34 : 17 for D_2O and $P_3(1:2) = 90:10$ for HOD. The surprisal analysis with $\langle E_{av}\rangle = 27.2$ and 23.1 kcal mol^{-1} (before adjustment for zero-point energies) for reactions (22′D *a*) and (22′D *b*) respectively gave $P_{1,3}(0) = 14$ and $P_3(0) = 51$ and the renormalized full distributions are $P_{1,3}(0\text{–}3) = 14:41:30:14$ for D_2O and $P_3(0\text{–}2) = 51:44:5$ for HOD. We now can calculate $\beta_{D_2O} = 0.45 \times 0.41 + 0.82 \times 0.30 + 1.11 \times 0.14 = 0.59$ and $\beta_{HOD} = 1.0 \times 0.44 + 1.75 \times 0.05 = 0.53$. Taking into account that the relative emission efficiency, $S'_v(HOD, \nu_3)/S'_v(D_2O, \nu_3) = 4.47$ (table 1), the branching ratio is $k_a/k_b = 1.5 \pm 0.3$ for reaction (22′D). In this example, the large $P_3(0)$ value for the HOD distribution introduces uncertainty into the branching ratio; nevertheless, these data serve to illustrate the method.

3.3. *Information-theoretic analysis*

The information theory developed by Levine and Bernstein [33, 44] compares the experimental distribution of the products, $P(v)$, with the prior distribution, $P^0(v)$, calculated with the assumption of equal probability for all energetically allowed quantum states of the products with energy E. The surprisal of the vibrational distribution is defined by

$$I(v) = -ln[P(v)/P^0(v)]. \tag{E9}$$

For an atom plus diatonic product, $P^0(v)$ is calculated [33] from

$$P^0(v) = \sum_0^{J(v)^*} P^0(v, J), \tag{E10}$$

where $J^*(v)$ is the highest allowed rotational level for the vibrational level v, and $P^0(v, J)$ is given by the following, where the internal energy of the product is $E_I = E_{vibr} + E_{rot}$ and v^* is the highest accessible vibrational level:

$$P^0(v, J) = \frac{(2J+1)(E - E_I)^{1/2}}{\sum_0^{v^*}\sum_0^{J^*(v)}(2J+1)(E-E_I)^{1/2}}. \tag{E11}$$

To extend the formalism to a reaction giving an asymmetric top molecule plus an atom as products, with vibrational and rotational states described by v_1, v_2, v_3 and J, K_a, K_c, the prior in equation (E10) is replaced by $P^0(v_1, v_2, v_3, J)$, which needs summation over $2J \pm 1$ sublevels owing to the asymmetry splitting. The summation over rotational levels could be done either explicitly, using conventional equations

for an asymmetric top, or by substitution of summation by integration, which gives a simpler expression. The difference between numerical summation and integration for $J < 60$ was insignificant [12], and the following has been used for the prior:

$$P^0(v_1, v_2, v_3) = (E - E_{\text{vib}})^2 \Big/ \sum_0^{v3^*} \sum_0^{v1^*} \sum_0^{v2^*} (E - E_{\text{vib}}). \tag{E-12}$$

For H_2O, the vibrational states are represented by two quantum numbers $v_{1,3}$ and v_2, and equation (14) takes the form

$$P^0(v_{1,3}, v_2) = \sum_{n=0}^{v_{1,3}} P^0(v_1 + n, v_2, v_3 - n) \tag{E-13}$$

and the prior for the stretching vibrations is defined as

$$P^0(v_{1,3}) = \sum_0^{v_2^*} P^0(v_{1,3}, v_2) \tag{E-14}$$

where v_2^* is the highest bending vibration allowed for a given $v_{1,3}$ stretching vibrational state.

The experimental and prior distributions plus the surprisal plots for $P_{1,3}(v_{1,3})$ for the OH + HBr and HI reactions are presented in figure 6. Surprisal plots show $I(v_{1,3})$ vs.$f_{v_{1,3}}$, where $f_{v_{1,3}} = E_v(v_{1,3}, v_2 = 0)/\langle E_{\text{av}} \rangle$; with $E_v(v_{1,3}) = \sum_{n=0}^{v_{1,3}} k_n E_v(v_1 + n, 0, v_3 - n)$, where k_n is the Boltzmann coefficient from equation (E4). The surprisal analysis of D_2O follows the scheme developed for H_2O. The vibrational surprisal plots

$$-I(f_{v_{1,3}}) = \lambda_{1,3}^0 + \lambda_{1,3} f_{v_{1,3}} \tag{E15}$$

are linear, and the intercepts provide estimates for the $P_{1,3}(v_{1,3} = 0)$ components of the distributions.

The ν_1 (O–D stretching) populations of HOD are coupled with the populations in the ν_2 (bending) levels, and the two vibrational degress of freedom are ν_3 and $\nu_{1,2}$. The prior for the equilibrated vibrational states of HOD is defined as

$$P^0(v_{1,2}, v_3) = \sum_{n=0}^{n^*} P^0(v_1 + n, v_2 - 2n, v_3) \tag{E-16}$$

where n^* is the highest n number allowed for a given $c_{1,2}$ vibrational state. The prior distribution for ν_3 can be calculated from the following, where $v_{1,2}^*$ is the highest allowed level for a given v_3 state:

$$P^0(v_3) = \sum_0^{v_{1,2}^*} P^0(v_{1,2}, v_3). \tag{E-17}$$

The experimental and statistical distributions plus the surprisal plots for the OD + HBr and HI reactions are compared in figure 7. The surprisal plots are linear, and the intercepts give estimates for the relative population of $v_3 = 0$:

$$-I(f_{v_3}) = \lambda_3^0 + \lambda_{v_3} f_{v_3}. \tag{E-18}$$

For ideal data the difference between this $P_3(0)$ value and the one assigned from the spectrum provide an estimate for the population of the 'dark' (000) and (010) vibrational levels.

The slopes of the surprisal plots measure the difference between the experimental distribution and the prior (statistical) distribution. The large negative λ_{v_3} and $\lambda_{v_{1,3}}$

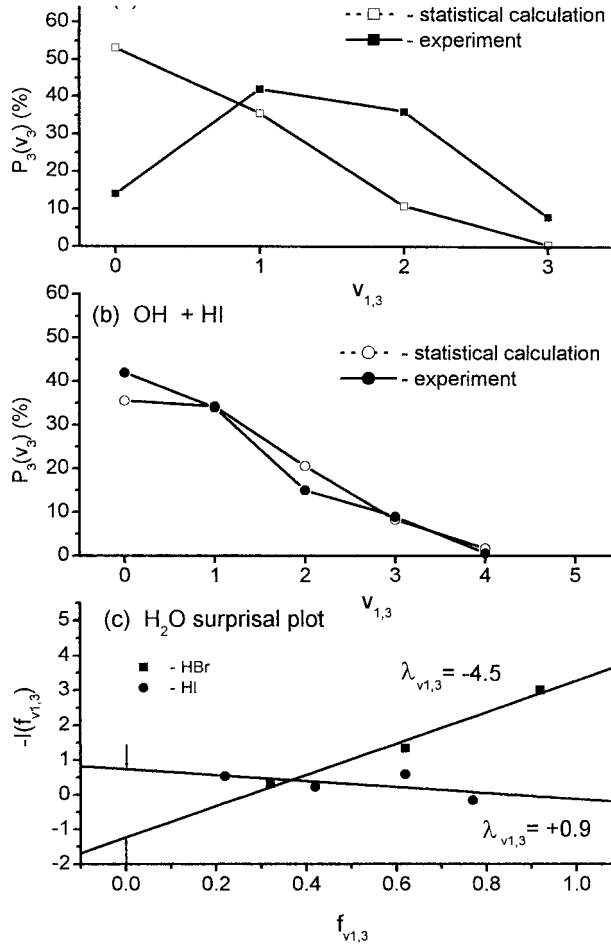

Figure 6. Comparison of the observed $P_{1,3}(v_{1,3})$ distribution for H_2O (full symbols) and the prior distribution (open symbols) from (*a*) the OH + HBr reaction and (*b*) the OH + HI reaction; (*c*) surprisal plot for the $P_{1,3}(v_{1,3})$ distribution vs. $f_{v_{1,3}}$ for HBr (squares) and HI (circles); the $P_{1,3}(0)$ values were obtained from the linear extrapolations indicated by the arrows.

values for the direct abstraction reactions reinforce the $\langle f_{v_3} \rangle$ value as a gauge of the energy distributions in the stretching modes. For the HBr reaction, the $\lambda_{v_3} = -6.1$ value for HOD is substantially higher than the slope of the surprisal for the H_2O distribution, $\lambda_{v_{1,3}} = -4.5$; this difference is largely a consequence of the different statistics for the two priors. The bending distributions of H_2O also have been treated by surprisal analysis. Although the $P(v_2)$ distributions from HBr, HI and GeH_4 give linear surprisals, the slopes are nearly zero, i.e. the bending distributions are close to the statistical limits (see table 3).

4. Results

4.1. *Reactions with inorganic compounds*

4.1.1. *Highly exothermic reactions: HBr, DBr, H_2S, HI and GeH_4*

Reactions of OH($^2\Pi$) radicals with HBr, HI and GeH_4 proceed without potential energy barriers [71, 72], and the barrier for H_2S is very small; see table 2. The

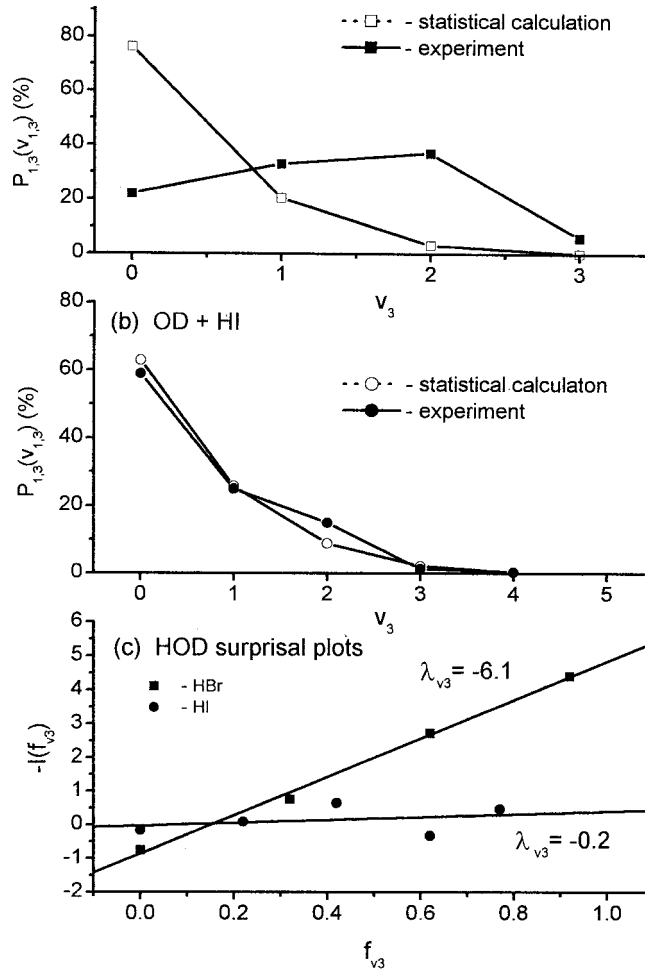

Figure 7. Comparison of the observed $P_3(v_3)$ distribution for HOD (full symbols) and the prior distribution (open symbols) from (*a*) the OD + HBr reaction and (*b*) the OD + HI reaction; (*c*) surprisal plot for the $P_3(v_3)$ distribution vs. f_{v_3} for HBr (squares) and HI (circles); the $P_3(0)$ values obtained from the intercepts can be compared with the values from simulation (see text).

formation of $Br^*(^2P_{1/2})$ and $I^*(^2P_{1/2})$ atoms, either in the primary reaction or as a result of V–E energy transfer, can be neglected [12, 15]. This series provides examples ranging from direct abstraction, HBr and H_2S, to more complicated mechanisms, HI and GeH_4, as identified from the vibrational distributions. A complete description, see table 3, will be given for these reactions; more abbreviated presentations will be made for the other reactions. The method for establishing the $P_{1,3}(0)$ and $P_3(0)$ components of the distributions and the utilization of $P_{1,3}(v_{1,3})$ and $P_3(v_3)$ to obtain the energy deposited in the bending and stretching modes of water are especially important points. The current interpretations of these reactions are virutally unchanged from the published work [15, 17].

HBr and DBr. The vibrational distributions of the H_2O, HOD and D_2O molecules from the following reaction are prototypical for direct abstraction:

Table 2. Thermodynamic and kinetic data for the $OH + HR \rightarrow H_2O + R$ reactions.

Reagent	k (298 K) (cm^3 molecule^{-1} s^{-1})	E_a (kcal mol^{-1})	Reference	D_0(H—R) (kcal mol^{-1})	Reference	$-\Delta H_0^{o\,a}$ (kcal mol^{-1})	$\langle E_{av} \rangle^b$
1. HBr	1.1×10^{-11}	0.0 ± 0.4	[26]	86.6 ± 0.1	[73]	31.5	33.6
2. H_2S	4.8×10^{-12}	0.16–0.82	[26]	89.9 ± 0.7	[73]	28.2	32.1[b]
3. HI	3.0×10^{-11}	0	[26]	70.4 ± 0.1	[73]	47.7	49.8
4. GeH_4	8.8×10^{-11}	0[c]	[15]	82 ± 2	[73]	36.0	38.4
5. HCl	7.9×10^{-13}	0.7 ± 0.2	[26]	102.2 ± 0.1	[73]	15.9	18.7
6. NH_3	1.6×10^{-13}	1.8 ± 0.4	[26]	106.7 ± 0.3	[73]	11.4	15.6
7. C_2H_6	2.6×10^{-13}	2.14 ± 0.20	[25]	99.5 ± 0.5	[73]	18.6	23.1
8. neo-C_5H_{12}	8.5×10^{-13}	1.54 ± 0.20	[25]	99.6 ± 1.4	[74]	18.5	22.4
9. cyclo-C_5H_{10}	5.1×10^{-12}	0.56 ± 0.14	[25]	96.0 ± 1.0	[75, 76]	22.1	25.1
10. cyclo-C_6H_{12}	7.5×10^{-12}	0.69 ± 0.16	[25]	96.6 ± 1.0	[75, 76]	21.5	24.6
11. n-C_4H_{10}	2.5×10^{-12}	0.88 ± 0.20	[25]	96.7 ± 0.5	[73, 77]	21.4	24.7
12. n-$C_{10}H_{22}$	1.2×10^{-11}		[25]			21.4[e]	24.7
13. iso-C_4H_{10}	2.3×10^{-12}	0.55 ± 0.20	[25]	95.0 ± 0.6	[73, 77]	23.1	25.5[b]
14. 2,2,4-Trimethylpentane	3.6×10^{-12}	0.88 ± 0.16	[25]	97.0 ± 0.6	[78]	21.1	23.5[b]
15. CH_3OH	9.4×10^{-13}	0.83 ± 0.07	[26]	94.5 ± 0.2	[73]	23.6	26.8
16. C_2H_5OH	3.5×10^{-12}	0.47 ± 0.20	[26]	93.6 ± 1	[74]	24.5	27.4
17. CH_3OCH_3	2.8×10^{-12}	0.52 ± 0.07	[79, 80]	93.8 ± 1	[81]	24.5	27.2
18. $C_2H_5OC_2H_5$	1.4×10^{-11}	-0.40 ± 0.05	[79, 82]	92.3 ± 1	[83]	25.8	28.2
19. $CH_3OCH_2OCH_3$	4.6×10^{-12}	≈ -0.8	[84]			24.5[f]	26.9

20. $CH_3OC_2H_4OH$	1.1×10^{-11}	≈ -1.3	[84]			25.8[g]	28.2
21. $CH_3C(O)CH_3$	1.8×10^{-13}	1.1 ± 0.1	[85]	98.9 ± 1.8	[74]	19.3	22.7
22. $CH_3C(O)C_2H_5$	1.2×10^{-12}	-0.2 ± 0.2	[85]	93.0 ± 1.4	[74]	25.2	27.7
23. $C_2H_5C(O)C_2H_5$	2.1×10^{-12}	0.0 ± 0.2	[86, 87]			25.2[h]	27.7
24. $CH_3C(O)C_3H_7$	4.9×10^{-12}		[86]			25.2[h]	27.7
25. HC(O)H	9.4×10^{-12}	-0.5 ± 0.30	[26]	87.3 ± 0.1	[73, 88]	30.8	33.2
26. $CH_3C(O)H$	1.6×10^{-11}	-0.51 ± 0.15	[26]	87.9 ± 0.3	[73]	30.2	32.6
27. CH_3SCH_3	4.4×10^{-12}	0.47 ± 0.10	[26, 89]	92.0 ± 1.4	[90]	26.1	28.9
28. $C_2H_5SC_2H_5$	1.5×10^{-11}	0.0 ± 0.4	[24]	≈ 90.0	[91]	28.1	30.5
29. CH_3SH	3.3×10^{-11}	-0.8 ± 0.3	[26]	86.1 ± 0.5	[73]	32.0	34.4
30. C_2H_5SH	4.3×10^{-11}	-0.8 ± 0.2	[24]			32.0[i]	34.4

[a] ΔH_0^0 was calculated from bond energies; $D_0(\text{H–R}) - D_0(\text{H–OH})$ with $D_0(\text{H–OH}) = 118.1\,\text{kcal mol}^{-1}$. For reactions with multiple pathways, the listed ΔH_0^0 is for the most exoergic path. If only $D_{298}(\text{H–R})$ was available, conversion to 0 K was made using Kirchoff's equation, which gives $D_0(\text{H–R}) = D_{298}(\text{H–R}) - 1.5\,\text{kcal mol}^{-1}$ from the assumption that the heat capacity of R is identical with RH.

[b] $\langle E_{\text{av}} \rangle = -\Delta H_0^0 + E_a + nRT$ ($n = 3.5$ for HCl, HBr, HI and 4.0 for other HR). For some $\langle E_{\text{av}} \rangle$, the listed value may be for the upper/lower limit of ΔH_0^0 and E_a, e.g. H_2S. E_a was taken as 0.0 for abstraction from tertiary C–H bonds.

[c] Implied from comparison with $OH + CH_4$ and $OH + SiH_4$ reactions with $E_a = 3.8$ and $0.095\,\text{kcal mol}^{-1}$ [15] respectively.

[d] Corrected for the activation energy of R + HI or HBr reactions (see Berkowitz *et al.* [73] and the text).

[e] Assumed to be similar to reagent 11.

[f] Assumed to be similar to reagent 17.

[g] Assumed to be similar to reagent 18.

[h] Assumed to be similar to reagent 22.

[i] Assumed to be similar to reagent 29.

$$OH + HBr \rightarrow H_2O + Br \quad (1)$$

$$OD + HBr \rightarrow HOD + Br \quad (1D)$$

$$OH + DBr \rightarrow HOD + Br \quad (1')$$

$$OD + DBr \rightarrow D_2O + Br. \quad (1'D)$$

The thermochemistry with zero-point energies (13.2, 11.5 and 9.7 for H_2O, HOD and D_2O, 5.3 and 3.9 for OH and OD and 3.8 and 2.7 kcal mol^{-1} for HBr and DBr respectively) gives $\langle E_{av} \rangle = 33.6$, 33.9, 34.1 and 34.6 kcal mol^{-1} for reactions (21). Excitation of up to the third O–H stretching or the fourth O–D stretching levels is possible. The emission from reactions (21*a*) and (21*b*) is strong (see figure 1) and data were collected for the best experimental conditions. The emission from reactions (1′) and (1′D) is weaker than from reactions (1) and (1D), because of the kinetic-isotope effect, $k_1/k_{1'} = 1.9$ [72, 92], and the lower Einstein coefficients for D_2O emission.

The distributions for reactions (21*a*) and (21*b*) were $P_{1,3}(1\text{–}3) = 49 : 41 : 10$ and $P_3(1\text{–}3) = 43 : 49 : 8$ from simulation of the 3200–3900 cm^{-1} bands. The highest v_2 energy for each stretching level is close to the thermochemical limit. The linear surprisal plot ($\lambda_{v_{1,3}} = -4.5 \pm 0.3$; $\lambda^0_{1,3} = -1.25 \pm 0.21$, with error limits from the standard deviation of the plot in figure 6 (*c*)) gives $P_{1,3}(0) = 14 \pm 2$, and the overall distribution for H_2O is $P_{1,3}(0\text{–}3) = 14 : 42 : 36 : 8$; the bending distribution in $v_3 = 0$ was assumed to follow the distribution in $v_3 = 1$ (see table 3). The full HOD vibrational distribution in table 3, $P_3(0\text{–}3) = 22 : 34 : 38 : 6$, was obtained in the following way. The linear surprisal plot ($\lambda_{v_3} = -6.1 \pm 0.1$) shown in figure 7 (*c*) gave $\lambda^0_3 = -1.05 \pm 0.10$ and $P_3(0) = 22 \pm 2$. The $P_3(0) = 17 \pm 3$ value from simulation of the 2400–3000 cm^{-1} part of the spectrum does not include $P_3(0,0)$ and $P_3(1,0)$, which were estimated as the difference between $P_3(0) = 22$ from the surprisal plot and $P_3(0) = 17$ from simulation. The mean fractions of vibrational energy for H_2O and HOD are $\langle f_v \rangle = 0.62$ and 0.60 respectively. Since the ν_3 and ν_2 modes are isolated in HOD and H_2O respectively, the energy released to the OH bond (stretch excitation) and to the bending mode can be calculated: $\langle f_{v_3} \rangle = 0.62$ and $\langle f_{v_2} \rangle = 0.31$. The overall bending distribution is only slightly inverted with the inversion more pronounced in the $v_{1,3} = 1$ level (and presumably $v_{1,3} = 0$).

The 3400–3800 cm^{-1} HOD emission spectrum in figure 1 (*c*) from reaction (1′), which is clearly different from that of reaction (1D), is mainly from $v_3 = 1$ with a broad distribution in $v_{1,2}$ (up to $v_{1,2} = 8$ in $v_3 = 0$ and $v_{1,2} = 7$ in $v_3 = 1$). The distributions, which are not given in table 3, are $P_3(0\text{–}3) = 34 : 54 : 10 : 1$ and $P_{1,2}(0\text{–}8) = 13 : 16 : 22 : 15 : 16 : 5 : 7 : 2 : 3$; the latter contradicts the expectation of a preferential release of energy into the new O–D bond, since 80% of the molecules are in $v_1 = 0$ and 1 states. An explanation [12] for the apparent over-population of $v_3 = 1$ is collisional transfer from $v_3 = 0$ with high $v_{1,2} \geq 7$ excitation to $v_3 = 1$ levels with reduction of the $v_{1,2}$ quantum number by 3. The observed $\langle f_v(\text{HOD}) \rangle$ of 0.51 with a 3:2 ratio between the $v_{1,2}$ mode and the v_3 mode is a lower limit to the true $\langle f_v(\text{HOD}) \rangle$, and the distribution between the $v_{1,2}$ and v_3 sets of levels probably has been distorted by relaxation. This relaxation is more serious for HOD from reaction (1′) than from reaction (1D), because in the latter case a large fraction of the energy initially is in the more isolated $\nu_3 = 2$ level.

Table 3. Vibrational distributions from reactions with inorganic compounds.[a]

	H_2O											HOD											
Reagent	$v^e_{1,3}$	$v_2=0$	1	2	3	4	5	≥ 6	$P_{1,3}$[b]	$P_{1,3}$[c]	$P^0_{1,3}$[d]	v_3	$v^e_{1,2}=0$	1	2	3	4	5	6	≥ 7	P_3[b]	P_3[c]	P_3[e]	P^0_3[d]
1. HBr	0	2.2	3.3	2.6	2.0	1.1	0.9	1.7	—	14	53.1	0	3.0	2.8	3.6	5.9	2.1	3.4	1.0	0.4	—	22	22 ± 3	76.2
	1	7.7	11.4	9.0	7.2	3.9	3.0		49	42	35.5	1	7.1	6.1	6.5	5.1	4.2	2.7	1.8	0.8	43	34	34	20.5
	2	14.6	15.3	3.4	2.5				41	36	10.9	2	12.7	9.9	7.2	5.0	2.3	0.8			49	38	38	3.2
	3	5.6	2.7						10	8	0.5	3	2.9	2.8	0.1						8	6	6	0.1
	P_2	30.1	32.7	15.0	11.7	5.0	3.9	1.7				$P_{1,2}$	25.7	21.6	17.4	16.0	8.6	7.0	2.8	1.2				
	P^0_2[d]	41.4	26.2	15.8	8.9	4.6	2.1	1.0				$P^0_{1,2}$[d]	22.3	15.8	21.4	13.7	12.9	7.0	4.7	2.2				
2. H_2S	0	3.0	5.2	4.1	1.9	1.0	0.6	1.2	—	17	55.9	0	6.6	1.1	6.6	1.1	1.9	1.1	1.6	0.8	—	23	21 ± 4	77.0
	1	9.8	13.5	11.2	6.6	1.8			52	43	34.6	1	10.4	6.4	10.0	3.5	4.5	1.1			45	35	36	20.0
	2	18.8	15.9	2.3					44	37	9.4	2	19.4	9.4	9.4	3.0					52	40	41	2.9
	3	3.2							4	3	0.1	3	2.0								3	2	2	0.05
	P_2	34.8	34.6	17.6	8.5	2.8	0.6	1.2				$P_{1,2}$	38.4	16.9	26.0	7.6	6.4	2.2	1.6	0.8				
	P^0_2[d]	44.8	26.6	14.9	7.9	3.8	1.6	0.5				$P^0_{1,2}$[d]	24.8	17.1	22.4	13.7	11.6	5.9	3.4	0.9				
3. HI	0	7.9	7.6	7.9	8.2	4.7	1.9	3.8	—	41	35.3	0	6.1	5.0	8.2	4.8	4.6	6.0	5.3	14.0	—	59	54 ± 4	62.9
	1	6.8	6.6	6.8	7.1	4.0	1.6	0.9	58	34	34.2	1	4.2	3.9	3.5	1.8	4.4	5.7	3.2	0.7	60	25	27.4	25.8
	2	6.5	4.8	1.2	1.8	0.3	0.1		25	15	20.6	2	3.1	3.9	1.0	3.4	2.5	3.0			36	15	16.5	8.9
	3	2.6	2.6	2.3	1.2				15	9	8.3	3	0.6	0.6	0.4						3.4	1.4	1.6	2.2
	4	0.6	0.2						1.4	1	1.7	4	0.4	0.1							1.1	0.4	0.5	0.3
	P_2	24.4	21.8	18.2	18.3	9.0	3.6	4.7				$P_{1,2}$	14.4	13.5	13.1	10.0	11.5	14.7	8.5	14.7				
	P^0_2[d]	31.9	22.9	16.2	11.1	7.2	4.6	5.9				$P^0_{1,2}$[d]	13.1	10.3	15.8	11.9	13.4	9.6	9.1	16.8				

4. GeH_4	0	6.1	7.1	6.5	7.6	2.2	1.6	2.0	—	33	47.0	0	6.9	5.3	8.4	8.5	4.4	5.5	2.6	2.6	—	41	44 ± 2	72.0
	1	7.8	9.1	8.5	9.7	2.9	1.9	0.5	60	40	36.0	1	5.7	5.2	6.2	2.8	1.1	2.2	3.1	2.8	52	31	29	22.7
	2	7.9	7.1	2.9	2.9				31	21	14.6	2	6.9	5.3	2.8	2.1	3.4	2.6			41	24	23	4.9
	3	3.3	2.5	0.2					9	6	2.3	3	1.9	1.8							7	4	4	0.5
	P_2	25.1	25.8	18.1	20.2	5.1	3.5	2.5				$P_{1,2}$	21.4	17.6	17.4	13.4	8.9	10.3	5.7	5.4				
	P_2^0 [d]	38.5	25.0	16.0	9.8	5.6	3.0	2.2				$P_{1,2}^0$ [d]	18.9	13.7	19.7	13.6	13.5	8.4	6.5	5.7				
5. HCl[h]	No H_2O emission was observed											0	14	9	8	2					—	33[h]	ws[g]	
												1	49	18							100	67		
												$P_{1,2}$	63	27	8	2								
6. NH_3[h]	0	19	10	3					—	32[h]	89.3	0	14	9	10	3					—	36[h]	ws[g]	95.1
	1	51	17						100	68	10.7	1	52	12							100	64[h]		4.9
	P_2	70	27	3								$P_{1,2}$	66	21	10	3								

[a] Except for the NH_3 results, which are new, the results in this table are based on spectra acquired in previously published work [10, 12, 15]; however, the HBr and H_2S spectra have been refitted with the improved simulation model.
[b] Population in v_3 or $v_{1,3} = 0$ is neglected.
[c] $P_v(0)$ determined from extrapolation of linear surprisal plots; the least-squares uncertainty is generally $\pm$ 10–15%.
[d] Statistical prior distribution.
[e] $P_3(0)$ determined from fitting the HOD spectra in the 2500–2900 cm^{-1} region; the uncertainty is from fitting several spectra. The $v_{1,2} = 0$ and 1 states of $v_3 = 0$ are dark states and populations of these states must be estimated; see text for details of each reaction.
[f] $v_{1,3} = v_1 + v_3$, $v_{1,2}$ is the maximum value of v_2 in the group of v_1, v_2 resonant states; $v_2(H_2O) = 6$ and $v_2(HOD) = 7$ were the highest bending levels in the models for spectral simulation.
[g] ws = weak signal and analysis of the 2500–2900 cm^{-1} region was not possible.
[h] See text for the method of estimation of $P_{1,3}(0)$ and $P_3(0)$.

The stretching distribution of D_2O from reaction (1′D) is $P_{1,3}(0\text{–}4) = 14 : 37 : 26 : 19 : 5$. The vibrational levels of D_2O are populated up to energetic limit $(v_2, v_{1,3}) = (1, 4)$ and nearly to the limit for (3,3) and (5,2). The vibrational distribution for reaction (1′D) gives $\langle f_v(D_2O)\rangle = 0.58$ with a bending excitation that is nearly the same as reaction (1).

The results from reactions (1) provided evidence that our spectral simulation model was satisfactory [12] and that the vibrational excitation of water was $\langle f_v\rangle = 0.61$ with $\langle E_{v_2}\rangle/\langle E_{v_3}\rangle \approx 0.50$. Since the distributions from the reactions with DBr provided little new information and since the spectra were more difficult to acquire and simulate, the OH and OD reactions with DR reagents, henceforth, were studied only for cases in which product branching was studied. One reservation is the low $v_2 = 1$ population for $v_3 = 1$ and 2 levels of HOD relative to the $v_{1,3} = 1$ and 2 levels of H_2O, which seems to exist for most reactions; this difference probably is a defect of the simulation procedure. To the extent that our assignment of the bending distribution to $P_{1,3}(0)$ underestimates the excitation, the $\langle f_2\rangle$ values may be lower limits.

H_2S. The chemiluminescent spectra from the reactions

$$\mathrm{OH\,(OD)} + \mathrm{H_2S} \rightarrow \mathrm{H_2O\,(HOD)} + \mathrm{SH} \qquad (2, 2\mathrm{D})$$

were recorded for the best conditions, and the vibrational distributions are given in table 3 [17]. The H_2O distribution is $P_{1,3}(1\text{–}3) = 52 : 44 : 4$, and the bending distribution of $v_{1,3} = 1$ level has a slight inversion with the maximum population in $v_2 = 1$. The uncertainties of D_0(HS–H) and E_a, about 1.5 kcal mol^{-1} in total, are consistent with excitation of $v_{1,3} = 3$. Because of the closeness of $\langle E_{av}\rangle$ to energy of $v_{1,3} = 3$, the $P_{1,3}(3)$ point was not included in a conventional surprisal analysis. Solving the inverse problem, we found that $\langle E_{av}\rangle = 32.1$ kcal mol^{-1} satisfied a linear surprisal plot, $-\lambda_{v_{1,3}} = 3.9 \pm 0.4$, $\lambda^0_{1,3} = -1.0 \pm 0.03$ for the three $v_{1,3}$ points and gives $P_{1,3}(0\text{–}3) = 17 \pm 4 : 43 : 37 : 3$. From this value for $\langle E_{av}\rangle$ and the upper limit $\Delta H^o_0 = -28.9$ kcal mol^{-1}, an activation energy of $E_a = 0.8$ kcal mol^{-1} can be deduced. Although this value exceeds the currently recommended $E_a = 0.16$ kcal mol^{-1} [26], it lies in the upper range of reported $E_a = 0.79 \pm 0.38$ kcal mol^{-1} values [93, 94].

The HOD distribution slightly favours $v_3 = 2$, with $P_3(0\text{–}3) = 21 : 36 : 41 : 2$. $P_3(0)$ was obtained from the spectral simulation and assuming that populations in (0,0) and (1,0) were equal to those of the (2,0) and (3,0) states. The surprisal plot for $OD + H_2S$ is linear with a slope of $-\lambda_{v_3} = 5.5 \pm 0.4$; the intercept, $\lambda^0_3 = -0.95 \pm 0.20$, corresponds to $P_{1,3}(0\text{–}3) = 23 \pm 3 : 35 : 40 : 2$, which agrees with the experimentally determined $P_3(0) = 21$.

Both H_2O and HOD distributions correspond to $\langle f_v\rangle = 0.57$ and the $\langle E_{v_2}\rangle/\langle E_{v_3}\rangle$ ratio is 0.40. The energy disposal for the H_2S reaction closely resembles that from HBr. However, the $-\lambda_{v_{1,3}}$ values, 3.9 vs. 4.5, the $-\lambda_{v_3}$ values, 5.5 vs. 6.1, and $\langle E_{v_2}\rangle/\langle E_{v_3}\rangle = 0.40$ vs. 0.50 show that the energy released to the new bond has a slightly broader distribution with somewhat less bending excitation for H_2S than for HBr. Surprisal plots, calculated using a prior that included two rotational degrees of freedom of HS (model II), are linear but steeper than for model I. However, $P_3(0) = 18$ from the intercept of the model II plot is in poorer agreement with the experimental value than $P_3(0)$ from model I, suggesting that HS can be considered as a single body. The $OH + H_2S$ reaction seems to resemble the $F + H_2S$ reaction [95] for which little energy is released to the SH fragment. The energy disposal pattern for

reaction (22) also is in accord with *ab initio* calculations [96], which found a transition state in the entrance channel for direct abstraction. The weak hydrogen-bonded [96] adducts, $H_2S{\cdot}HO$ and $SH{\cdot}OH_2$, seem to have no apparent effect on the energy disposal. The HBr and H_2S distributions can be taken as representative for direct abstraction. Since $\langle f_{v_3}\rangle + \langle f_{v_2}\rangle \simeq 1.0$, the old bond must receive very little energy in these reactions.

HI and GeH₄. The intense emission in the 2200–3000 cm^{-1} range allowed the $P_3(0)$ contributions to be evaluated with confidence for the HI and GeH_4 reactions:

$$OH\,(OD) + HI \rightarrow H_2O\,(HOD) + I \qquad (3, 3D)$$

$$OH\,(OD) + GeH_4 \rightarrow H_2O\,(HOD) + GeH_3. \qquad (4, 4D)$$

The distributions decline with increasing $v_{1,3}$ for both reactions, but the range of v_2 extends to the thermochemical limit for each $v_{1,3}$ or v_3 level, except from $v_{1,3}$ or $v_3 = 1$ reactions from (3) and (3D). In spite of the available energy being higher than for the HBr or H_2S reactions, the vibrational distributions of H_2O and HOD from both HI and GeH_4 are not inverted in the stretching mode, but the bending excitation is significantly broader (see table 3) than for reactions with HBr and H_2S.

The surprisal plots, see figures 6 and 7, for the HI reactions are linear with slopes close to zero; $\lambda_{v_{1,3}} = 0.9 \pm 0.4$ and $\lambda_{v_3} = -0.2 \pm 0.5$. These values may be compared with $\lambda_{v_{1,3}} = -4.5$ and $\lambda_{v_3} = -6.1$ for the HBr reaction. The full stretching distributions for reaction (3) and (3D) are $P_{1,3}(0\text{–}4) = 41 \pm 4 : 34 : 15 : 9 : 1$ and $P_3(0\text{–}4) = 59 \pm 5 : 25 : 15 : 1.4 : 0.4$. The $P_3(0) = 59$ value from the $\lambda_3^0 = -0.90 \pm 0.4$ of the surprisal agrees with $P_3(0) = 54 \pm 4$ from the spectral simulation with the populations in the dark states assigned by analogy to the statistical limit. Comparison of the $P_2(v_2)$ distribution in table 3 with $P_2^0(v_2)$ suggests a very slight overpopulation in the $v_2 = 2$–4 levels relative to the statistical limit. The $\langle f_v\rangle$ values for the HI reaction are 0.36 (H_2O) and 0.38 (HOD). The bending contribution is $\langle f_{v_2}\rangle = 0.47$, which exceeds the statistical fraction $\langle f_{v_2}\rangle^0 = 0.41$. The energy released to the new bond is only $\langle f_{v_3}\rangle = 0.30$. The energy disposal pattern clearly shows that the dynamics for OH + HI differ from OH + HBr. The most likely explanation is that the OH radical initially attacks the I atom, the H atom of HI then migrates to the oxygen atom and H_2O is ejected; the HI reaction is not a direct process in contradistinction to the HBr and H_2S reactions.

The surprisal plots for GeH_4 reactions are also linear, but the slopes are intermediate between those of HBr and HI. Three priors were tested [15] in which GeH_3 was treated as an atom (I), a rotating symmetric top (II) and a rotating symmetric top with six vibrations (III); the surprisal plots of $P_3(v_3)$ for HOD were linear with slopes $\lambda_{v_3} = -3.5 \pm 0.3$, -5.4 ± 0.2 and -10.8 ± 0.2 respectively. The renormalized $v_3 = 0$ populations obtained from these plots are $P_3(0) = 41$, 34 and 24 respectively and the $P_3(0) = 41 \pm 2$ value of model I agrees best with the measured population, $P_3(0) = 44 \pm 2$. This suggests that GeH_3 does not receive much internal energy (as already found for SH). The slopes of the surprisal plots for H_2O are $\lambda_{v_{1,3}} = -1.5 \pm 0.1$ (model I), -3.7 ± 0.3 (model III) and -9.8 ± 0.3 (model III), and the $P_{1,3}(0)$ values from the intercepts are 33 ± 2, 24 ± 3 and 15 ± 2. The energy disposal for GeH_4 is intermediate between HBr and HI: $\langle f_v(H_2O)\rangle = 0.47$ and $\langle f_v(HOD)\rangle = 0.45$ with $\langle E_{v_2}\rangle/\langle E_{v_3}\rangle = 1.0$. The energy in the H_2O bending mode, $\langle E_{v_2}\rangle = 7.7\,kcal\,mol^{-1}$, with $\langle f_{v_2}\rangle = 0.43$, is nearly equal to the model I statistical value of $\langle f_{v_2}\rangle^0 = 0.44$. The decline in the $-\lambda_{v_3}$ values (6.1, 3.5 and 0.2) for the HBr,

GeH_4 and HI reactions clearly identifies a less specific release of energy to the new OH bond for the series.

Inspection of table 3 shows that $P_{1,3}(v_{1,3})$ and $P_3(v_3)$ are not identical and an extension of the discussion of section 3.1.2 is helpful. As a first approximation, the initial deposit of energy is to the local mode of the new bond. Since a local H_2O mode is an equal mixture of ν_1 and ν_3 normal modes, a $P_3(0)$ population obtained for the O–H mode of HOD can be related to $P_{1,3}(0)$ in H_2O. If the old O–H bond was a pure spectator and received no energy; the whole $P_{1,3}(v_{1,3})$ distribution would coincide with the $P_3(v_3)$ distribution. On the other hand, if the old bond receives some energy, the resulting $P_{1,3}(v_{1,3})$ distribution can be obtained as a product of two local distributions. In this case, $P_{1,3}(0)$ is only the fraction of $P_3(0)$ corresponding to $P_1(0)$. Suppose that the old bond receives a statistical fraction of $\langle E_{av}\rangle$. For the HBr reaction, the statistical fraction for $P^{old}_{local}(0)$ is 0.74 and, if $P^{new}_{local}(0) = P_3(HOD) = 0.23$, the combined $P_{1,3}(0) = 0.17$, which is slightly larger than the $P_{1,3}(0) = 0.14$. The statistical value for the HI reaction is $P^{old}_{local}(0) = 0.61$. Combining this with the $P_3(v_3)$ distributions from HOD, taken as $P^{new}_{local}(0)$, gives $P_{1,3}(0) = 0.36$, which is smaller than $P_{1,3}(0) = 0.42$ from table 3. For GeH_4 the statistical population is $P^{old}_{local}(0) = 0.70$, and the predicted $P_{1,3}(0) = 0.29$ is again smaller than the $P_{1,3}(0) = 0.33$. The argument above explains why $P_3(0) > P_{1,3}(0)$ for the reactions of table 3 and suggests that the old OH bond is more involved in the dynamics for HI and GeH_4 than for HBr. This also is evident from comparing the sum of $\langle f_{v_2}\rangle$ and $\langle f_{v_3}\rangle$, which is 0.77 and 0.90 for HI and GeH_4 respectively.

4.1.2. *Moderately exothermic reactions: HCl, DCl and NH_3*

HCl. These reactions are less exoergic than the HBr reaction, and excitation of just the first stretching level is possible. The HCl and NH_3 reactions have small activation energy barriers, and the rate constants are 14 and 70 times smaller than for HBr. These reactions were studied at elevated reactant concentrations, and longer Δt (≈ 0.35 ms), the the possibility of vibrational relaxation and energy transfer must be considered. Spectra in the 2500–3900 cm^{-1} range from reactions (25) and in the 3200–4000 cm^{-1} range for reactions (26) are shown in figure 8:

$$OH\,(OD) + HCl \rightarrow H_2O\,(HOD) + Cl \qquad (5, 5D)$$

$$OH\,(OD) + DCl \rightarrow HDO\,(D_2O) + Cl. \qquad (5', 5'D)$$

The most striking feature is the absence of H_2O chemiluminescence from reaction (5), whereas the HOD emission intensities are comparable with those from the OD reactions with hydrocarbons. The 3200–3900 cm^{-1} chemiluminescence from reaction (5*b*) is predominantly the ν_3 fundamental band of HOD; however, a 27% contribution from (011) also was required. Emission from the ν_1 and $2\nu_2$ modes of HOD in the 2600–3000 cm^{-1} range could not be observed because this region was always overlapped by relatively strong HCl emission. As explained below, HCl($v = 1$) is formed by energy transfer from HOD.

The observation of both HOD and HCl emission from reaction (5D), whereas neither H_2O nor HCl is observed from reaction (5), was duplicated in many experiments [16]. The secondary kinetic-isotope [97] effect for reaction (5) is $k_{OH}/k_{OD} = 0.95$. If the same fractions of H_2O and HOD molecules are produced with one quantum of stretching excitation, the I_{H_2O}/I_{HOD} ratio should be the product of the ratio of Einstein coefficients and k_{OH}/k_{OD}, $0.33 \times 0.95 = 0.31$. Our

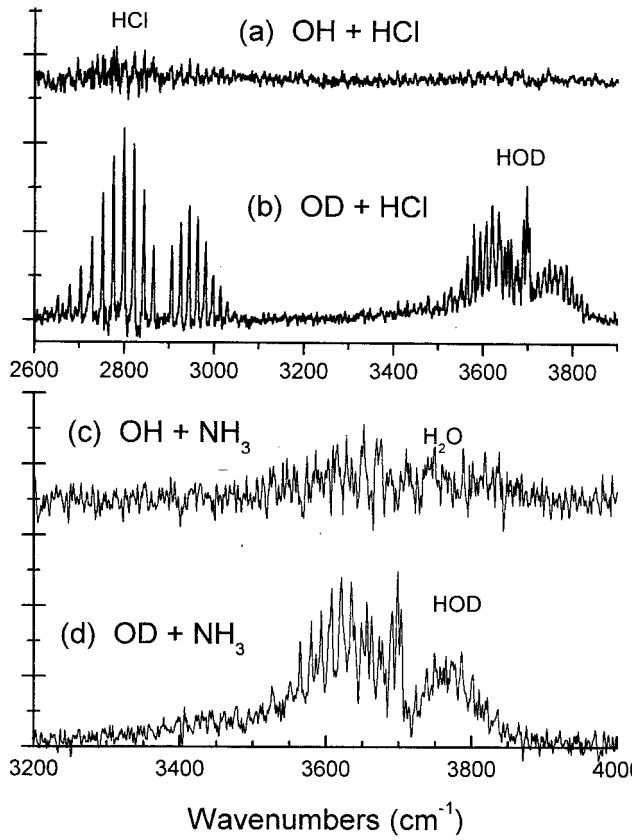

Figure 8. Chemiluminescent spectra from the OH (OD) + HCl and NH_3 reactions. The much stronger HOD emission is a consequence of more favourable emission probabilities plus quenching of vibrationally excited H_2O by HCl. The HCl fundamental emission in (*b*) is from V–V exchange with excited HOD; see text for discussion of quenching and V–V exchange by the HCl reactions.

estimate for the I_{H_2O}/I_{HOD} ratio from (5) and (5D) is 0.07 ± 0.07. The dilemma posed by the absence of the H_2O emission is discussed at the end of this section after reaction (5D) is analysed.

To estimate $P_3(0)$ from reaction (5D), comparisons were made between the OD + HCl and the OD + HBr (and OH + HBr) reactions. The fraction of HOD molecules from (5D) with $v_3 \neq 0$ can be estimated using

$$f(v_3 \neq 0) = \beta_{HCl} = (k_{HBr}/k_{HCl})([HBr]/[HCl]) \times (I_{HCl}/I_{HBr})[\beta_{HBr} S'_v(\nu_3, Pr_{HBr})/S'_v(\nu_3, HOD)], \quad \text{(E-19)}$$

where I_{HCl} and I_{HBr} are the integrated emission intensities, $S'_v(\nu_3, Pr_{HBr})$ and $S'_v(\nu_3, HOD)$ are the v_3 band-sum intensities for the products of HBr and HCl reactions and β are coefficients that depend on the vibrational distributions (defined in section 3.3). The spectra from all three reactions used for the calculation were recorded at 0.7 Torr for $[HCl] = 1.9 \times 10^{13}$, $[HBr] = 1.5 \times 10^{13}$, $[H_2] = [D_2] = 1.7 \times 10^{13}$ and $[NO_2] = 4.5 \times 10^{13}$ molecules cm^{-3}. The HOD and H_2O intensities were linearly dependent on the HCl and HBr concentrations in this range, which

shows that vibrationally excited HOD and H_2O molecules were not quenched. The integrated intensities were, in arbitrary units, 1.03 (OD + HCl), 7.02 (OH + HBr) and 11.4 (OD + HBr). The H_2O spectrum from the OH + HBr experiment corresponded to $P_{1,3}(0\text{–}3) = 24 : 42 : 28 : 6$ [12], which gives $\beta_{HBr} = 0.46$. The HOD emission from reaction (5D) can be considered as a pure $S'_v(\nu_3, \mathrm{HOD})$ band, since the (001) → (000) and (011) → (010) transitions have the same band strengths. For $k_{5D} = 8.0 \times 10^{-13}$ [97] and $k_1 = 1.1 \times 10^{-11}\,\mathrm{cm^3\ molecule^{-1}\,s^{-1}}$, we obtain $f(v_3 \neq 0) = 0.56$. The HOD distribution from OD + HBr [12] was $P_3(0\text{–}3) = 33 : 35 : 29 : 3$, which corresponds to $0.93S'_v(\nu_3, \mathrm{HOD})$. If our secondary kinetic-isotope effect for OD + HBr ($k_{OH}/k_{OD} = 1.16$) is used, $f(v_3 \neq 0) = 0.78$. Although this calculation is based on several approximations, the average value, $P_3(1) = 0.67$, indicates that most HOD molecules are produced with one quanta of O–H stretching vibration. According to the above estimates, the energy disposal for reaction (5D) seems normal for a direct abstraction reaction.

The most probable excitation mechanism of HCl($v = 1$) is energy transfer from the nearly resonant bending levels of H_2O (or HOD):

$$\mathrm{H_2O(or\ HOD)}(2\nu_2) + \mathrm{HCl}(v = 0) \rightarrow H_2O(HOD) + HCl(v = 1) + 226(-104)\ \mathrm{cm^{-1}}. \quad (\mathrm{Q1, QD1})$$

The band-sum intensity of the HCl, H_2O and HOD transitions in absorption are 4.75×10^{-18}, 7.57×10^{-20} and 5.64×10^{-19} respectively. With account of the cubic dependence on the transition frequency, the ratio of emission intensities for the three bands is $50.2(\mathrm{HCl}) : 1.0(2\nu_2, \mathrm{H_2O}) : 5.1(2\nu_2, \mathrm{HOD})$, and the HCl emission *could* indirectly identify the presence of $H_2O\,(2\nu_2)$ or HOD $(2\nu_2)$. However, Zittel and Masturzo found that HCl($v = 1$) formation from $H_2O\,(2\nu_2)$ + HCl was a small part (< 0.1) of the rate constant ($4.7 \times 10^{-11}\,\mathrm{cm^3\ molecule^{-1}\,s^{-1}}$), and the major product is just $H_2O(v_2 = 1)$. The stretching levels of H_2O and the ν_3 level of HOD are more than $500\,\mathrm{cm^{-1}}$ above HCl($v = 1$) and V–V exchange rate with HCl($v = 0$) is not important [50]. In fact the relaxation of $H_2O(v_{1,3} = 1)$ by HCl mainly proceeds with formation of $H_2O(v_2 = 2)$ [49, 50]. On the other hand, the O–D stretch mode of HOD can be involved in V–V exchange, and the following reaction would augment reaction (28*b*) as a source of HCl $(\nu = 1)$:

$$\mathrm{HOD}\,(\nu_1) + \mathrm{HCl}(v = 0) \rightarrow \mathrm{HOD} + \mathrm{HCl}(v = 1) - 163\ \mathrm{cm^{-1}}. \quad (\mathrm{QD2})$$

Formation of HCl $(v = 1)$ in the OD + HCl system from a secondary step was verified [16] by comparing the HOD and HCl emission intensities; plots of I_{HOD} and I_{HCl}/I_{HOD} vs. [HCl] are both linear for $[\mathrm{HCl}) < 3 \times 10^{13}$ molecules $\mathrm{cm^{-3}}$, i.e. the I_{HCl} intensity is proportional to $[\mathrm{HCl}]^2$. The slope of the I_{HCl}/I_{HOD} plot was used [16] to estimate $k_{QD1} + k_{QD2} = 6 \times 10^{-11}\ \mathrm{cm^3\ molecule^{-1}\ s^{-1}}$ with an uncertainty of about 50%. This rate constant is much larger than the value ($< 4.7 \times 10^{-12}\,\mathrm{cm^3\,molecule^{-1}\ s^{-1}}$) for (Q1), which explains the higher (by a factor of 3–6) I_{HCl} from reaction (5D) than from reaction (5).

On the basis of an indirect analysis for the yield of H_2O ($2\nu_2$ and $3\nu_2$), the lack of emission from $H_2O\,(\nu_{1,3})$ and HCl, and the presently accepted rate constant for $H_2O(v_{1,3} = 1)$ + HCl, we suggested earlier [16] that reaction (5) must mainly release energy to the translational motion of the products. However, new studies of several reactions with similar $\langle E_{av} \rangle$ and rate constants give normal H_2O and HOD vibrational distributions, and it seems unlikely that the OH + HCl reaction is unique.

Another explanation of why the HCl and H_2O emissions were so weak now seems more plausible. First of all, the branching fraction for HCl($v = 1$) formation from reaction (Q1) is very small and HCl($v = 1$) is not a monitor for $H_2O(\nu_2 = 2)$. Second, even if the total quenching [50] rate constant, $8.4 \pm 1.2 \times 10^{-12}\,cm^3\,s^{-1}$, for $H_2O(\nu_{1,2} = 1)$ is correct, the local [HCl] concentration in the reaction zone may be 2–3 times higher than the calculated homogenous concentration because of incomplete mixing at high HCl flow rates. Thus, quenching of $H_2O(\nu_{1,3} = 1)$ by HCl is probably more important than originally thought, and the energy disposal by reactions (25*a*) and (5D) must be similar.

DCl. Reactions (5′) and (5′D) are three times slower than reactions (5) [97] and the transition probabilities for $D_2O(\nu_{1,3})$ and $HOD(\nu_{1,2})$ are factors of 6 and 10 smaller than for $HOD(\nu_3)$. Thus, observation of emission from reactions (5′) was difficult. The only distinct emission was from the fundamental band of DCl in the 1900–2200 cm^{-1} range, which was an order of magnitude more intense from reaction (5D) than from reaction (5′) for similar experimental conditions. The weak (001) bond of D_2O in the 2600–2900 cm^{-1} range from (5′D), see figure 4 (*b*), may correspond to a substantial excitation of stretching vibrations of D_2O. On the basis of energy defect arguments, the energy transfer rate from D_2O ($2\nu_2$) to DCl probably is faster than from HOD ($2\nu^2$), which can exlain the stronger DCl emission from reaction (5′D). The overall pattern for the emission intensities seems to follow that of reactions (5).

NH_3. The reaction rates with NH_3 are four times slower than that for HCl, and the activation energy is comparable with that for ethane:

$$OH(OD) + NH_3 \rightarrow H_2O(HOD) + NH_2 \qquad (6, 6D)$$

Reaction (6) is 3 kcal mol^{-1} less exothermic than reaction (5), but excitation of one stretching level is possible. The spectra shown in figure 8, which were recorded at 0.53 Torr and $[NH_3] = 1.3 \times 10^{14}$ molecules cm^{-3} with $[OH] = [OD] = 2.5 \times 10^{13}$ molecules cm^{-3}, are new data. The H_2O emission is hardly above the experimental limit of sensitivity, but the HOD emission from reaction (6D) obviously exceeds the noise level. The HOD spectrum corresponds to emission from (001) + (011) in 100 : 22 proportion. As in the HCl case, comparison of the H_2O and HOD intensities from OH (OD) + HBr with that from NH_3 was made at the same pressure (0.7 Torr) to estimate the fraction of water molecules in non-emitting vibrational states using equation (E-19). The integrated intensities were equal (in arbitrary units) to 0.031 ($OH + HN_3$), 3.1 (OH + HBr), 0.095 ($OD + NH_3$) and 7.6 (OD + HBr). (These are the values after normalization for the order of magnitude lower concentration of HBr.) Normalization for rate constants is straightforward: $k_1(OH)/k_6(OH) = 68.8$ and the intensity ratio for NH_3 to HBr becomes 2.1 : 3.1. The emission strength from (1) is $0.44S'_v(\nu_3, H_2O)$, as can be calculated from the $P_{1,3}(\nu_{1,3})$ distribution, which was the same as for the HCl experiment described above. Since all the intensity from reaction (6) is from $v_{1,3} = 1$ with $0.44S'_v(\nu_3, H_2O)$ band strength, we obtain $P_{1,3}(0) = (2.1/3.1) \times (0.44/0.44) = 0.68$, i.e. the estimated distribution for reaction (6) is $P_{1,3}(0 : 1) = 32 : 68$. After normalization for rate constants using $k_{OH}/k_{OD} = 0.93$ for NH_3 [98] and 1.16 for HBr (see section 3.2), the intensity ratio of NH_3 to HBr becomes 5.2 : 7.6. According to the HOD distribution from OD + HBr, the observed emission corresponds to $0.93S'_v(\nu_3, HOD)$. The HOD emission from $OD + NH_3$ reaction is a pure $S'_v(\nu_3, HOD)$ band ($\alpha_1 = 1$); thus, we obtain $P_3(1) = (5.2/7.6) \times 0.93 = 0.64$. The final distribution is $P_3(0 : 1) = 36 : 64$.

Assuming that the $P_2(v_2)$ and $P_{1,2}(v_{1,2})$ distributions in the $v_{1,3}$ and $v_3 = 0$ states are close to statistical, we estimate $\langle f_v \rangle \cong 0.56$ and $\langle f_{v_2} \rangle \cong 0.18$ for reaction (6) and $\langle f_v \rangle \cong 0.55$ and $\langle f_{v_3} \rangle \cong 0.77$ for reaction (6D). On the basis of these new data, the OH (OD) + NH_3 reaction appears to be a normal, direct H atom abstraction reaction.

4.2. *Reactions with saturated hydrocarbons*

The 298 K rate constants and activation energies recommended by Atkinson *et al.* [24–26] are listed in table 2 for (1) ethane and neopentane, (2) cyclo-C_5H_{10} and cyclo-C_6H_{12}, (3) *n*-C_4H_{10} and *n*-$C_{10}H_{22}$ with mixed primary and secondary H atoms and (4) iso-C_4H_{10} and 2,2,4-trimethylpentane. The results to be presented in table 4 are based on new spectra and slightly different thermochemistry to that used before [16]. According to the structure–activity relationship (SAR) [99], the rate constants are additive for contributions from the CH_3, CH_2 and CH groups with account taken of the groups adjacent to the carbon atom from which a hydrogen atom is abstracted, and SAR will be used to discuss product branching. We have used the C–H bond dissociation energy values recommended by Berkowitz *et al.* [73], who critically reviewed the literature. The recommended changes mainly arise from the activation energies of the R + HI or R + HBr reactions used in thermochemical cycles. In Benson's work, activation energies of 1 ± 1 for R + HI and 2 ± 1 kcal mol^{-1} for R + HBr reactions were assumed, whereas Gutman and coworkers discovered that these reactions have negative activation energies. In the review of McMillen and Golden [74], which is one of the more complete compilations of bond dissociation energies, some of the thermochemical data are based on the iodine or bromine cycles, and their recommended bond dissociation energies have been adjusted in a few cases. A recent evaluation of theoretical bond energies also is instructive [100]. These changes in D(C–H) are important because of the sensitivity of the prior distribution to $\langle E_{av} \rangle$ and the concomitant effect on the estimates of $P_{1,3}(0)$ and $P_3(0)$ from surprisal plots.

4.2.1. *Primary H atom reactions (ethane, neopentane)*

The activation energy ($E_a = 1.54$ kcal mol^{-1}) for neo-C_5H_{12} is lower than for C_2H_6 ($E_a = 2.14$ kcal mol^{-1}) and the rate coefficients per H atom are 0.71×10^{-13} and 0.43×10^{-13} cm^3 molecule^{-1} s^{-1} respectively. The SAR coefficient underestimates this effect, giving 0.56 and 0.45×10^{-13} cm^3 s^{-1}.

$$\text{OH (OD)} + C_2H_6 \rightarrow H_2O \text{ (HOD)} + C_2H_5; \qquad (7, 7D)$$

$$\text{OH (OD)} + \text{neo-}C_5H_{12} \rightarrow H_2O \text{ (HOD)} + C_5H_{11}. \qquad (8, 8D)$$

The recommended values of E_a and D_0(H–R) give $\langle E_{av} \rangle = 23.1$ and 22.4 kcal mol^{-1} for reactions (7) and (8). The second stretch level is very close to the energy limit (within 90% of $\langle E_{av} \rangle$) and formation of v_3 or $v_{1,3} = 2$ cannot be accompanied by bending excitation. Spectra were measured at 0.5 Torr ($\Delta t \approx 0.2$ ms) and reagent concentrations of 2.6×10^{13} for C_2H_6 (figures 2 and 3) and 1.9×10^{13} molecules cm^{-3} for C_5H_{12} and vibrational relaxation need not be considered. The vibrational distributions (table 4) obtained from the simulation, $P_{1,3}(1:2) = 82:18$ and $P_3(1:2) = 79:21$, from C_2H_6 extend to the energy limit. Since emission in the 2400–3000 cm^{-1} range was weak, both $P_3(0)$ and $P_{1,3}(0)$ were estimated by surprisal analysis. The plots consists of only two points, and linearity was assumed. The

Table 4. Vibrational distribution from reactions with hydrocarbons.[a]

	H_2O										HOD										
Reagent	$v_{1,3}$	$v_2 = 0$	1	2	3	4	5	$P_{1,3}$[b]	$P_{1,3}$[c]	$P^0_{1,3}$[d]	v_3	$v_{1,2} = 0$	1	2	3	4	5	P_3[b]	P_3[c]	P_3[e]	P^0_3[d]
7. C_2H_6	0	9.6	6.2	3.3	1.6	0.5		—	21	71.7	0	9.9	6.8	7.9	4.1	2.6		—	31	ws	85.6
	1	43.6	18.3	3.0				82	65	27.5	1	50.9	1.1	3.2				79	55		13.1
	2	14.2						18	14	0.87	2	14.3						21	14		0.32
8. neo-C_5H_{12}	0	9.2	5.7	3.2	1.1	0.3		—	20	73.1	0	10.1	6.6	8.2	4.3	2.7		—	32	ws	87.4
	1	48.2	19.5	1.3				86	69	26.4	1	54.7	2.3	1.1				86	58		12.4
	2	11.5						14	11	0.52	2	9.5						14	10		0.21
9. cyclo-C_5H_{10}	0	7.5	5.1	3.3	1.9	0.9	0.2	—	19	67.0	0	5.2	3.8	5.1	3.3	2.6	1.1	—	21	14 ± 3	84.0
	1	25.9	20.8	7.1	1.2			68	55	30.5	1	43.7	2.3	4.5				63	50	55	15.2
	2	17.5	8.5					32	26	2.56	2	28.2	1.3					37	29	31	0.79
10. cyclo-C_6H_{12}	0	7.7	5.2	3.3	1.8	0.8	0.2	—	19	68.7	0	5.2	3.8	5.0	3.3	2.6	1.1	—	21	16 ± 4	84.9
	1	29.0	19.1	8.3	0.6			71	57	29.3	1	44.8	2.7	5.5				67	53	57	14.5
	2	16.5	7.5					29	24	1.92	2	24.0	1.9					33	26	27	0.60
11. n-C_4H_{10}	0	7.7	5.1	3.0	1.5	0.7	0.2	—	18	68.7	0	7.1	4.8	6.8	2.4	1.2	0.5	—	19	23 ± 4	84.9
	1	24.7	18.2	8.9	4.2			68	56	29.3	1	27.0	4.4	10.3	7.5			63	51	49	14.5
	2	15.3	10.6					32	26	1.92	2	20.9	7.3					37	30	28	0.60

12. n-$C_{10}H_{22}$	0	7.3	4.8	2.9	1.3	0.6	0.1	—	17	68.7	0	6.3	4.2	5.2	3.3	1.3	0.5	—	19	21 ± 3	84.9
	1	25.7	19.4	9.4	0.6			67	55	29.3	1	41.8	4.6	2.6				62	50	49	14.5
	2	16.0	12.0					33	28	1.92	2	28.2	1.9					38	31	30	0.60
13. iso-C_4H_{10}[f]	0	7.2	4.4	2.6	1.3	0.4	0.1	—	16	66.8[f]	0	6.2	4.2	5.2	2.8	1.8	0.6	—	21[f]	ws	83.9
	1	26.2	21.0	8.1	1.1			66	56	30.6	1	41.7	5.9	3.4				65	51		15.3
	2	16.9	11.2					34	28	2.63	2	25.8	2.2					35	28		0.82
14. 2,2,4-trimethylpentane[f]	0	8.8	5.6	3.3	1.6	0.5	0.1	—	20	70.7[f]	0	7.1	4.9	5.9	3.2	2.1	0.7	—	24[e]	ws	86.1
	1	40.7	15.9	3.2	2.1			78	62	28.2	1	45.1	6.6	3.8				73	55		13.5
	2	11.4	6.6					22	18	1.15	2	18.6	2.3					27	21		0.40

[a] These distributions are derived from new spectra; however, the results are similar to earlier work [16].
[b] Population in v_3 or $v_{1,3} = 0$ is neglected.
[c] $P_v(0)$ determined from extrapolation of linear surprisal plots; the least-squares uncertainty is generally ± 10–15%.
[d] Statistical prior distribution.
[e] $P_3(0)$ determined from fitting the HOD spectra in the 2500–2900 cm^{-1} region; the uncertainty is from fitting several spectra. The $v_{1,2} = 0$ and 1 states of $v_3 = 0$ are dark states and populations of these states must be estimated; see text for details of each reaction.
[f] These distributions are for the overall reaction; see text for distribution from abstraction of the tertiary C—H atoms.

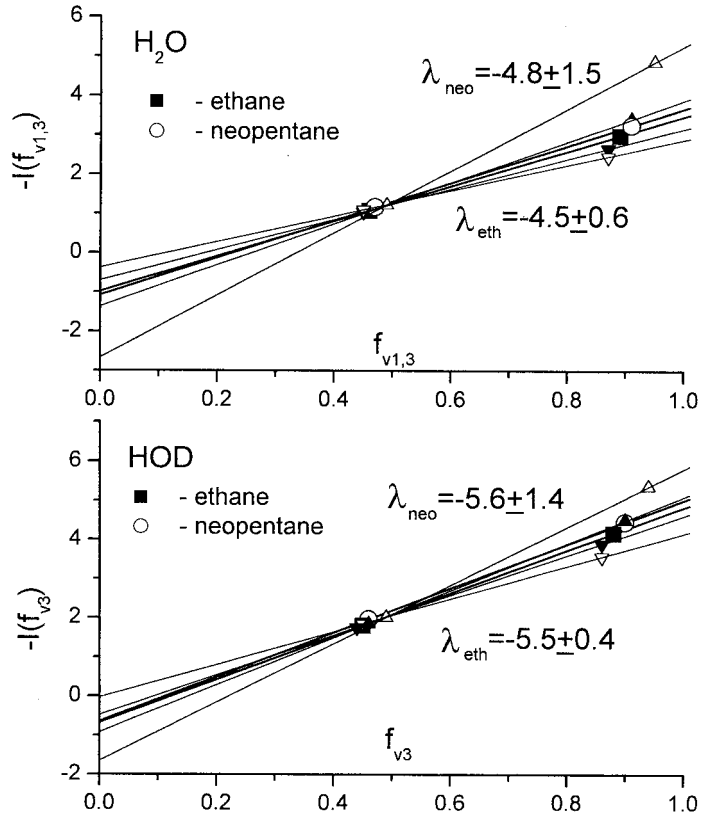

Figure 9. Vibrational surprisal plots for $P_{1,3}(v_{1,3})$ of H_2O and $P_3(v_3)$ for HOD from the C_2H_6, and $(CH_3)_4C$ reactions. The thin lines with closed triangles (ethane) and open triangles (neopentane) symbols show how an uncertainty in $\langle E_{av}\rangle$ of ± 0.50 and $\pm 1.0\,\text{kcal mol}^{-1}$ affects the plots for C_2H_6 and $(CH_3)_4C$ respectively. Since the intercepts provide estimates of $P_{1,3}(0)$ and $P_3(0)$, the uncertainty in $\langle E_{av}\rangle$ affects the vibrational distributions.

intercepts and slopes of the surprisals depend on the bond dissociation energy used to obtain $\langle E_{av}\rangle$, as illustrated by figure 9; the thick lines correspond to $\langle E_{av}\rangle$ from table 2 and the thin lines are for limits of $\pm 0.5\,\text{kcal mol}^{-1}$ for C_2H_6 and $\pm 1.0\,\text{kcal mol}^{-1}$ for neo-C_5H_{12}. The plots give $\lambda^0_{1,3} = -0.98 \pm 0.28$, $\lambda_{v_{1,3}} = -4.5 \pm 0.6$ and $\lambda^0_3 = -0.67 \pm 0.20$, $\lambda_{v_3} = -5.5 \pm 0.4$ for C_2H_6 and $\lambda^0_{1,3} = -1.07 \pm 0.60$, $\lambda_{v_{1,3}} = -4.8 \pm 1.5$ and $\lambda^0_3 = -0.63 \pm 0.40$, $\lambda_{v_3} = -5.6 \pm 1.3$ for neo-C_5H_{12}, and the corresponding uncertainties in dark state populations are $P_{1,3}(0) = 21 \pm 5$, $P_3(0) = 31 \pm 3$ for C_2H_6 and $P_{1,3}(0) = 20 \pm 8$, $P_3(0) = 32 \pm 6$ for neo-C_5H_{12}. The stretching distributions are sharply inverted. To calculate the total vibrational energy, we assumed that the bending distributions in $v_{1,3} = 0$ and $v_3 = 0$ follow the statistical distributions. The results, table 4, for reactions (7) and (8) are similar, and $\langle f_v(H_2O)\rangle = 0.51$ and 0.50 and $\langle f_v(HOD)\rangle = 0.47$ and 0.46. Only 16–17% of this energy is released as bending excitation, which is a factor of 2 less than for HBr or H_2S. On the basis of Cohen's claim [78] that the C–H bonds of neopentane are not completely representative of primary C–H bonds, the $P_{1,3}(0\text{–}2) = 21 : 65 : 14$ and $P_3(0\text{–}2) = 31 : 55 : 14$ distributions from ethane were chosen as representative for primary H atom abstraction from alkanes.

4.2.2. *Secondary H atom reactions (cyclo-C_6H_{12}, cyclo-C_5H_{10})*

The reactions with cycloalkanes are an order of magnitude faster and about 3 kcal mol^{-1} more exoergic than reactions (7) and (8) and one more quantum of bending excitation is allowed. Good spectra from

$$\mathrm{OH\,(OD) + cyclo\text{-}C_5H_{10} \rightarrow H_2O\,(HOD) + cyclo\text{-}C_5H_9}, \qquad (9, 9\mathrm{D})$$

$$\mathrm{OH\,(OD) + cyclo\text{-}C_6H_{12} \rightarrow H_2O\,(HOD) + cyclo\text{-}C_6H_{11}} \qquad (10, 10\mathrm{D})$$

were obtained for reagent concentrations of $(1.3\text{–}1.9) \times 10^{13}$ molecules cm^{-3} and $\Delta t = 0.25$ ms, and simulation of the 2400–3000 cm^{-1} bands gave $P_3(0)$ values. If we assume that the number of HOD molecules in the dark (000) and (010) states are equal to those in (020) and (030) states, which approximately corresponds to the statistical distribution, then the HOD distribution becomes $P_3(0\text{–}2) = 14 : 55 : 31$ for cyclopentane and 16 : 57 : 27 for cyclohexane. The $v_{1,3}$ and $v_3 = 2$ components are two times higher than for ethane or neopentane.

The bond dissociation energies of cyclo-C_5H_{10} and cyclo-C_6H_{12} given in [74] are 94.5 and 95.5 kcal mol^{-1} at 298 K. The surprisal parameters for cyclo-C_5H_{10} with $\langle E_{\mathrm{av}}\rangle = 28 \pm 1$ kcal mol^{-1} are $\lambda^0_{1,3} = -0.57 \pm 0.08$, $\lambda_{1,3} = -4.5 \pm 0.3$ and $\lambda^0_3 = -0.72 \pm 0.06$, $\lambda_{v_3} = -5.5 \pm 0.2$ with $P_{1,3}(0) = 26 \pm 2$ and $P_3(0) = 28 \pm 2$. The cyclohexane values for $\langle E_{\mathrm{av}}\rangle = 27.2$ kcal mol^{-1} are $\lambda^0_{1,3} = -0.47$, $\lambda_{v_{1,3}} = -3.2$ and $\lambda^0_3 = -0.91$, $\lambda_{v_3} = -5.7$ with $P_{1,3}(0) = 25$, $P_3(0)27$ with similar error limits for the ± 1 kcal mol^{-1} uncertainty in $\langle E_{\mathrm{av}}\rangle$. The average distributions from the cyclo-C_5H_{10} and cyclo-C_6H_{12} reactions are $P_{1,3}(0\text{–}2) = 29 : 49 : 22$ and $P_3(0\text{–}2) = 29 : 46 : 25$. The factor of 2 disagreement between the $P_3(0)$ values obtained from the simulation and from the surprisal analysis is larger than can be explained by an uncertainty in $\langle E_{\mathrm{av}}\rangle$ of 1 kcal mol^{-1}. The implication is that these $\langle E_{\mathrm{av}}\rangle$ values may be incorrect. Stein and Rabinovitch [75] expressed the C–H bond energies of cyclanes in terms of the strain energies (SE) in the cyclanes and cycloalkene molecules:

$$D(\text{cyclane C–H}) = D(\text{standard secondary C–H}) + [\mathrm{SE(cycloalkene)} - \mathrm{SE(cyclane)}]/2. \qquad (\mathrm{E20})$$

The strain energies were taken from [76], SE(cyclo-C_5H_{10}) = 6.2 kcal mol^{-1}, SE(cyclo-C_5H_8) = 5.7 kcal mol^{-1}, SE(cyclo-C_6H_{12}) = 0.0 kcal mol^{-1} and SE(cyclo-C_6H_{10}) = 1.3 kcal mol^{-1}. The standard secondary D(C–H) was taken as 97.7 kcal mol^{-1} [73], and thus D_{298}(cyclo-C_5H_9–H) = 97.4 and D_{298}(cyclo-C_6H_{11}–H) = 98.1 kcal mol^{-1} or 96.0 and 96.6 kcal mol^{-1} at 0 K. Fujisaki *et al.* [76] correlated the primary kinetic-isotope effects for the $\mathrm{H + RH\,(D) \rightarrow H_2\,(HD) + R}$ reactions with bond dissociation energies and expressed the results as $k_{\mathrm{H}}/k_{\mathrm{D}} = (A_{\mathrm{H}}/A_{\mathrm{D}}) \exp[(E_{\mathrm{D}} - E_{\mathrm{H}})/RT]$. The activation energy difference $E_{\mathrm{D}} - E_{\mathrm{H}}$ was correlated with the bond dissociation energies of the C–H bond being broken. The Evans–Polanyi empirical relation was used as a starting point:

$$E_{\mathrm{D}} - E_{\mathrm{H}} = a[D(\mathrm{C\text{–}H})] + b, \qquad (\mathrm{E21})$$

where a and b are constants. We used their $E_{\mathrm{D}} - E_{\mathrm{H}}$ values for neopentane, isobutane, cyclopentane and cyclohexane, which are 2.63 ± 0.11, 1.86 ± 0.15, 2.15 ± 0.06 and 2.31 ± 0.06 kcal mol^{-1} respectively. The neopentane and isobutane values and D_{298}(C–H) were employed to calculate $a = 0.17$ and $b = -14.51$. The D_{298}(C–H) values for cyclopentane and cyclohexane were determined to be 98.0 and

98.9 kcal mol^{-1} or 96.5 and 97.4 kcal mol^{-1} at 0 K, which agree with those obtained from the strain energy considerations. We used $\langle E_{av}\rangle = 25.1$ for cyclopentane and $\langle E_{av}\rangle = 24.6$ kcal mol^{-1} for cyclohexane for the final surprisal analysis, which gave $\lambda^0_{1,3} = -1.05$, $\lambda_{v_{1,3}} = -4.4$ and $\lambda^0_3 = -1.17$, $\lambda_{v_3} = -6.2$ with $P_{1,3}(0) = 19$ and $P_3(0) = 21$ for cyclopentane. The cyclohexane numbers are nearly identical. These $P_3(0)$ values agree better with the results derived from the spectra, and they were used for the distributions given in table 4. The average distributions are representative of secondary C–H bonds in cyclanes: $P_{1,3}(0\text{–}2) = 19 : 56 : 25$ and $P_3(0\text{–}2) = 21 : 51 : 27$. According to these distributions, $\langle f_v\rangle = 0.55$ and the vibrational energy is shared between bending and stretching modes in a 1 to 4 ratio, which is slightly higher than for primary C–H bonds.

4.2.3. *Mixed primary and secondary H atoms (*n*-butane and* n*-decane)*

Abstraction from secondary C–H bonds dominates over primary abstraction at 298 K and the SAR coefficients assign a contribution to the CH_3 groups of about 13% for *n*-C_4H_{10},

$$\mathrm{OH\,(OD)} + n\text{-}\mathrm{C_4H_{10}} \rightarrow \mathrm{H_2O\,(HOD)} + \mathrm{C_4H_9}, \qquad (11, 11\mathrm{D})$$

and only about 3% for *n*-$C_{10}H_{22}$. The $P_{1,3}(1 : 2) = 68 : 32$ and $P_3(1 : 2) = 63 : 37$ vibrational distributions from *n*-butane are identical to those from cyclopentane. Neglecting the primary hydrogens, i.e. doing surprisal calculations with $\langle E_{av}\rangle = 24.7$ kcal mol^{-1}, gives $\lambda^0_{1,3} = -1.15$, $\lambda_{v_{1,3}} = -4.6$ and $\lambda^0_3 = -1.30$, $\lambda_{v_3} = -6.4$, and the distributions are $P_{1,3}(0\text{–}2) = 18 : 56 : 26$ and $P_3(0\text{–}2) = 19 : 51 : 30$. The $P_3(0)$ contribution obtained from spectral simulation matches that from the surprisal analysis. After assignment of statistical populations to $v_{1,3} = 0$ and $v_3 = 0$ states, the butane distributions, table 4, give $\langle f_v\rangle = 0.58$ with $\langle E_{v_2}\rangle = 0.23$. In our previous work [16], the contribution of primary C–H bonds to reaction (11) was neglected, but now, having obtained distributions for primary C–H bonds, we can extract distributions for the secondary H atoms. Using the SAR primary-to-secondary ratio of 0.13 : 0.87 and the primary distributions for ethane, the 'pure' secondary distributions are $P_{1,3}(0\text{–}2) = 18 : 54 : 28$ and $P_3(0\text{–}2) = 19 : 49 : 32$.

The $P(1) : P(2)$ ratios from *n*-decane are virtually identical to those for *n*-butane, and the full HOD distribution obtained from the simulation, $P_3(0\text{–}2) = 21 : 49 : 30$, also is very close to that from *n*-butane. The dissociation energy for secondary C–H bonds in *n*-decane is not known; calculation with the help of equation (36) using the measured [76] $E_D - E_H = 2.25$ kcal mol^{-1} value for *n*-decane gives a bond dissociation energy identical to that for *n*-butane. The surprisals were calculated for the prior distributions corresponding to $\langle E_{av}\rangle = 24.7$ kcal mol^{-1} giving $P_{1,3}(0) = 17$, $P_3(0) = 19$; $\langle f_v\rangle = 0.56$ and the division between stretching and bending energies are the same as for *n*-butane.

4.2.4. *Reactions including tertiary C–H bonds (isobutane and 2,2,4-trimethylpentane)*

Iso-C_4H_{10} has nine primary and one tertiary hydrogen atoms which contribute to products in a 20 : 80 proportion according to the SAR. The rate constant calculated using this ratio, 2.4×10^{-12} cm^3 molecule^{-1} s^{-1}, agrees with the experimental value. Simulation of the spectra gave $P_{1,3}(1 : 2) = 66 : 34$ and $P_3(1 : 2) = 65 : 35$. To determine a distribution specific for the tertiary hydrogen reaction, we used the primary distributions from ethane and assumed that the observed distributions

followed the SAR rule. This gave $P_{1,3}(1:2) = 62:39$ and $P_3(1:2) = 61:40$. Surprisal plots were made with $\langle E_{av}\rangle = 25.5 \pm 1.0\,\text{kcal mol}^{-1}$, corresponding to abstraction from a tertiary C–H bond with zero activation energy. The surprisal parameters were $\lambda_{v_{1,3}} = -4.5 \pm 0.5$ and $\lambda_{v_3} = -6.3 \pm 0.6$ and complete distributions for the tertiary reaction are $P_{1,3}(0\text{–}2) = 14:53:33$ and $P_3(0\text{–}2) = 19:49:32$. Given the uncertainties, the distributions from tertiary and secondary abstraction are very similar. For superposition of primary and tertiary C–H abstraction, the distributions become $P_{1,3}(0\text{–}2) = 16 \pm 3:56:28$ and $P_3(0\text{–}2) = 21 \pm 3:51:28$, which give $\langle f_v(H_2O)\rangle = 0.58$ and $\langle f_v(HOD)\rangle = 0.52$, and $\langle E_{v_3}\rangle/\langle E_{v_2}\rangle = 0.24$ for the overall reaction.

2,2,4-Trimethylpentane, commonly called isooctane, contains fifteen primary, two secondary and one tertiary hydrogen, which, according to the SAR, should contribute in 18 : 30 : 52 proportions. The predicted rate constant, $4.6\times 10^{-12}\,\text{cm}^3\,\text{s}^{-1}$, slightly overestimates the true rate constant. Simulation of the spectra gave $P_{1,3}(1:2) = 78:22$ and $P_3(1:2) = 73:27$, which have notably less population in $v_{1,3}$ and $v_3 = 2$ than the isobutane reaction. Since the relative contribution of the primary hydrogens does not differ much from the isobutane reaction and since the distributions for secondary hydrogen abstraction should follow those of butane, the difference in the nature of tertiary H bonds in isooctane and isobutane (T_{001} and T_{000}, respectively, according to Cohen's classification [78]) can be examined for an explanation of the low $P_3(2)$ and $P_{1,3}(2)$. The T_{001} bond energy value is more than $2\,\text{kcal mol}^{-1}$ higher, but both reactions have negative apparent activation energies for tertiary C–H abstraction [78]. Taking $97.0\,\text{kcal mol}^{-1}$ for the tertiary bond energy of iso-C_8H_{18} gives $\langle E_{av}\rangle = 23.5\,\text{kcal mol}^{-1}$, similar to the available energy for ethane. From the point of view of the available energy, the trimethylpentane reaction is equivalent to the reactions of primary and secondary hydrogens in 70 : 30 ratio, which may explain the low excitation for v_3 and $v_{1,3} = 2$. The best agreement with the measured $P_{1,3}(1:2)$ and $P_3(1:2)$ was obtained from the superposition of ethane and cyclohexane distributions, $P_{1,3}(0\text{–}2) = 20:60:21$ and $P_3(0\text{–}2) = 24:54:22$. They can be compared with estimates from the surprisal plots using $\langle E_{av}\rangle = 23.5 \pm 0.8\,\text{kcal mol}^{-1}$: $P_{1,3}(0\text{–}2) = 20 \pm 5:63:18$ and $P_3(0\text{–}2) = 24 \pm 4:55:21$, with $\langle f_v\rangle = 0.53$.

In summary, slightly lower $\langle f_v\rangle \approx 0.50$ and $\langle E_{v_2}\rangle/\langle E_{v_3}\rangle \approx 0.20$ were found from primary H atom abstraction compared with the other C–H abstraction reactions with $\langle f_v\rangle \approx 0.55$ and $\langle E_{v_2}\rangle/\langle E_{v_3}\rangle \approx 0.25$. However, within the error limits, which are determined to a great extent by the uncertainties in the $\langle E_{av}\rangle$ values, the nature of the hydrogen atom in the hydrocarbon molecule had little effect on the energy disposal. The common energy disposal pattern for the primary, secondary and tertiary C–H bonds presumably reflects the similarity of the dynamics after passing the transition states, which have different barrier heights and somewhat different properties [30, 31, 101]. The fraction of the energy released to bending excitation is distinctly smaller for reactions with hydrocarbons than for the HBr and H_2S reactions; see the summary in table 8. The fact that the sum of $\langle f_{v_2}\rangle$ and $\langle f_{v_3}\rangle$ is very close to 1.0 for reactions (7)–(14) indicates that the old OH bond is nearly a spectator.

4.3. *Reactions with oxygen-containing organic compounds*

Four classes of oxygen-containing organic compounds were studied: (1) alcohols (methanol, ethanol); (2) ethers (dimethyl and diethyl ether, dimethoxy-methane, methoxy-ethanol); (3) ketones (acetone, 2-butanone, 2-pentanone and 3-pentanone);

(4) aldehydes (formaldehyde, acetaldehyde). Except for the aldehydes [18, 21], the results in tables 5 and 6 are from new studies. Since the $\langle E_{av} \rangle$ are below 28 kcal mol^{-1} (except for H_2CO and CH_3CHO), only two stretching quanta can be excited and the dynamics of these reactions can be compared with hydrocarbons. Although many studies have been dedicated to the kinetics and mechanisms of OH reactions with alcohols, ethers and ketones [79, 80, 82, 84–88, 102–115], accurate thermochemical data still are not available for several reactions. If necessary, the C–H bond energies tabulated in [74] were revised in view of more recent experimental and theoretical work. The contributions from different product channels were estimated using the SAR method [99].

Alcohol, ether and ketone molecules have strong intermolecular interactions with water [116–119], which result in fast relaxation rates for vibrationally excited water molecules. If possible, spectra were taken for a range of reactant concentrations, and distributions were then assigned for each spectrum. For every reaction, a critical reagent concentration was determined below which the distributions did not change, and averages of two or three spectra taken below the critical concentration were used for assignment of the nascent distributions given in tables 5 and 6. The concentrations of CH_3OH and C_2H_5OH could not be reduced enough to be confident about the critical limits, as explained below.

4.3.1. *Alcohols*

The reaction with methanol proceeds via two paths

$$OH\,(OD) + CH_3OH \rightarrow H_2O\,(HOD) + CH_2OH \qquad (15a, 15Da)$$

$$\rightarrow H_2O\,(OD) + CH_3O \qquad (15b, 15Db)$$

but abstraction from the oxygen site contributes only 14% [102, 103]. $D_0(HOCH_2–H)$, which is known with high accuracy [73, 107], is 5 kcal mol^{-1} lower than in ethane and it is close to the tertiary C–H bond energy in isobutane. The $\langle E_{av} \rangle$ values for reactions (15*a*) and (1) are 26.8 and 18.9 kcal mol^{-1} respectively. The methanol concentration could not be decreased lower than $\sim 5.0 \times 10^{13}$ molecules cm^{-3}, otherwise the spectra were too noisy for simulation, and at this concentration the distributions were still changing. Somewhat lower reactant concentrations were possible for experiments with $OD + CH_3OD$, which were carried out to eliminate contributions from reaction (15D*b*) to the HOD emission, and the lowest concentration giving credible HOD spectra was 2.6×10^{13} molecules cm^{-3}. The reported distributions from methanol must be considered as lower limits to the vibrational excitation. The stretching populations from reactions (15*a*) and (15*b*) are $P_{1,3}(1:2) = 76:24$, $P_3(1:2) = 75:25$ and $P_3(1:2) = 69:31$ from the $OD + CH_3OD$ reaction; all distributions show less population in $v_3 = 2$ than the reaction of isobutane. The surprisal calculation with $\langle E_{av} \rangle = 26.8$ kcal mol^{-1} (neglecting channel (15*b*)) gives $\lambda^0_{1,3} = -0.17 \pm 0.10$, $\lambda_{v_{1,3}} = -2.6 \pm 0.2$ and $\lambda^0_3 = -0.15 \pm 0.08$, $\lambda_{v_3} = -4.2 \pm 0.2$; the small error limits are just from the uncertainty in the C–H bond energy. The corresponding full distributions are $P_{1,3}(0–2) = 35 \pm 3:49:16$ and $P_3(0–2) = 41 \pm 3:44:15$ with $\langle f_v(H_2O) \rangle = 0.44$, $\langle f_v(HOD) \rangle = 0.43$ and $\langle E_{2v} \rangle / \langle E_{3v} \rangle = 0.44$. Unfortunately, the 2400–2900 cm^{-1} emission from reactions (15D*a*) and (15D*b*) was too weak to obtain a $P_3(0)$ population from the HOD spectra.

Table 5. Vibrational distribution from reactions with alcohols and ethers.[a]

Reagent	H_2O										HOD										
	$v_{1,3}$	$v_2=0$	1	2	3	4	5	$P_{1,3}$[b]	$P_{1,3}$[c]	$P^0_{1,3}$[d]	v_3	$v_{1,2}=0$	1	2	3	4	5	P_3[b]	P_3[c]	P_3[e]	P^0_3[d]
15. Methanol, CH_3OH[f]	0	13.5	9.5	6.2	3.7	2.1		—	35	64.5	0	9.3	6.8	9.7	6.2	5.9	3.1	—	41	ws	82.5
	1	28.9	11.8	8.2				76	49	31.6	1	35.6	5.7	2.0	0.7			75	44		16.3
	2	9.4	6.6					24	16	3.9	2	12.4	2.9					25	15		1.2
16. Ethanol, C_2H_5OH[g]	0	12.4	8.7	5.6	3.5	1.8	0.9	—	33	63.2	0	8.3	6.1	8.6	5.8	5.2	2.7	—	33	39 ± 7	81.8
	1	19.0	16.1	10.7	2.3			72	48	32.2	1	29.8	5.1	5.7	2.5			67	45	44	16.8
	2	14.2	4.8					28	19	4.6	2	17.3	3.5					33	22	17	1.4
17. Dimethyl ether, CH_3OCH_3	0	13.1	8.9	5.7	3.5	2.0	0.8	—	34	63.2	0	7.9	5.8	8.2	5.5	5.0	2.6	—	35	ws	81.5
	1	26.1	14.8	5.1	1.3			72	47	32.2	1	27.7	4.9	10.0	1.4			68	44		17.1
	2	12.4	6.6					28	19	4.6	2	18.1	2.9					32	21		1.5
18. Diethyl ether, $C_2H_5OC_2H_5$[g]	0	12.9	8.7	5.8	3.6	2.1	0.9	—	34	62.2	0	7.8	5.8	8.3	5.7	5.2	2.8	—	32	39 ± 5	81.0
	1	19.7	11.8	10.2	5.3			71	47	32.5	1	30.8	6.2	4.0	1.5			66	45	40	17.5
	2	12.4	5.6					29	19	5.3	2	19.2	2.8					34	23	21	1.6
19. Dimethoxymethane, $CH_3OCH_2OCH_3$	0	16.5	11.1	7.4	4.5	2.5	1.0	—	43	64.5	0	10.4	7.7	11.0	7.3	6.9	3.7	—	51	47 ± 9	82.5
	1	25.7	13.3	4.6	1.8			79	45	31.6	1	34.7	3.4	3.2	0.7			79	39	42	16.3
	2	8.3	3.6					21	12	3.9	2	9.9	1.1					21	10	11	1.2
20. Methoxyethanol, $CH_3OC_2H_4OH$[g]	0	14.3	9.7	6.5	4.4	2.2	1.0	—	38	62.2	0	8.9	6.6	9.4	6.2	5.8	3.1	—	43	40 ± 7	81.0
	1	23.0	15.9	5.8	1.2			74	46	32.5	1	29.9	7.2	5.1	1.8			73	42	44	17.5
	2	10.6	5.4					26	16	5.3	2	13.0	3.0					27	15	16	1.6

[a] The data in this table are new.
[b] Population in v_3 or $v_{1,3}=0$ is neglected.
[c] $P_v(0)$ determined from extrapolation of linear surprisal plots; the least-squares uncertainty is generally $\pm$ 10–15%.
[d] Statistical prior distribution.
[e] $P_3(0)$ determined from fitting the HOD spectra in the 2500–2900 cm^{-1} region; the uncertainty is from fitting several spectra. The $v_{1,2}=0$ and 1 states of $v_3=0$ are dark states and populations of these states must be estimated; see text for details of each reaction.
[f] Results are for the overall reaction, see text for separation of the contribution from the OH site.
[g] Results are for abstraction at the CH_2 site.

The contribution of abstraction from the OH position to the H_2O and HOD distribution's was subtracted in the following manner. $\langle E_{av} \rangle$ is 18.9 kcal mol^{-1} for $E_a = 1.4$ kcal mol^{-1} [99], which is sufficient to excite only one O–H vibrational level. The contribution of reaction (15*b*) to the population of the first stretching level cannot exceed 14%, which gives $P_{1,3}(1:2) = 66:24$ and $P_3(1:2) = 65:25$ or, in the renormalized form, $P_{1,3}(1:2) = 73:27$ and $P_3(1:2) = 72:28$, for reactions (15*a*) and (15D*b*). The latter distribution agrees with the $P_3(1:2) = 69:31$ distribution obtained from the $OD + CH_3OD$ experiment. The surprisal parameters calculated with $\langle E_{av} \rangle = 26.8$ kcal mol^{-1} are $\lambda_{v_{1,3}} = -3.0$ and $\lambda_{v_{1,3}} = -4.6$, and the full distributions are $P_{1,3}(0\text{–}2) = 30:51:19$ and $P_3(0\text{–}2) = 36:46:18$. The correction leads to an increase in the population inversion and to $\langle f_v \rangle = 0.45$. However, the vibrational excitation from reaction (15*a*) is less than from most hydrocarbons. Reaction (15*b*) gives only $v_3 = 0$ and 1 and it is not possible even to estimate the energy disposal. However, the logic used above to subtract the $v_3 = 1$ and $v_{1,3} = 1$ contributions from the total distributions suggests that the energy disposal probably is normal for abstraction from the OH bond with $\langle f_v \rangle \approx 0.5$.

The branching ratios at 298 K for the three channels with ethanol,

$$\begin{aligned} OH\,(OD) + CH_3CH_2OH &\rightarrow H_2O\,(HOD) + CH_3CHOH, && (16a, 16Da)\\ &\rightarrow H_2O\,(HOD) + CH_3CH_2O, && (16b, 16Db)\\ &\rightarrow H_2O\,(HOD) + CH_2CH_2OH, && (16c, 16Dc) \end{aligned}$$

(16*a*) : (16*b*) : (16*c*) = 90 : 5 : 5 [24], and abstraction from the CH_2 group is dominant. For the reasons already stated, the C–H dissociation energy for CH_2 given by McMillen and Golden [74] was elevated by 2 kcal mol^{-1}, which gives $\langle E_{av} \rangle = 27.4$ kcal mol^{-1}. The difference between the bond energies in CH_2 and CH_3 groups in ethanol is about 1 kcal mol^{-1}, which is smaller than the difference between the primary and secondary C–H bonds in alkanes. Because of the lower E_a, the available energy of reaction (16*a*) is nearly equal to that of reaction (15*a*). Reactions (42) slightly favour v_3 and $v_{1,3} = 2$ relative to reactions (15); see Table 5. However, the $P_3(v_3)$ distribution from $OD + CH_3OD$ is nearly the same as for reactions (16). The surprisal calculations with $\langle E_{av} \rangle = 27.4 \pm 1.0$ kcal mol^{-1} for (16*a*) and (16D*a*) give $\lambda^0_{1,3} = -0.27 \pm 0.29$, $\lambda_{v_{1,3}} = -2.8 \pm 0.4$ and $\lambda^0_3 = -0.52 \pm 0.22$, $\lambda_{v_3} = -4.9 \pm 0.4$; the full distributions are $P_{1,3}(0\text{–}2) = 33 \pm 5 : 48 : 19$ and $P_3(0\text{–}2) = 33 \pm 4 : 45 : 22$. It was possible to evaluate $P_3(0) = 39 \pm 7$ by simulation of the $\Delta v_1 = -1$ HOD spectra, and the result is in reasonable agreement with the surprisal prediction. Corrections for channels (16*b*) and (16*c*) were ignored, since they would be smaller than for methanol, and $\langle f_v(H_2O) \rangle = 0.48$, $\langle f_v(HOD) \rangle = 0.47$ and $\langle E_{2v} \rangle / \langle E_{3v} \rangle = 0.44$. The oxygen atom lowers the C–H bond energies in alcohols and ethers, and the effect spreads for 2–3 carbon atoms beyond the α-carbon [82, 105]; thus, $\langle E_{av} \rangle$ for channel (16*c*) would not be much lower than that for reaction (16*a*).

Despite the similarity in rate constants and $\langle E_{av} \rangle$, $\langle E_{vib} \rangle$ is lower and $\langle E_{2v} \rangle / \langle E_{3v} \rangle$ is higher for CH_3OH and C_2H_5OH relative to reactions with hydrocarbons. This tendency also holds for methyl and ethyl ether; see below. The presence of the oxygen atom is playing some role in the dynamics that affects the vibrational energy released to the water product.

4.3.2. *Ethers*

The vibrational excitation of H_2O and HOD in the reaction with dimethyl ether,

$$OH\,(OD) + CH_3OCH_3 \rightarrow H_2O\,(HOD) + CH_3OCH_2 \qquad (17, 17D)$$

is identical to that from ethanol. Good and Francisco [110] reported $D_0(CH_3OCH_2\text{–}H) = 95.6\,\text{kcal mol}^{-1}$ from *ab initio* calculations, which exceeds the $D_0(C\text{–}H) = 91.6\,\text{kcal mol}^{-1}$ recommended by McMillen and Golden [81]. Appearance potential measurements [111] give $D_0(CH_3OCH_2\text{–}H) = 92.3 \pm 2\,\text{kcal mol}^{-1}$. We used $93.8\,\text{kcal mol}^{-1}$, which gives $\langle E_{av}\rangle = 27.6\,\text{kcal mol}^{-1}$ for the surprisal analysis and $\lambda^0_{1,3} = -0.22 \pm 0.20$, $\lambda_{v_{1,3}} = -2.7 \pm 0.4$ and $\lambda^0_3 = -0.43 \pm 0.20$, $\lambda_{v_{1,3}} = -4.8 \pm 0.2$; the uncertainty corresponds to a $\pm 1\,\text{kcal mol}^{-1}$ variation in the C–H bond energy. The full distributions are $P_{1,3}(0\text{–}2) = 34 : 47 : 19$ and $P_3(0\text{–}2) = 35 : 45 : 21$, with $\langle f_v(H_2O)\rangle = 0.45$, $\langle f_v(HOD)\rangle = 0.47$ and $\langle E_{2v}\rangle/\langle E_{3v}\rangle = 0.41$. These H_2O and HOD distributions are consistent with a direct abstraction mechanism. According to extensive *ab initio* calculations [119], the hydrogen bonded $OH \cdot CH_3OCH_3$ complex plays no role in the abstraction dynamics, although the presence of two types of hydrogen atoms does complicate the number of transition states needed to describe reaction (17).

The SAR predicts the overwhelming domination by secondary abstraction for diethyl ether:

$$OH\,(OD) + C_2H_5OC_2H_5 \rightarrow H_2O\,(HOD) + CH_3CHOCH_2CH_3. \qquad (18, 18D)$$

According to Kondo and Benson [83], the C–H bond dissociation energy of the CH_2 group is $90.3\,\text{kcal mol}^{-1}$ to which we added a $2\,\text{kcal mol}^{-1}$ generic correction. In ethers, the difference between the C–H bond energies in CH_2 and CH_3 groups in α- and β-positions with respect to the oxygen atom is $1.3\,\text{kcal mol}^{-1}$. Since abstraction from the CH_2 group of $C_2H_5OC_2H_5$ has a negative temperature dependence ($E_a \approx -0.5\,\text{kcal mol}^{-1}$ [82]), whereas reaction (17) has a positive temperature coefficient ($E_a = 0.6\,\text{kcal mol}^{-1}$ [79, 80]), the $\langle E_{av}\rangle$ are similar. Surprisal calculations with $\langle E_{av}\rangle = 28.2\,\text{kcal mol}^{-1}$ give $\lambda^0_{1,3} = 0.21 \pm 0.18$, $\lambda_{v_{1,3}} = -2.6 \pm 0.4$ and $\lambda^0_3 = -0.54 \pm 0.22$, $\lambda_{v_{1,3}} = -5.0 \pm 0.4$; the uncertainty corresponds to a $1\,\text{kcal mol}^{-1}$ variation in C–H bond energy. The full distributions, $P_{1,3}(0\text{–}2) = 34 \pm 4 : 47 : 19$ and $P_3(0\text{–}2) = 32 \pm 4 : 45 : 23$, differ only slightly from those of dimethyl ether; $\langle f_v\rangle = 0.47$ with $\langle E_{2v}\rangle/\langle E_{3v}\rangle = 0.45$.

Two more complex ethers, dimethoxymethane

$$OH\,(OD) + CH_3OCH_2OCH_3 \rightarrow H_2O\,(HOD) + \text{products} \qquad (19, 19D)$$

and methoxyethanol

$$OH\,(OD) + CH_3OC_2H_4OH \rightarrow H_2O\,(HOD) + \text{products} \qquad (20, 20D)$$

were selected for study. These reactions gave less population in $v_{1,3}$ and $v_3 = 2$ than reaction (17) and (18). The experimental distributions are $P_{1,3}(1 : 2) = 79 : 21$ and $P_3(1 : 2) = 79 : 21$ for reaction (19) and (19D) and $P_{1,3}(1 : 2) = 74 : 26$ and $P_3(1 : 2) = 73.27$ for reaction (20) and (20D). The thermochemistries of reactions (19) and (20) are not known, and estimates of the available energies were made on the basis of the kinetic data [84, 109] for these reactions. Sauer *et al.* [114] found that abstraction from CH_3 and CH_2 groups connected to oxygen atoms in $CH_3O\text{-}CH_2OCH_3$ had branching fractions of approximately 68:32, which correspond to the reactivity per hydrogen atom for CH_3 and CH_2 groups of 0.52×10^{-12} and

0.74×10^{-12} cm^3 molecule^{-1} s^{-1}, respectively. Apparently, the C–H bond energy of the CH_2 group is closer to that of the CH_3 group than to the C–H bond energy of the CH_2 group of diethyl ether, since the estimated reactivity per atom of the latter is 3.4×10^{-12} cm^3 molecule^{-1} s^{-1}. The ΔH^0_o value for reaction (19) was assumed to be similar to reaction (17). Surprisal plots with $\langle E_{av} \rangle = 26.9$ kcal mol^{-1} give $\lambda_{v_{1,3}} = -1.8$ and $\lambda_{v_3} = -3.2$. The full distributions and energy disposal parameters for reaction (19) are $P_{1,3}(0\text{–}2) = 43 : 45 : 12$ and $P_3(0\text{–}2) = 51 : 39 : 10$; $\langle f_v \rangle = 0.40$ with $\langle E_{2v} \rangle / \langle E_{3v} \rangle = 0.61$. The rate constant for reaction (20) is similar to that for reaction (18), and we assume that abstraction is mainly from the CH_2 groups with $\langle E_{av} \rangle = 28.2$ kcal mol^{-1}, i.e. the C–H bond energy of the methylene groups is the same as that for α-carbon in diethyl ether. Surprisal calculations for reaction (20) gave $\lambda_{v_{1,3}} = -2.2$ and $\lambda_{v_3} = -4.0$; the full distributions are $P_{1,3}(0\text{–}2) = 38 : 46 : 16$ and $P_3(0\text{–}2) = 43 : 42 : 15$ with $\langle f_v \rangle = 0.43$ and $\langle E_{2v} \rangle / \langle E_v \rangle = 0.51$. Reactions (19) and (20) have somewhat lower $\langle f_v \rangle$ values and less inverted $P_3(v_3)$ distributions than for $(CH_3)_2O$ and $(C_2H_5)_2O$ reactions, and the bend-to-stretch excitation ratio also is higher. These trends accentuate those noted in comparing distributions from hydrocarbons to those from reactions (15)–(18).

4.3.3. *Ketones*

The C–H bond energy in acetone is larger than in dimethyl ether and, with the 2 kcal mol^{-1} correction, the 98.9 kcal mol^{-1} value is comparable with the primary C–H bond energy of alkanes. Accordingly, the rate of reaction,

$$OH\,(OD) + CH_3C(O)CH_3 \rightarrow H_2O\,(HOD) + CH_3C(O)CH_2, \qquad (21, 21D)$$

is slow and the H_2O emission was too weak to be useful. However, the HOD emission reaction from (21D), which could be analysed, gave a definite population in $v_3 = 2$, and $P_3(1 : 2) = 82 : 18$. Surprisal calculations with $\langle E_{av} \rangle = 23.1$ kcal mol^{-1} gave $\lambda^0_3 = -0.66 \pm 0.40$, $\lambda_{v_3} = -5.5 \pm 0.9$; the uncertainty corresponds to a 1 kcal mol^{-1} change in D(C–H). The full distribution is $P_3(0\text{–}2) = 31 \pm 5 : 57 : 12$, with estimates for $\langle f_v(HOD) \rangle$ and $\langle f_{3v} \rangle$ of 0.49 and 0.75 respectively. Our experiments were not designed to measure relative emission intensities. However, qualitative comparisons with ethane are in accord with abstraction, rather than addition, as the main reaction path at room temperature for OH+acetone [120].

The reaction rates with ketones containing carbon atoms in the β-position [85, 87] are an order of magnitude faster than the reaction with acetone:

$$OH\,(OD) + CH_3C(O)CH_2CH_3 \rightarrow H_2O\,(HOD) + CH_3C(O)CHCH_3 \quad (22a, 22Da)$$

$$\rightarrow H_2O(HOD) + CH_3C(O)CH_2CH_2, \quad (22b, 22Db)$$

$$OH\,(OD) + CH_3CH_2C(O)CH_2CH_3 \rightarrow H_2O\,(HOD) + CH_3CH_2C(O)CHCH_3 \quad (23a, 23Da)$$

$$\rightarrow H_2O\,(HOD) + CH_3CH_2C(O)CH_2CH_2. \quad (23b, 23Db)$$

The SAR gives branching ratios of $(22a) : (22b) = 53 : 40$ and $(23a) : (23b) = 57 : 43$. The importance of both channels was confirmed by studying the $OD + CD_3C(O)CD_2CH_3$ reaction; see section 3.2. Hydrogen abstraction from the

Table 6. Vibrational distribution from reactions with alcohols and ethers.[a]

	H_2O										HOD										
Reagent	$v_{1,3}$	$v_2=0$	1	2	3	4	≥ 5	$P_{1,3}$[b]	$P_{1,3}$[c]	$P^0_{1,3}$[d]	v_3	$v_{1,2}=0$	1	2	3	4	5	≥ 6	P_3[b]	P_3[c]	P_3[e]	P^{0d}_3
21. Acetone, $CH_3C(O)CH_3$[f]	0									72.4	0	8.8	6.0	7.9	4.6	3.6			—	31	ws	87.0
	1				ws					27.0	1	43.5	5.6	7.9					82	57		12.8
	2									0.68	2	11.8							18	12		0.3
22. 2-Butanone, $CH_3C(O)C_2H_5$[f,g]	0	17.0	11.6	7.7	4.6	2.7	1.1	—	45	62.8	0	12.5	9.2	13.4	9.0	8.4	4.7		—	57	ws	81.5
	1	19.4	13.2	9.1	1.5			79	43	32.4	1	27.8	2.0	4.2	0.8				82	35		17.1
	2	8.2	3.8					21	12	4.8	2	6.0	2.1						19	8		1.5
23. 3-Pentanone, $C_2H_5C(O)C_2H_5$[f,g]	0	18.6	12.5	8.2	5.0	2.8	1.1	—	48	62.8	0	14.3	10.7	15.1	10.1	9.4	5.2		—	65	ws	81.5
	1	25.4	13.5	2.2	0.5			81	42	32.4	1	20.5	3.2	5.7	0.4				86	30		17.1
	2	7.2	2.3					19	10	4.8	2	5.2							14	5		1.5
24. 2-Pentanone, $CH_3C(O)C_3C_7$[f]	0	22.0	14.9	9.8	6.0	3.6	1.4	—	58	62.8	0	15.6	11.6	16.7	11.3	10.8	6.1		—	72	ws	81.5
	1	20.6	11.3	4.1				85	36	32.4	1	17.1	4.5	2.3	0.8				88	25		17.1
	2	6.5						15	6	4.8	2	2.2	0.8						12	3		1.5
25. Formaldehyde, H_2CO	0	4.5	5.6	4.5	3.6	1.7	1.1	—	21	53.7	0	6.0	4.3	6.5	3.1	2.7	1.1	1.9	—	29	26 ± 4	75.9
	1	10.7	13.4	11.0	8.5	4.0		60	47	35.5	1	10.3	7.9	8.0	3.7	2.6	2.7	1.8	50	36	37	20.6
	2	12.2	9.5	5.3				34	27	10.4	2	14.9	8.2	4.8	3.0	3.9			47	33	35	3.3
	3	4.6						6	5	0.4	3	1.7	0.7						3	2	2	0.1
26. Acetaldehyde, $CH_3C(O)H$	0	5.7	5.9	4.9	3.5	1.7	1.3	—	23	55.1	0	4.0	3.4	4.0	3.4	3.7	3.5	3.1	—	28	25 ± 4	76.5
	1	12.9	13.4	11.2	8.1			59	46	34.9	1	14.1	5.9	10.7	2.7	2.6	3.1		52	38	39	20.3
	2	19.3	9.9					38	29	9.8	2	19.9	10.2	2.5	0.9				44	32	34	3.1
	3	2.2						3	2	0.2	3	1.7	0.7						3	2	2	0.08

[a] The data for the ketones are new; the results for H_2CO and $CH_3C(O)H$ were reported previously [18, 21].
[b] Population in v_3 or $v_{1,3}=0$ is neglected.
[c] $P_v(0)$ determined from extrapolation of linear surprisal plots; the least-squares uncertainty is generally $\pm$ 10–15%.
[d] Statistical prior distribution.
[e] $P_3(0)$ determined from fitting the HOD spectra in the 2500–2900 cm^{-1} region; the uncertainty is from fitting several spectra. The $v_{1,2}=0$ and 1 states of $v_3=0$ are dark states and populations of these states must be estimated; see text for details of each reaction.
[f] The bending distributions in $v_{1,3}=0$ and $v_3=0$ were taken to be the same as the statistical distributions.
[g] The $P_3(0)$ and $P_{1,3}(0)$ values may be too large because the surprisal plot ignored the smaller $\langle E_{av}\rangle$ corresponding to abstraction from CH_3; see text

α-methyl group in reactions (22) can be neglected, since the rate is expected to be similar to the rate of reaction (21) (the SAR gives a branching fraction of 7%). The maximum available energy for these reactions is determined by the CH_2 bond energy in the α-position. After the $2\,kcal\,mol^{-1}$ correction for the value given in [74], $\langle E_{av}\rangle = 27.7\,kcal\,mol^{-1}$, which is the same as for ethanol and dimethyl ether and $5\,kcal\,mol^{-1}$ higher than for acetone. The spectra from these reactions showed noticeably less $v_{1,3}$ or $v_3 = 2$ excitation than spectra from reactions (16) or (17). The surprisal calculations gave $\lambda_{v_{1,3}} = -1.6$, $\lambda_{v_3} = -2.8$ for reactions (22) and $\lambda_{1,3} = -1.3$, $\lambda_{v_3} = -2.0$ for reactions (23). The full distributions, Table 6, have less population in v_3 or $v_{1,3} = 2$ and higher *apparent* population in v_3 or $v_{1,3} = 0$ than the reactions with alcohols or simple ethers. The $\langle f_v\rangle$ values are about 0.40 with bending-to-stretch excitation ratios of $\sim$0.80. However, abstraction from the β-CH_3 group with $\langle E_{av}\rangle$ several $kcal\,mol^{-1}$ less than $27.7\,kcal\,mol^{-1}$ has not been taken into account, and the distributions from channels (*a*) and (*b*) need to be separated to gain further insight about reactions (22) and (23).

If channels (a) and (b) are direct abstraction, total vibrational distributions can be built as a superposition of distributions from reaction with ethyl ether (reactions (18)) and ethane (reactions (7)) using the SAR coefficients. For reactions (23), the calculated full distributions would be $P_{1,3}(0\text{–}2) = 28 : 56 : 16$ and $P_3(0\text{–}2) = 34 : 47 : 19$. These correspond to $P_{1,3}(1 : 2) = 77 : 23$ and $P_3(1 : 2) = 72 : 28$, which do not agree with the experimental $P_{1,3}(1 : 2) = 81 : 19$ and $P_3(1 : 2) = 86 : 14$ distributions. The $P_{1,3}(v_{1,3})$ distribution of D_2O from $OD + CD_3C(O)CD_2CH_3$, see section 3.2, show that abstraction from the methylene group is normal for a direct reaction; therefore, this comparison indicates that the methyl groups in the β-position must give less energy to the stretch mode and more to the bending mode than reactions with a 'normal' primary C–H bond. This expectation was proven by analysis of the HOD spectrum from $OD + CD_3C(O)CD_2CH_3$. Inspection of the spectra in figure 5 shows that reactions (22Da) plus (22Db) give more $v_3 = 2$ emission than does the HOD spectrum from $OD + CD_3C(O)CD_2CH_3$. Surprisal analysis of $P_3(1\text{–}2) = 90 : 10$ from reaction (22′D*b*) gave $\lambda_{v_3} = -3.8$ and $P_3(0\text{–}2) = 51 : 44 : 5$ with $\langle f_v(HOD)\rangle = 0.45$ and $\langle f_3\rangle = 0.54$ for abstraction from the β-methyl group. On the basis of the larger rate constants for reactions (22) and (23), relative to acetone, several laboratories have suggested that these reactions occur via a six- or seven-membered ring adduct [87, 112, 113]; the seven-membered H-bonded structure is currently favoured. The H_2O and HOD vibrational distributions from reactions (22b, 22Db) and (23b, 23Db) support the hypothesis that the reaction is not direct and an intermediate complex aids abstraction at the β-position.

Whatever the structure of this complex, its importance should increase for a CH_2 group in the β-position relative to a CH_3 group. To examine such a case we studied 2-pentanone:

$$OH\,(OD) + CH_3C(O)CH_2CH_2CH_3$$

$$\rightarrow H_2O\,(HOD) + CH_3C(O)CHCH_2CH_3 \qquad (24a, 24Da)$$

$$\rightarrow H_2O(HOD) + CH_3C(O)CH_2CHCH_3. \qquad (24b, 24Db)$$

According to the SAR equations, the branching ratio for (24*a*) : (24*b*) should be 18 : 76. The experiments were conducted for exactly the same conditions as for 3-pentanone. The HOD spectra from reactions (22) or (23) and (24) were clearly

different. The $P_{1,3}(1:2) = 85:15$ and $P_3(1:2) = 88:12$ distributions from (24) have less population in the second level than reactions (22) and (23). The surprisal calculations with $\langle E_{av}\rangle = 27.7\,\text{kcal mol}^{-1}$ give $\lambda^0_{1,3} = 0.78$, $\lambda_{v_{1,3}} = -0.5$ and $\lambda^0_3 = -1.14$, $\lambda_{v_3} = -1.2$. The full distributions are $P_{1,3}(0\text{–}2) = 58:36:6$ and $P_3(0\text{–}2) = 72:25:3$, and the energy disposal parameters are $\langle f_v\rangle = 0.35$ and $\langle E_{2v}\rangle/\langle E_{3v}\rangle = 1.3$. The $\langle f_v\rangle$ value probably is a lower limit, since the bond dissociation energy of the β-CH_2 group of 2-pentanone could be closer to the standard CH_2 bond dissociation energy in alkanes, which would give $\langle E_{av}\rangle \cong 25\,\text{kcal mol}^{-1}$. The low energy would lead to a steeper surprisal plot with lower $P_3(0)$ and $P_{1,3}(0)$ values, increased $\langle f_v\rangle$ and a bend-to-stretch ratio of 0.8–0.9. In any case, abstraction from the β-CH_2 group releases less vibrational energy to water than abstraction from an α-CH_2 group. These results support the claim for a seven-membered ring intermediate that aids the C–H abstraction process of reaction from β-CH_2 or β-CH_3 groups.

4.3.4. *Aldehydes*

Studies of formaldehyde and acetaldehyde have been reported [18, 21] together with the results for the secondary reactions of formyl and acetyl radicals with OH, H, NO_2 and NO. The secondary reactions proceed by recombination followed by unimolecular deoomposition. Abstraction from the CH_3 group of $CH_3C(O)H$ is negligible and the following are the primary reactions:

$$\text{OH (OD)} + CH_2O \rightarrow H_2O\,(HOD) + HCO, \qquad (25, 25D)$$

$$\text{OH (OD)} + CH_3C(O)H \rightarrow H_2O\,(HOD) + CH_3CO. \qquad (26, 26D)$$

The most recent determination [88] of $D_0(\text{HCO–H}) = 87.3 \pm 0.1\,\text{kcal mol}^{-1}$ is $0.7\,\text{kcal mol}^{-1}$ larger than recommended in [73]. This small adjustment causes no change in the previous analysis [18]. Reactions (25) and (26) were studied with either $[NO_2] \gg [H_2]$ or $[H_2] \gg [NO_2]$ so that secondary reactions of hydroxyl radicals with HCO or CH_3CO yielding water molecules were suppressed. The H_2O and HOD spectra gave decreasing distribution with $P_{1,3}(1\text{–}3) = 60:34:6$ and $59:38:3$ and $P_3(1\text{–}3) = 50:47:3$ and $52:44:3$ for reactions (25) and (26), respectively. The emission in the 2400–3000 cm^{-1} region of the HOD spectra was strong enough for simulation, which gave $P_3(0) = 26 \pm 4$ and 25 ± 4 for reactions (25) and (26D), respectively. These uncertainties are one-half of the population in the (0, 0, 0 and 0, 1, 0) states, which were assigned by analogy to the statistical distribution. The $P_{1,3}(v_{1,3})$ and $P_3(v_3)$ distributions in table 6 are the averages from four independent spectra.

The surprisal plots gave $P_{1,3}(0) = 21.2 \pm 3.9$ and $P_3(0) = 29 \pm 3$ for reaction (25) and $P_{1,3}(0) = 23.0 \pm 3.8$ and $P_3(0) = 28 \pm 3$ for reaction (26); these uncertainties are from the four independent distributions. The full HOD distributions, $P_3(0\text{–}3) = 29:36:33:2$ for reaction (25D) and 28:38:34:2 for reaction (26D), are in good agreement with the experimental values of $P_3(0)$. The average $\langle f_v\rangle$ values are 0.53 ± 0.02 for reaction (25) and 0.52 ± 0.02 for reaction (26), and the ratios of bending-to-stretch excitation are 0.52 and 0.47. These values and the slopes of the surprisal plots closely resemble those from the H_2S reaction, and the mechanism seems to be direct abstraction, as also indicated by the *ab initio* molecular dynamics simulation [115]. The second C–H bond of CH_2O and the O–H bond of the hydroxy radical appear not be be involved in the dynamics. The weak long-range interaction

Table 7. Vibrational distribution from reactions with sulphur-containing organic compounds.[a]

Reagent	H_2O										HOD											
	$v_{1,3}$	$v_2=0$	1	2	3	4	≥ 5	$P_{1,3}$[b]	$P_{1,3}$[c]	$P^0_{1,3}$[d]	v_3	$v_{1,2}=0$	1	2	3	4	5	≥ 6	P_3[b]	P_3[c]	P_3[e]	P^0_3[d]
27. Dimethylsulphide, CH_3SCH_3	0	9.0	11.7	5.7	2.8	1.3	0.4	—	31	61.3	0	6.2	1.9	6.2	1.9	3.2	2.2	3.5	—	33	25 ± 4	80.3
	1	13.8	18.1	8.9	4.2			66	45	32.8	1	23.7	3.4	10.7	7.7	2.6			64	43	48	17.9
	2	15.5	8.6					34	24	5.9	2	20.2	3.5	3.3					36	24	27	1.8
	P_2	38.3	38.4	14.6	7.0	1.3	0.4				$P_{1,2}$	50.1	8.8	20.2	9.6	5.8	2.2	3.5				
	P^0_2[d]	46.8	27.3	14.7	7.1	3.1	1.1				$P^0_{1,2}$[d]	27.4	18.1	23.3	13.6	10.7	4.8	2.1				
28. Diethylsulphide, $C_2H_5SC_2H_5$[f]	0	9.6	8.5	5.2	1.5	0.8	0.4	—	26	58.9	0	6.7	4.5	6.7	4.5	4.1	2.3	2.3	—	29	31 ± 5	79.1
	1	18.0	15.7	9.6	2.7			62	46	34.0	1	18.7	6.9	8.9	5.4	0.2			58	42	40	18.7
	2	23.1	4.0					36	27	7.1	2	24.4	2.4	0.8					40	28	28	2.2
	3	1.3						2	1		3	1.3							2	1	1	
	P_2	52.0	28.2	14.8	4.2	0.8	0.4				$P_{1,2}$	51.1	13.8	16.4	7.9	4.3	2.3	2.3				
	P^0_2[d]	45.2	26.7	15.0	7.8	3.6	1.9				$P^0_{1,2}$[d]	24.9	17.0	22.3	13.8	11.9	5.9	3.5				
29. Methyl mercaptan, CH_3SH	0	11.5	14.9	8.5	5.2	2.5	1.6	—	44	52.6	0	12.6	8.5	12.6	8.4	2.9	2.3	4.7	—	50	52 ± 5	74.8
	1	10.5	13.7	7.8	4.7	1.3		69	38	35.2	1	12.1	4.0	6.7	1.7	1.2	0.3		54	27	26	21.3
	2	8.9	6.6	0.5				28	16	11.5	2	15.3	2.6	1.7	0.6				42	21	20	3.8
	3	1.8						3	2	0.7	3	1.3	0.2						4	2	2	0.2
	P_2	32.7	35.2	16.8	9.9	3.8	1.6				$P_{1,2}$	41.3	15.8	21.1	10.7	4.1	2.6	4.7				
	P^0_2[d]	41.1	26.2	15.7	8.9	4.7	3.1				$P^0_{1,2}$[d]	21.4	15.4	21.3	13.8	13.0	7.3	7.1				

30. Ethyl mercaptan, C_2H_5SH	0	7.6	9.8	5.6	3.4	1.6	1.0	—	29	52.6	0	8.4	6.9	8.4	6.9	3.3	1.9	1.8	—	37	38 ± 4	74.8
	1	13.1	16.9	9.6	5.8	1.7		66	47	35.2	1	17.1	4.1	4.5	1.9	1.0			46	29	29	21.3
	2	10.9	8.3	0.8				29	20	11.5	2	20.2	4.0	6.6	0.7				50	32	31	3.8
	3	4.0						5	4	0.7	3	2.2							4	2	2	0.2
	P_2	35.6	35.0	16.0	9.2	3.3	1.0				$P_{1,2}$	47.9	15.0	19.5	9.5	4.3	1.9	1.8				
	$P_2^{0\,d}$	41.1	26.2	15.7	8.9	4.7	3.1				$P_{1,2}^{0\,d}$	21.4	15.4	21.3	13.8	13.0	7.3	7.1				

[a] The data for $(C_2H_5)_2S$ and C_2H_5SH have not been previously published. The distributions for DMS are those of [17]. The CH_3SH spectra were refitted for comparison with C_2H_5SH; however, the changes relative to those of [20] are insignificant. The $v_{1,2} = 0$ and 1 populations of $P_3(0)$ in this table were taken to be the same as those for $v_{1,2} = 2$ and 3.

[b] Population in v_3 or $v_{1,3} = 0$ is neglected.

[c] $P_v(0)$ determined from extrapolation of linear surprisal plots; the least-squares uncertainty is generally $\pm$ 10–15%.

[d] Statistical prior distribution.

[e] $P_3(0)$ determined from fitting the HOD spectra in the 2500–2900 cm^{-1} region; the uncertainty is from fitting several spectra. The $v_{1,2} = 0$ and 1 states of $v_3 = 0$ are dark states and populations of these states must be estimated; see text for details of each reaction.

[f] The emission from $v_{1,3}$ and $v_3 = 3$ provides strong support for a bond dissociation energy of the CH_2 group ≤ 92 kcal mol^{-1}. The round-off in the renormalization underestimates the $P_{1,3}(3)$ and $P_3(3)$ populations.

between the H atom of OH and the carbonyl oxygen [115] has no obvious effect on the energy disposal. The high-quality spectra from reactions (25) and (26) and the subsequent analysis reinforces the claim that the distributions from reactions (22)–(24) are abnormal for H atom abstraction from carbonyl compounds.

Two other models were used [18] for the prior distributions for reaction (25): model II included the rotational degrees of freedom of HCO and model III included all degrees of freedom of HCO (the HCO fragment is treated as an atom in model I). Models II and III gave $-\lambda_{v_{1,3}} = 5.5 \pm 0.9$ and 8.1 ± 1.0 and $-\lambda_{v_3} = 6.4 \pm 0.2$ and 8.3 ± 0.2 respectively. The $P_3(0) = 24 \pm 2$ and 21 ± 2 values are smaller than from model I. Just as for the H_2S example, the $P_3(0)$ values from the model I surprisal seem to match the experimental result.

4.4. *Reactions with sulphur-containing organic compounds*

The reactions of hydroxyl radicals with sulphur-containing compounds are of practical importance, because they are the initial steps in the oxidation of these substances in the troposphere [89–90, 121–125]. Two separate mechanisms have been recognized for $(CH_3)_2S$ (DMS), direct abstraction of H atoms and reversible addition of OH to the sulphur atom [122, 123]. The latter leads to products other than OH and DMS only in the presence of oxygen. In addition to reviewing the published work [17, 19, 20], new results from reactions with C_2H_5SH and $(C_2H_5)_2S$ are reported in table 7. The emphasis here will be on the difference in the vibrational distributions of water formed from sulphides vs. thiols. The rate coefficients for reactions (27–30) have been extensively studied, and recommended values are given in table 2 along with the available energies.

4.4.1. *Sulphides: CH_3SCH_3 and $C_2H_5SC_2H_5$*

The emission from

$$\mathrm{OH\,(OD) + CH_3SCH_3 \rightarrow H_2O\,(HOD) + CH_2SCH_3} \qquad (27, 27\mathrm{D})$$

was strong, even for reactant concentrations of $(4\text{–}6) \times 10^{13}$ molecules cm^{-3}. The stretching distribution of H_2O is $P_{1,3}(1:2) = 66:34$ and the bending distribution has a slight inversion for $v_{1,3} = 1$. The HOD stretching distribution is inverted; $P_3(0\text{–}2) = 25:48:27$. The surprisal plot for HOD gives $-\lambda_{v_3} = 4.9$ and $\lambda_3^0 = 0.55$, giving $P_3(0\text{–}2) = 33:43:25$. The H_2O surprisal plot gives $-\lambda_{v_{1,3}} = 2.8$; the intercept is $\lambda_{1,3}^0 = 0.30$, corresponding to $P_{1,3}(0\text{–}2) = 31:45:24$. These distributions give $\langle f_v(\mathrm{H_2O})\rangle = 0.50$ and $\langle f_v(\mathrm{HOD})\rangle = 0.52$ with $\langle E_{v_2}\rangle / \langle E_{v_3}\rangle = 0.48$. Although reaction (27) involves primary C–H bonds, the ratio of bend-to-stretch energies resembles those of H_2S, H_2CO ethanol and diethyl ether more than hydrocarbons.

Abstraction from the CH_2 group and the CH_3 group is possible from DES:

$$\mathrm{OH\,(OD) + C_2H_5SC_2H_5 \rightarrow H_2O\,(HOD) + C_2H_5SCH_2CH_2} \qquad (28a, 28\mathrm{D}a)$$

$$\mathrm{\rightarrow H_2O\,(HOD) + C_2H_5SCHCH_3.} \qquad (28b, 28\mathrm{D}b)$$

The C–H bond energy in the methyl group was assumed to be similar to that of the primary bond in alkanes, a value of ≈ 90 kcal mol^{-1} was assigned to the methylene group by Ekwenchi *et al.* [91]. The difference between the primary (DMS) and secondary (DES) bond energies for the CH_3 and CH_2 groups adjacent to the S atom is about 2.0 kcal mol^{-1}. This seems reasonable by analogy to ethers and $\langle E_{\mathrm{av}}\rangle = 30.5$ kcal mol^{-1} was used for reaction (28*b*), which will dominate the overall

reaction. The experimental distributions are $P_{1,3}(1\text{–}3) = 62 : 36 : 2$ and $P_3(0\text{–}3) = 31 : 40 : 28 : 1$. The linear surprisal plot for HOD has a slope of $-\lambda_{v_3} = 5.2$ and an intercept of $\lambda_3^0 = -0.68$, giving $P_3(0\text{–}3) = 29 : 42 : 28 : 1$ in good agreement with the measured $P_3(0) = 31$. The H_2O surprisal plot has a smaller slope, $-\lambda_{v_{1,3}} = 3.3$ with $\lambda_{1,3}^0 = -0.57$, giving the total distribution $P_{1,3}(0 : 1 : 2 : 3) = 26 : 46 : 27 : 1$. These distributions correspond to $\langle f_v \rangle = 0.48$ with $\langle E_{2v} \rangle / \langle E_{3v} \rangle = 0.35$.

4.4.2. *Thiols: CH_3SH (CH_3SD) and C_2H_5SH*

The reaction

$$\text{OH (OD)} + \text{CH}_3\text{SH} \rightarrow \text{H}_2\text{O (HOD)} + \text{products} \qquad (29, 29\text{D})$$

is eight times faster than the DMS reaction, and good spectra were obtained for conditions that avoid relaxation [17, 20]. Abstraction from sulphur can give v_3 and $v_{1,3} = 3$ and the distributions of table 7 have small populations in the third level, but the distributions are not inverted. The H_2O surprisal plot gave $-\lambda_{v_{1,3}} = 0.8 \pm 0.5$, an intercept of $\lambda_{1,3}^0 = 0.44 \pm 0.12$ and a total distribution $P_{1,3}(0\text{–}3) = 44 : 38 : 16 : 2$. The experimental distribution for HOD also shows a declining population; $P_3(0\text{–}3) = 52 : 26 : 29 : 2$. The surprisal analysis gave $\lambda_3^0 = -0.33 \pm 0.15$ and $-\lambda_{v_3} = 3.2 \pm 0.2$, with $P_3(0) = 50$. These distributions give $\langle f_v(\text{H}_2\text{O}) \rangle = 0.39$ and $\langle f_v(\text{HOD}) \rangle = 0.38$, with $\langle E_{2v} \rangle / \langle E_{3v} \rangle = 0.73$. The reduced $\langle f_v \rangle$, but enhanced bending excitation, of the vibrational distributions from CH_3SH relative to $(CH_3)_2S$ has been thoroughly documented in two separate studies [17, 20]; the difference is a consequence of the interaction of OH with the SH site in reaction (29).

A special study [20] was devised to determine the product branching from the reactions of OH and OD radicals with CH_3SD:

$$\text{OH} + \text{CH}_3\text{SD} \rightarrow \text{HOD} + \text{CH}_3\text{S} \qquad (29'a)$$

$$\rightarrow \text{H}_2\text{O} + \text{CH}_2\text{SD} \qquad (29'b)$$

$$\text{OD} + \text{CH}_3\text{SD} \rightarrow \text{D}_2\text{O} + \text{CH}_3\text{S} \qquad (29'\text{D}a)$$

$$\rightarrow \text{HOD} + \text{CH}_2\text{SD} \qquad (29'\text{D}b)$$

The spectra shown in figure 10 from $OH + CH_3SD$ display the overlapped H_2O and HOD emission in the 3200–3900 cm^{-1} range and the HOD emission in the 2400–2900 cm^{-1} range. The overlapped HOD and H_2O emissions were separated by simulating the HOD spectrum in a normal manner and adding the H_2O spectrum from $OH + CH_3SCH_3$. The distribution of HOD is $P_3(0\text{–}2) = 71 \pm 6 : 27 : 2$; the $P(v_3 = 0)$ component was obtained from simulation of the 2400–2900 cm^{-1} band of the spectrum. As expected, excitation of the 'passive' O–H vibration in reaction ($29'a$) was low, with 71% of the molecules in the ground $v_3 = 0$ state. This distribution is close to the statistical distribution, $P_3^0(0\text{–}2) = 75 : 21 : 4$.

The HOD emission in the 3200–3900 cm^{-1} range from $OD + CH_3SD$ shown in figure 10(*d*) clearly demonstrates abstraction from the methyl group. That part of the spectrum which extends to 4100 cm^{-1} is the 011–000 combination band emission from D_2O centred at 3965 cm^{-1} [55]. The HOD spectrum from reaction ($29'\text{D}b$) was assumed to be identical to that from $OD + CH_3SCH_3$ in order to separate the HOD and D_2O emission in the 3200–4200 cm^{-1} range. The HOD spectrum was normalized to match the least noisy spectrum from reaction ($29'\text{D}b$) in the 3200–3500 cm^{-1}

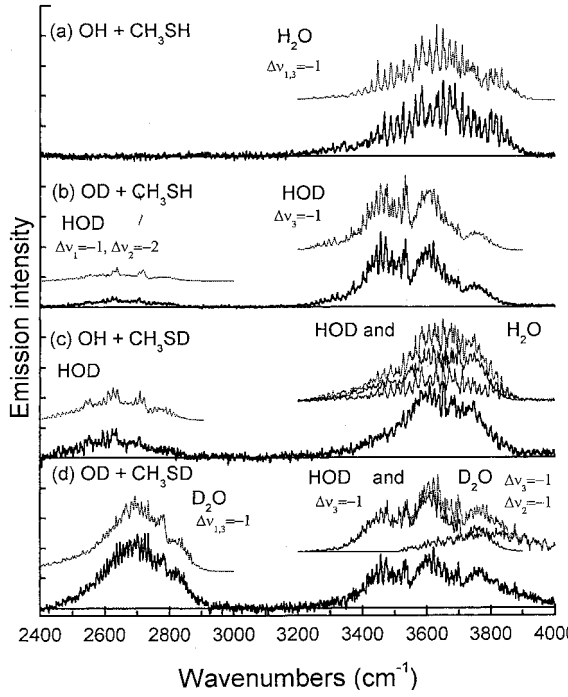

Figure 10. Comparison of emission spectra from OH (OD) with CH_3SH and CH_3SD. The branching between abstraction from carbon vs. sulphur is clearly demonstrated by the D_2O and HOD emission from the $OD + CH_3SD$ reaction. Comparison of the $\Delta v = -1$ emission of HOD in (b) and (c) illustrates the preferred excitation of ν_3 from $OD + CH_3SH$ and $\nu_{1,2}$ from $OH + CH_3SD$. The $\Delta v_3 = -1 + \Delta v_2 = -1$ combination band of D_2O also is observed in (d); the combination bands H_2O and HOD are discussed in [15]. The simulated spectra are plotted above the experimental and the individual and combined simulated spectra are shown for H_2O and HOD in (c) and HOD and D_2O in (D).

region and subtracted from the combined spectrum. The resulting spectrum was assigned to the combination $\nu_2 + \nu_3$ emission from D_2O. The D_2O stretching distribution obtained by simulation of the 2500–2900 cm^{-1} band is $P_{1,3}(1\text{–}3) = 65 : 32 : 3$. The relative areas associated with the D_2O and HOD emission intensities were measured in the 2400–2900 and 3200–3900 cm^{-1} ranges respectively to determine the product branching. The weak HOD emission in the 2400–2900 cm^{-1} range was neglected and that band was assigned to the $\Delta v_3 = -1$ transitions of D_2O. The average ratio was $I_{HOD}/I_{D_2O} = 1.12 \pm 0.22$ from seven experiments. The expermental intensity ratio was converted to the ratio of HOD to D_2O yields, using equation (E18) with $\beta = 0.41 \pm 0.03$ and $\beta_{HOD} = 0.90 \pm 0.05$; the result is $[HOD]/[D_2O] = 0.13 \pm 0.01$ for a branching fraction of 0.11 ± 0.04.

To determine the branching fraction for the $OH + CH_3SD$ reaction, the HOD emission intensity from five experimental spectra was obtained as the difference between the total integrated intensity in the 3200–4000 cm^{-1} range and the intensity of the H_2O contribution. The average $I_{H_2O}/I_{HOD} = 0.44 \pm 0.04$ ratio was converted to a branching fraction of 0.24 ± 0.08. Since the rate coefficients $(3.24 \pm 0.19) \times 10^{-11}$ and $(3.17 \pm 0.15) \times 10^{-11}$ cm^{-3} $molecule^{-1}\,s^{-1}$, were found for the $OH + CH_3SD$ and $OH + CH_3SH$ reactions are equal [121], a similar

branching ratio can be predicted for $OH + CH_3SH$ reaction. The 0.24 ± 0.08 value, which is more than twice as large as the branching fraction for reaction (29′D), was explained [20] as a large inverse secondary kinetic-isotope effect for reactions (29′*a*) and (29′D*a*), which proceed by an addition–rearrangement process.

Abstraction from the methyl group of ethyl mercaptan can be neglected, and only two competing channels are considered:

$$OH\,(OD) + C_2H_5SH \rightarrow H_2O\,(HOD) + C_2H_5S \qquad (30a, 30Da)$$

$$\rightarrow H_2O\,(HOD) + CH_3CHSH. \qquad (30b, 30Db)$$

$\langle E_{av} \rangle$ was assumed to be the same as that for CH_3SH. Simulations gave the following distributions: $P_{1,3}(1\text{–}3) = 66 : 29 : 5$ and $P_3(0\text{–}3) = 38 : 29 : 31 : 2$. The slight minimum for $P_3(2)$ suggests that both reaction channels are important: the high population for $v_3 = 0$ can be due to channel (30D*a*), whereas the large population for $v_3 = 2$ is from channel (30D*b*). The surprisal plot for HOD has $-\lambda_{v_3} = 4.0 \pm 0.3$ and $\lambda_3^0 = -0.24$, giving an overall distribution of $P_3(0\text{–}3) = 37 : 29 : 32 : 2$ in agreement with the measured $P_3(0) = 38$. The H_2O surprisal plot gives $-\lambda_{v_{1,3}} = 2.4 \pm 0.2$ and $\lambda_{1,3}^0 = -0.25$, with an overall distribution of $P_{1,3}(0\text{–}3) = 29 : 47 : 20 : 4$. These distributions correspond to $\langle f_v \rangle = 0.44$ with $\langle E_{2v} \rangle / \langle E_{3v} \rangle = 0.48$. The enhanced $\langle f_v \rangle$ and the reduced $\langle f_{v_2} \rangle$, relative to reaction (29), suggests that abstraction from the CH_2 group is competing with abstraction from the SH bond. As explained in the next paragraph, channels (29*a*) and (30*a*) are thought to involve mainly addition of OH radical to the sulphur atom followed by transfer of the hydrogen atom on sulphur to the oxygen atom of OH, rather than direct abstraction.

The larger rate constant for CH_3SH relative to H_2S and $(CH_3)_2S$ prompted Wilson and Hirst [126] to investigate the reaction by *ab initio* calculations; they concluded in favour of direct H atom abstraction from S–H, because this transition state was slightly lower in energy than the transition state for adduct formation. Since direct abstraction was inconsistent with the vibrational energy disposal results, Muiño [127] reinvestigated the $OH + CH_3SH$ system using a somewhat larger basis set, as was required [128, 129] to identify the $OH{\cdot}(CH_3)_2S$ adduct. A weakly bonded adduct ($3.3\,kcal\,mol^{-1}$ before consideration of zero-point energy) with the oxygen atom of the OH radical directed toward the sulphur atom of CH_3SH was identified [127], and a rearrangement pathway to products was characterized. Thus, the conclusions from the experimental vibrational distributions and the *ab initio* calculations are self-consistent, and an addition–rearrangement mechanism dominates over the direct abstraction pathway.

4.5. *Unimolecular decomposition of vibrationally excited ethanol and acetic acid*

Unimolecular dehydration is a reaction pathway for alcohols and acids. Infrared emission from water has been observed from the two-carbon members of both series, i.e. ethanol [11, 13] and acetic acid [14], that were formed with $\approx 100\,kcal\,mol^{-1}$ of vibrational energy from recombination of H atoms with CH_2CH_2OH and CH_2COOH respectively. The results from ethanol will be summarized here, but [14] should be consulted for acetic acid. The emission in the 3200–4000 cm^{-1} range shows that H_2O elimination is the dominant reaction for ethanol, as previously demonstrated by activation via multiphoton absorption of CO_2-laser irradiation [130]:

$$C_2H_5OH \rightarrow H_2O + C_2H_4 \quad (31)$$

$$CH_3CH_2OD \rightarrow HOD + C_2H_4. \quad (31D)$$

Ethanol was generated by a secondary reaction in the $H + CH_2ICH_2OH(D)$ reaction system. In addition to the experiments, *ab initio* calculations were done with the Gaussian G92 package with optimization at the MP2(FC)/6-31G(d) and MP2(FULL)/6-311G(d,p) levels to characterize the transition state and threshold energy ($67\,kcal\,mol^{-1}$). Rate constants calculated by RRKM theory for H_2O eliminations are larger than those for CH_3–CH_2OH or C_2H_5–OH bond rupture for energies $\leq 100\,kcal\,mol^{-1}$. The following reactions were studied from D atom recombination with $CH_2CH_2OH(D)$:

$$CH_2DCH_2OH \rightarrow H_2O + CHDCH_2 \quad (32a)$$

$$\rightarrow HOD + C_2H_4, \quad (32b)$$

$$CH_2DCH_2OD \rightarrow HOD + CHDCH_2 \quad (32Da)$$

$$\rightarrow D_2O + C_2H_4. \quad (32Db)$$

Spectra were recorded for $\Delta t = 0.4\,ms$ and Ar pressure of 0.8 Torr, and vibrational relaxation of H_2O, HOD or D_2O should be minimal. The $91\,kcal\,mol^{-1}$ of available energy permits excitation of ≤ 8 stretching levels; however, only 3 quanta of OH or 4 quanta of OD stretch excitation were observed.

Interpretation of the spectra from reactions (31D) and (31) was straightforward, and the distributions were $P_{1,3}(1–3) = 65 : 27 : 8$ and $P_3(1–3) = 79 : 16 : 5$. Analysis of the 2400–$2900\,cm^{-1}$ region provided the $P_3(0)$ component and the total $P_3(0–3)$ distribution is $60 : 32 : 6 : 2$. The $P_{1,3}(0)$ component for reaction (31) was assigned from consideration of the $P_3(0)/P_3(1)$ ratio, and the statistics for v_3 vs. $v_{1,3}$ excitation, and the total $P_{1,3}(0–3)$ distribution is $50 : 33 : 13 : 4$. Since the $v_3 = 0$ and $v_{1,3} = 0$ components constitute $\geq 50\%$ of the distributions with extensive bending excitation, it is important to note that $P_3(0)$ and $P_{1,3}(0)$ have experimental support. The bending distributions of H_2O and HOD are extended with emission observed from the highest levels that are in our models, and a strong inverse correlation exists between the stretching and bending excitation; see table 8. These distributions give $\langle f_v \rangle = 0.16$ and 0.14 for reactions (31) and (31D) respectively, with $\langle E_{2v} \rangle / \langle E_{3v} \rangle = 1.2$. Comparison with the statistical distributions show that H_2O or HOD from reactions (31) and (31D) acquired somewhat more than the statistical amounts of energy. The bending mode clearly has excess energy; however, the HOD data show that the new OH bond also has about one quantum of energy beyond the statistical expectation [13].

The H_2O and HOD contributions to the 3300–$3900\,cm^{-1}$ region from reactions (32) where deconvoluted by assuming that the water spectrum from reaction (32*a*) was the same as that from reaction (31), and the H_2O spectrum was subtracted from the combined H_2O and HOD band. Fitting the 2400–$2900\,cm^{-1}$ and the HOD $\Delta v_3 = -1$ spectra gave $P_3(v_{0–3})$ for reaction (32*b*) as $83 : 14 : 2 : 0.4$ with a broad $P_{1,2}(v_{1,2})$ distribution; see table 8. $\langle f_v(HOD) \rangle$ is 0.12, but with only 19% of the vibrational energy in the v_3 stretch mode. This greatly reduced fraction (from 41%) relative to HOD from reaction (31D) is a consequence of OH being the passive mode, i.e. the OH bond is the old bond for reaction (32*b*), and most of the energy release is to the $v_{1,2}$ modes with populations extending to $v_2 = 8$. The ratio of H_2O

Table 8. Vibrational distributions from the unimolecular decomposition of ethanol.[a]

	H_2O											HOD										
Reagent	$v_{1,3}$	$v_2=0$	1	2	3	4	5	≥ 6	$P_{1,3}$[b]	$P_{1,3}$[c]	$P^0_{1,3}$[d]	Reagent	v_3	$v_{1,2}=0$	1	2	3	4	5	6	≥ 7	P_3[b]	P_3[e]	P^{0d}_3
31. C_2H_5O	0	13.6	13.0	7.7	6.0	5.3	2.7	1.2	—	50	61.3	31. C_2H_5OD	0	20.2	8.6	13.0	3.4	4.6	1.9	3.8	4.2	—	60 ± 3	78.4
	1	9.3	8.9	5.1	4.0	1.8	3.5	0.8	65	33	27.7		1	11.7	5.0	6.0	2.5	5.3	1.1	0.4		79	32	17.3
	2	4.3	3.7	1.6	2.1	1.5	0.3		27	13	8.5		2	3.5	1.8	0.8	0.3					16	6	3.5
	3	1.1	2.2	0.6					8	4	2.0		3	0.7	0.7	0.5						5	2	0.7
	P_2	28.3	27.8	15.0	12.1	8.6	6.5	2.0					$P_{1,2}$	30.3	21.9	20.3	6.2	9.9	3.0	4.2	4.2			
	P^{0d}_2	47.9	25.3	13.4	6.9	3.6	1.8	0.9					$P^{0}_{1,2}$[d]	28.6	16.9	19.8	11.4	9.8	5.4	4.1	3.7			
32. CH_2DCH_2OD (D_2O)	0	5.7	8.9	6.4	6.1	3.2	4.6	5.1	—	40	44.2	32. CH_2DCH_2OH	0	16.5	16.5	21.2	9.5	6.0	3.8	4.2	6.0	—	83 ± 4	78.4
	1	3.6	5.6	4.0	3.9	2.1	2.9	3.2	41	25	31.2		1	4.5	2.6	4.5	0.5	1.0	0.5	0.1		83	14	17.3
	2	5.9	5.0	4.0	1.6	0.8			29	17	15.4		2	1.1	1.0	0.3						15	2.4	3.5
	3	6.5	4.0	3.5					23	14	6.5		3	0.4								2	0.4	0.7
	4	4.2							7	4	2.4													
	P_2	25.9	23.5	17.9	11.6	6.1	7.5	8.3					$P_{1,2}$	22.4	20.1	25.9	10.0	7.0	4.5	4.3	6.0			
	P^{0d}_2	38.0	24.3	15.4	9.7	6.1	3.7	2.6					$P^{0}_{1,2}$	28.5	16.8	19.8	11.4	9.8	5.4	4.1	3.9			

[a] These data are from [15]. In this table, the prior is the full statistical model that includes the degrees of freedom of C_2H_4. The $P_3(0)$ values of HOD were obtained from the spectra; the $P_{1,3}(0)$ values for H_2O and D_2O were obtained by analogy to the HOD distributions with consideration of the relation between distributions in v_3 vs. v_1+v_3 and the vibrational surprisals.

[b] Population in v_3 or $v_{1,3}=0$ is neglected.

[c] $P_v(0)$ determined from extrapolation of linear surprisal plots; the least-squares uncertainty is generally ± 10–15%.

[d] Statistical prior distribution.

[e] $P_3(0)$ determined from fitting the HOD spectra in the 2500–2900 cm^{-1} region; the uncertainty is from fitting several spectra. The $v_{1,2}=0$ and 1 states of $v_3=0$ are dark states and populations of these states must be estimated; see text for details of each reaction.

and HOD intensities gave a primary kinetic-isotope effect of 1.8 ± 0.4 for (32*a*) vs. (32*b*).

The HOD molecules from reaction (32D*a*) make a negligible contribution to the emission in the 2400–2900 cm^{-1} region, and analysis of the D_2O spectra from reaction (32D*b*) gave $\langle f_v \rangle = 0.16$ with 45% of the energy in the bending mode. The D_2O spectrum corroborates the results from reaction (31). The HOD spectrum from reaction (32Da) was nearly identical to that of reaction (31D). From the ratio of HOD and D_2O intensities, the primary kinetic-isotope effect for reactions (32D*a*) and (32D*b*) was estimated as 1.4 ± 0.3.

The vibrational distributions for H_2O formed from unimolecular decomposition of acetic acid, which also proceeds via a four-membered state, is similar to that of reaction (31) with $\langle f_v \rangle \cong 0.23$ and with extended bending excitation. Since only H_2O spectra from CH_3COOH were obtained, the $P_{1,3}(0)$ contribution was estimated by extrapolation. We have confidence in the results of table 8 as being representative of unimolecular four-centred H_2O elimination reactions from stable molecules with high threshold energies. An interesting point is that the sum of $\langle f_{v_3} \rangle$ and $\langle f_{v_2} \rangle$ is close to unity, which implies that the old OH bond is more of a spectator for the elimination reactions than is the case for OH + HI or GeH_4.

5. Discussion

5.1. *Infrared chemiluminescence from water—general aspects*

Bernath [131] has reviewed recent developments in the field of infrared emission spectroscopy. Our own work based on the chemiluminescence observed from chemical reactions in a fast-flow reactor with an FT spectrometer plus an InSb detector illustrates how reaction kinetics and dynamics can be inferred from emission spectra of triatomic, as well as diatomic, product molecules. In this programme, we have analysed emission from HCN, HNC, HNO, CO_2, COS and the three isotopic molecules of water. Except for OCS [9], the anharmonic shifts are sufficiently large that vibrational distributions in the ν_1 and ν_2 modes could be obtained from the strong $\Delta v_3 = -1$ spectra. Rotational relaxation of the product molecules in the flow reactor generally is complete except for reactions giving HF [7, 35, 95, 132]. The partial pressures of the Ar carrier gas and the reagent should be varied to ascertain the degree of vibrational relaxation. Except for the collisional coupling between ν_1 and ν_3 levels of H_2O and ν_1 and ν_2 levels of HOD, the vibrational relaxation of H_2O and HOD was not important for the shortest reaction times and Ar pressure ≤ 0.5 Torr, and the reported results should be close to nascent distributions. Our spectral simulation model is based on the best available spectroscopic data for H_2O, HOD and D_2O. Nevertheless, simulations are never as reliable as direct measurements; the Einstein coefficients for the combination levels are probably the least reliable part of the model. In general, the stretching distributions should have uncertainties of $\pm 10\%$; the bending distributions are less reliable because of the difficulty of assigning populations to the ν_3 and $v_{1,3} = 0$ levels, which have high bending excitation. These uncertainties also affect product branching ratios that are based on the relative integrated intensities.

The opportunity to observe emission from H_2O, HOD and D_2O from the same chemical reaction makes the study of water-forming reactions unusual in several ways. By combining information deduced from the spectra of H_2O and HOD, vibrational energy distributions in the new bond, the old bond and in the bending

mode can be inferred. Also, the two independent spectra, plus the spectra from D_2O, provide a consistency check of the results for a given reaction. With the current interptetation of the OH (OD) + HCl reactions, no evidence exists, nor was any expected, for an isotope effect on the energy disposal pattern. The emission spectra from the OD stretch mode of HOD, $\Delta v_1 = -1$, provides relative populations in $v_3 = 0$ and 1 levels. These experimental $v_3 = 0$ populations of HOD confirm the $P_3(0)$ values deduced from the intercepts of vibrational-surprisal plots of the $P_3(v_3 \geq 1)$ distribution, which was assigned from the $\Delta v_3 = -1$ spectra. Therefore, linear surprisal plots could be used with confidence to assign the $v_{1,3} = 0$ population of the $P_{1,3}(v_{1,3})$ distribution of H_2O. These first-generation data derived from steady-state emission spectra can be augmented in the future by experiments at higher resolution, by time-resolved emission studies [131, 133], and by high-resolution absorption measurements [38, 134] at low pressure to measure rotational energy distributions.

Vibrational distributions of products are useful for identification of overall reaction mechanisms, as well as for studies of microscopic reaction dynamics. For example, inverted vibrational distributions of HF and HCl that extend to the thermochemical limit identify H atom abstraction by F or Cl atoms [35]. On the other hand, abstraction of F or Cl by an attacking H atom gives narrow, inverted, HF and HCl vibrational distributions that do not extend to the thermochemical limit [6, 45, 135]. Monotonically declining distributions with small $\langle f_v \rangle$ are signatures for unimolecular HF or HCl elimination from vibrationally excited molecules [7, 136, 137]. Comparison of the numerous examples given in this review for direct H atom abstraction by OH radicals and with the distributions from unimolecular elimination of H_2O from ethanol and acetic acid show that these trends in energy disposal patterns exist for water-forming reactions too. In fact, this criterion was the basis for assigning addition–rearrangement mechanisms to the reactions of OH with HI, GeH_4, CH_3SH and C_2H_5SH. Although D(H–CO) and D(H–CH_2CO) are quite low, both radicals react with OH by recombination followed by H_2O elimination rather than by H atom as judged by the low $\langle f_v(H_2O) \rangle$ and declining populations for higher vibrational levels [18, 21].

Since atom + radical or OH + radical reactions have fast rates, secondary reactions can be observed in the flow reactor for high concentrations of reactive atoms of hydroxyl radicals. One interesting secondary reaction, NO + HCO, gave a strong HNO spectrum [10]. The reaction of OH radicals with dimethyldisulphide [138] gave surprising results. Since the observed spectra were identical with that from the CH_3SH reaction, the following mechanism was suggested:

$$OH + CH_3S_2CH_3 \rightarrow CH_3SH + CH_3SO,$$

$$CH_3SH + OH \rightarrow H_2O + CH_3S.$$

The mechanism was proven by the OD reaction, which gave spectra that were identical to those from OD + CH_3SD. The primary step has such a large rate constant $(2.0 \pm 0.3) \times 10^{-10}$ cm^3 molecule^{-1} s^{-1}) that strong emission from the secondary step was easily observed. In some cases, IRCL from flow reactors provides a way to identify secondary reactions that may be difficult to observe by other means.

Table 9. Summary of energy disposal for water producing reactions.

Reagent	$\langle E_{av}\rangle^a$	$-\lambda_{1,3}{}^b$	$-\lambda_{v_3}{}^b$	$\langle E_{vib}\rangle$		$\langle f_v\rangle^c$		$\langle f_{v_2}\rangle^d$	$\langle f_{v_3}\rangle^e$	$\langle E_{v_2}\rangle/\langle E_{v_3}\rangle$
				H_2O	HOD	H_2O	HOD			
1. HBr	33.6	4.5	6.1	20.8	20.3	0.62	0.60	0.31	0.62	0.50
2. H_2S	32.1	3.9	5.5	18.3	18.5	0.57	0.57	0.28	0.70	0.40
3. HI	49.8	−0.9	0.2	18.3	18.7	0.37	0.38	0.47	0.30	1.57
4. GeH_4	38.4	1.5	3.5	18.1	17.6	0.47	0.45	0.43	0.42	1.0
5. HCl	18.7				≈10.0		≈0.54		≈0.83	
6. NH_3	15.6	5.2	5.6	≈8.7	≈8.8	≈0.54	≈0.55	≈0.18	0.77	≈0.23
7. C_2H_6	23.1	4.5	5.5	11.7	10.8	0.51	0.47	0.17	0.81	0.21
8. neo-C_5H_{12}	22.4	4.8	5.6	11.3	10.2	0.50	0.46	0.16	0.80	0.20
9. cyclo-C_5H_{10}	25.1	4.4	6.2	14.3	13.3	0.57	0.52	0.22	0.85	0.26
10. cyclo-C_6H_{12}	24.6	4.6	6.2	14.0	13.1	0.57	0.53	0.21	0.84	0.25
11. *n*-C_4H_{10}	24.7	4.6	6.4	14.7	14.7	0.59	0.58	0.23	0.78	0.29
12. *n*-$C_{10}H_{22}$	24.7	4.5	6.3	14.5	13.4	0.58	0.53	0.22	0.85	0.26
13. iso-C_4H_{10}	25.5	4.5	6.3	14.7	13.7	0.58	0.52	0.20	0.85	0.24
14. 2,2,4-Trimethylpentane	23.5	4.6	6.0	12.7	12.3	0.54	0.52	0.19	0.83	0.23
15. CH_3OH	26.8	2.8	4.4	11.9	11.6	0.44[f]	0.43[f]	0.29	0.66	0.44
16. C_2H_5OH	27.4	2.8	4.9	13.1	13.1	0.48	0.47	0.31	0.71	0.44
17. CH_3OCH_3	27.6	2.7	4.8	12.4	13.1	0.45	0.47	0.28	0.69	0.41
18. $C_2H_5OC_2H_5$	28.2	2.6	5.0	13.2	13.0	0.47	0.46	0.33	0.73	0.45
19. $CH_3OCH_2OCH_3$	26.9	1.8	3.2	11.1	10.9	0.41	0.40	0.35	0.57	0.61
20. $CH_3OC_2H_4OH$	28.2	2.2	4.0	12.1	12.0	0.43	0.42	0.32	0.63	0.51

21. $CH_3C(O)CH_3$	22.7	—	5.5	—	11.3		0.49	—	0.75	—
22. $CH_3C(O)C_2H_5$[g]	27.7	1.6	2.8	11.3	10.6	0.41	0.38	0.38	0.51	0.75
23. $C_2H_5C(O)C_2H_5$[g]	27.7	1.3	2.0	10.2	10.2	0.37	0.36	0.36	0.42	0.86
24. $CH_3C(O)C_3H_7$	27.7	0.5	1.2	9.3	9.7	0.34	0.35	0.45	0.34	1.3
25. CH_2O	33.2	3.2	5.1	18.0	18.3	0.54	0.55	0.33	0.64	0.52
26. $CH_3C(O)H$	32.6	3.3	4.9	16.4	17.7	0.50	0.54	0.31	0.66	0.47
27. CH_3SCH_3	28.9	2.8	4.9	14.3	15.2	0.50	0.52	0.30	0.63	0.48
28. $C_2H_5SC_2H_5$	30.5	3.3	5.2	14.2	14.9	0.47	0.48	0.24	0.69	0.35
29. CH_3SH	34.4	0.8	3.2	13.3	13.2	0.39	0.38	0.41	0.56	0.73
30. C_2H_5SH[h]	34.4	2.4	4.0	15.3	14.9	0.45	0.43	0.33	0.68	0.48
31. C_2H_5OH[i]	90.9			14.9	—	0.16		0.51	—	
31D. C_2H_5OD[i]	92.6			—	12.4	—	0.14	—	0.42	1.20
33. $CH_3C(O)OH$[i]	61			14.5		0.23		0.57	—	

[a] In kcal mol^{-1}; the $\langle E_{av} \rangle$ values for OD reactions are 0.3 kcal mol^{-1} higher because of zero-point energy changes. For reactions with multiple pathways $\langle E_{av} \rangle$ is listed for the most exoergic path; see text for discussion of contributions from different pathways.
[b] Internal degrees of freedom of the product radical were ignored in the calculation of prior distribution (except for reactions (31), (31D) and (33)).
[c] $\langle f_v \rangle = \langle E_v \rangle / \langle E_{av} \rangle$; [d] $\langle f_{v_2} \rangle = \langle E_{v_2} \rangle / \langle E_{vib} \rangle$; [e] $\langle f_{v_3} \rangle = \langle E_{v_3} \rangle / \langle E_{vib} \rangle$.
[f] These values increase to 0.45 if the contribution from abstraction at the OH site is removed.
[g] These $\langle f_v \rangle$ values are probably too low, because $\langle E_{av} \rangle$ from abstraction from the methyl groups was ignored in the surprisal plots; see text for separation of reaction channels.
[h] The higher $\langle f_v \rangle$, relative to CH_3SH, may be a consequence of the contribution from reaction with the CH_2 group.
[i] Unimolecular reactions.

5.2. *Energy disposal patterns with comparison to HF-forming reactions*

Each reaction was discussed in detail in section 4, and a summary of the energy disposal is given in table 9. The goal here is to provide an overview for the energy disposal from H atom abstraction reactions by OH(^{2}II) radicals. Numerous *ab initio* calculations [27–31, 98, 101, 106, 108] have established the similarity of the transition states for direct H atom abstraction reactions; the transition state is located in the early part of the entrance channel with the half-filled p orbital of OH′ directed toward the H atom and the H–O–H′ angle is close to the equilibrium value of H_2O. For the reactions considered here, the potential energy barriers decline from $\sim 2\,\text{kcal mol}^{-1}$ for primary C–H bonds to cases with no barriers, and even cases with weakly bound adducts in the entrance channel. On the other hand, the exoergicity of the reaction is released in the exit channel as the new O–H bond is formed. The radical fragment and the water molecule then separate. The potential energy surfaces closely resemble those for H atom abstraction reactions by F, Cl or O atoms with the added complexity that the new bond of H_2O is associated with formation of a triatomic molecule, which has a second stretch mode and a bending mode. Since the H atom is transferred between two heavy centres, the dynamics of OH-radical abstraction reactions is subject to the established kinematic restraints associated with the **H′–L–H** mass combination [1, 35–37, 44]. In this discussion we will use the vocabulary associated with quasi-classical trajectories on a repulsive-type potential energy surface, even though tunnelling seems to be important according to some models of the transition-state theory [27–31].

The fraction of the total energy released as vibrational energy of water in H atom abstraction reactions ranges from 0.62 (HBr) to $\sim$0.55 for several reactions (H_2S, hydrocarbons with secondary C–H bonds, $(CH_3)_2S$ and CH_2O), to $\sim$0.50 for hydrocarbons with primary C–H bonds and down to 0.40–0.45 for several oxygen-containing organic molecules. The $\langle f_v(H_2O)\rangle$ values for abstraction of H atoms from the CH_3 group of methyl amines seem to be similar to that of alcohols and ethers [139]. The global vibrational energy release, $\langle f_v(H_2O)\rangle$, is generally very close to the $\langle f_v(HF)\rangle$ values for F atoms reacting with the same reagent [34, 35], and the dynamics for H atom abstraction by F atoms is a useful starting point for understanding the vibrational energy disposal by OH radical reactions. A few reactions (H_2S and CH_3SCH_3) seem to have slightly higher $\langle f_v(H_2O)\rangle$ than $\langle f_v(HF)\rangle$, but for these two examples the F atom reactions may be the anomalous ones. The more numerous examples for which $\langle f_v(H_2O)\rangle$ is slightly lower than $\langle f_v(HF)\rangle$ are mainly oxygen-containing organic molecules, which have attractive interactions between H_2O and either an acidic H atom or basic oxygen atom in the radical fragment. These direct H atom abstraction reactions give inverted HF (v) and H_2O (v_3 or $v_{1,3}$) distributions and, with inclusion of bending energy of the water molecules or rotational energy of the HF molecules, the product energy distributions extend to the thermochemical limits. Since $\langle f_R(H_2O)\rangle$ is expected to be $\leq$0.10 by analogy with F atom reactions [35] and since the radical fragment receives little energy [95], the fraction of energy released as relative product translational motion is expected to be $\approx$0.4–0.5 for the H atom abstraction reactions by OH radicals. Although HF should share the propensity with H_2O for hydrogen-bonding-type attractive interactions with the radical fragment in the exit channel, the OH radical also can have attractive interactions in the entrance channel, as exhibitied by the seven-membered adduct of OH and ketones with β-CH_2 or β-CH_3 groups. On the basis of the difference in energy disposal, the mechanism for OH interacting with HI,

GeH_4 and CH_3SH clearly differs from that of F atoms reacting with these molecules. Thus, a direct analogy between F atom and OH reactions is not always applicable.

Another measure of vibrational energy disposal is the vibrational surprisal. The HF and DF vibrational distributions follow linear surprisals for priors in which the radical fragment was treated as an atom or the rotational degrees of freedom of the radical were included [34, 35]. With improved D(C–H) for several reagents, linear surprisal plots for HF(v) distributions are actually now more general without the need to restrict the available energy in the prior [34]. The estimate for $P_v(0)$ from extrapolation of the surprisal plots [35] for $F + CH_4$ has now been confirmed by experimental measurement of the HF($v = 0$) population [38]. The slopes of the HF vibrational surprisal plots are typically ($\lambda_v = -5.0 \pm 0.5$) for the three-body prior. The surprisal plots for the $P_{1,3}(H_2O)$ and P_3(HOD) distributions from direct abstraction also are linear and with slopes of $\sim(-4.0)$ and $\sim(-5.5)$ for H_2O and HOD respectively; see table 9. Since the priors and the $P_{1,3}(v_{1,3})$ and $P_3(v_3)$ distributions for the OH and OD reactions differ from each other, as well as those of F atom reactions, the slopes of these surprisal plots cannot be directly compared. However, the commonality of the linear surprisal plots reflects the similarity of the dynamics associated with the vibrational energy release to the stretching modes of water and to HF. The above analysis and the trajectory calculations for OH + HR reactions [32, 115] show that the vibrational energy is released as the new O–H bond is formed. However, the OH reactions have an important additional component, relative to F atom reactions, namely the energy released to the bending mode of water, which is both significant and variable. Understanding the release of energy to the bending mode of H_2O requires a major extension of the models used to describe F atom reactions. Nothing is currently known about the rotational energy distributions of water, and hence no comparison can be made with the rotational distributions of HF; the $\langle f_R(HF)\rangle$ values are usually small, ≤ 0.10, but they do increase to ≈ 0.15 for cases with very large reaction cross-sections. The larger $\langle f_R(OH)\rangle$ from O + HBr vs. O + HR reactions has been explained [36, 37] by the angular dependence of the potentials, i.e. the potential barrier increases more sharply for O–H–R than for O–H–Br with deviation from collinearity. The trend in $\langle f_R(HF)\rangle$ just noted with reaction cross-sections could also be explained by this argument.

For the **H′**–**L**–**H** category of atom transfer reactions in which the light atom is hydrogen, the transfer of the hydrogen atom to the attacking **H′** atom occurs very rapidly (and gives the characteristic corner-cutting trajectory on the highly skewed potential surface). It has been argued that this transfer is so rapid that the nuclear coordinates inside the polyatomic R group would not change from their equilibrium positions in the R–H molecule. If this is the case, the vibrational energy associated with relaxation (or reorganization [100]) of the R group will not be released to HF. The best evidence for this claim is the failure of HF(v, J) distribution to extend to the themochemical limit for reaction with C_6D_5–CH_3 and CH_3CHCH_2, because of the resonance stabilization energy of $C_6H_5CH_2$ and CH_2CHCH_2 radicals [140, 141]. The $CD_3C(O)H$ and CH_3OCH_3 + F atom reactions also may exhibit the effect of a small radical stabilization energy [141]. The low $\langle f_v(HF)\rangle$ and the failure of the HF (v, J) distributions to extend to the thermochemical from $F + N_2H_4$ may be a consequence of a very large organization energy of N_2H_3 [142]. The only OH radical reactions that can be examined for comparison are those with $CH_3C(O)H$ and CH_3OCH_3. The latter shows some evidence for an effect of a radical stabilization

energy, since $\langle f_v(H_2O)\rangle$ is less than for hydrocarbons of the same $\langle E_{av}\rangle$ and the distribution does not extend to the thermochemical limit. Within the uncertainty limits the results from $OH + CH_3C(O)H$ and CH_2O are the same, although a small contribution from abstraction at the CH_3 site could distort the comparison.

The $OH + H_2$ reaction has been a favourite target for theoretical models and kinetic studies [143]. However, the low available energy ($\sim 18\,kcal\,mol^{-1}$) and small rate constant render it unattractive for IRCL experiments. Crossed molecular-beam experiments [143] show that backwards scattering of H_2O is preferred. Although the results are not nearly as detailed as the extraordinary experimental and theoretical efforts with the $F + H_2$ reaction [134, 144], the overall pattern of the reactive scattering for $OH + H_2$ strongly resembles the $F + H_2$ reaction. An interesting subject for future investigations will be the reactivity of the $OH(^2\Pi_{1/2})$ excited ($140\,cm^{-1}$) spin–orbit state in abstraction reactions. Recent studies of $Cl(^2P_{1/2}) + H_2$ [145] and $F(^2P_{1/2}) + H_2$ [134] reactions find that the reactivity is higher than expected, because of non-adiabatic coupling of ground- and excited-state potentials. The reactive quenching of $OH(A\ ^2\Sigma^+)$ by H_2 also is relevant to understanding the excited-state potentials [146] of the $O + H_2$ system. Rotational alignment information [37, 147] about the H_2O product would assist in understanding the dynamics of water-forming reactions.

According to the principle of microscopic reversibility, the large $\langle f_v(H_2O)\rangle$ for the abstraction reaction implies that vibrational energy in H_2O would promote the reverse reaction. One must remember that $\langle f_T(H_2O)\rangle$ is 0.5–0.4 and a combination of both translational and vibrational energy in H_2O should be the most effective for promoting the reverse reaction. Experiments by Zare and coworkers [148] and by Crim and coworkers [149–150] have demonstrated enhancement of the endoergic reaction rates of H atoms and Cl atoms with H_2O and HOD by excitation of high overtone stretch levels of H_2O and HOD. Furthermore, excitation of the OH or OD modes of HOD provides control (a factor of 200) over the product branching for the $H + HOD$ reaction [148, 150]; the degree of control is less for Cl atom than for H atom reactions. Crim and coworkers [149, 151] found that the relative rates of reaction of Cl with the isoenergetic states of H_2O with 4 quanta of stretch excitation vs. 3 quanta of stretch and 2 quanta of bend were the same. On the other hand, the rate of reaction for 3 quanta of stretch vs 2 quanta of stretch and 2 quanta of bend were three times higher if all the energy was in the stretching state. The authors conclude that bend excitation is less efficient than stretch excitation near the threshold energy but equally efficient at higher vibrational energies. Bending excitation does play a role in promoting the reverse reaction, as would be expected from the energy disposal results. Smith and coworkers [152] have reported absolute rate constants for removal of $H_2O\,(04^-)$ molecules by H atoms, $(4.9 \pm 0.6) \times 10^{-10}$, and, for relaxation, $(2.2 \pm 0.2) \times 10^{-10}\,cm^3\,molecule^{-1}\,s^{-1}$, by collisions with H_2O. Examination of a representative water-forming reaction in both the forward and the reverse directions would provide an opportunity to understand selective energy disposal and energy consumption.

The overall vibrational energy disposal by the unimolecular HF and H_2O elimination reactions of C_2H_5F and C_2H_5OH are nearly the same, because the thermochemistry, transition-state structures and kinematics are very similar. The $\langle f_v(H_2O)\rangle$ value, 0.15–0.20, is much smaller than for H atom abstraction reactions by OH radicals, because the H atom first migrates to the F (or OH) moiety and subsequently HF (or H_2) recoils from the olefin as the repulsive potential energy is

released. According to our analysis, 17% and 24% of the potential energy is released to HF and H_2O from decomposition of C_2H_5F and C_2H_5OH [13]. Although the $\langle f_v(HF)\rangle$ and $\langle f_v(H_2O)\rangle$ values are nearly the same, slightly more than one-half of the vibrational energy of water is in the bending mode, and the dynamics for the H_2O elimination is more complex. The recent measurement [153] of $\langle f_T(H_2O)\rangle \cong 0.4$ from the infrared multiphoton dissociation of acetic acid is higher than an older measurement of $\langle f_T(HCl)\rangle = 0.20$ from CH_3CCl_3 [154]. Although the vibrational energy released to HX or H_2O seems rather generic in unimolecular elimination reactions [7, 13, 136, 137], the division of energy between translational motion and the internal energy of the olrefin may depend on the reaction. Substantial rearrangement of the internal coordinates must occur as the trajectory passes from the transition state to $C_2H_4 + H_2O$ products [13, 155].

5.3. *Bending mode vs. stretch modes of water as energy acceptors*

Vibrational distributions were assigned for bimolecular, direct hydrogen atom abstraction reaction by OH radicals, for bimolecular hydrogen atom abstraction reactions involving weakly bound OH·RH adducts and for truly unimolecular H_2O elimination reactions from stable molecules. Inspection of table 9 shows that the fraction of the vibrational energy in bending excitation ($\langle E_{v_2}\rangle/\langle E_{vib}\rangle = \langle f_{v_2}\rangle$) varies from 0.16 to 0.57. On the basis of the $\langle f_{v_2}\rangle$ values in table 9, the reactions can be placed in four broad categories: hydrocarbons (and NH_3) with $\langle f_{v_2}\rangle = 0.20 \pm 0.02$; HBr, H_2S, alcohols, ethers, aldehydes and $(CH_3)_2S$ with $\langle f_{v_2}\rangle = 0.30 \pm 0.02$; the third group with $\langle f_{v_2}\rangle = 0.35$–$0.41$ includes CH_3SH, C_2H_5SH and most ketones; the last category with $\langle f_{v_2}\rangle \geq 0.42$ includes the unimolecular H_2O elimination reactions plus GeH_4 and HI. The $\langle E_{v_2}\rangle/\langle E_{v_3}\rangle$ ratios naturally fall into the same four categories: 0.20–0.29, 0.40–0.52, ~ 0.75, and 1.0–1.6. The sum of $\langle f_{v_2}\rangle$ and $\langle f_{v_3}\rangle$ is approximately unity for the first two categories, although the sum seems slightly lower for the second category. The sum is 0.8–0.9 for the ketones and 0.93 for the thiols. The sum is only 0.80 for HI and GeH_4, suggesting that the new and old bonds are both involved in the dynamics. However, for elimination of H_2O from ethanol $\langle f_{v_3}\rangle + \langle f_{v_2}\rangle$ is 0.93, indicating that the old O–H bond only marginally participates in the dynamics. No obvious correlation seems to exist between $\langle f_{v_2}\rangle$ and the magnitudes of the OH + RH rate constants or the available energy of the reaction. The partitioning of energy between bending and stretch excitation of water, as well as the allocation of energy between $E_{vib}(H_2O)$, $E_R(H_2O)$ and $E_T(H_2O + R)$, must be related to the dynamics on the potential energy surface. This discussion above could be made in terms of $\langle E_{v_2}\rangle/\langle E_{av}\rangle$, the fraction of the total available energy in bending excitation; the $\langle f_{v_2}\rangle$ values in table 9 can be mutiplied by $\langle E_{vib}\rangle/\langle E_{av}\rangle$ to obtain the overall fraction in bending excitation.

A quasi-classical trajectory calculation [32] for a semi-empirical potential surface designed to represent the OH + HBr reaction provides some guidance. The extensive series of papers by Persky and coworkers [156, 157], which illustrates the relation between the potential energy surfaces and the reaction dynamics for $\mathbf{H'} + \mathbf{L}$–$\mathbf{H}$ triatomic systems, provides an excellent background, and the *ab initio* potentials that include the spin–orbit states for the O + HBr reaction also are instructive [158]. The trajectory calculations for OH + HBr were done with Clary's potential [40], which was constructed from extended LEPS-type interactions for the O–H–Br bonds being formed and broken plus a realistic potential for water and a switching function. Variational transition state and the trajectory calculations [32] of the rate constant

based on the entrance channel properties of this potential were in modest accord with the experimental rate constants [71, 72, 92] from 300 to 500 K. Since the potential did not have reliable long-range interactions between HBr and OH, the calculated rate constants below 300 K increased less rapidly than the experimental results. The LEPS part of the potential could be adjusted in the usual way [156, 157] to obtain qualitative agreement with the experiment $\langle f_v(H_2O)\rangle$. Although the calculation did show an inverse correlation between stretch and bend excitation of H_2O, the calculated $\langle f_{v_2}\rangle$ value was too low by a factor of 2. Furthermore, the parameters of the potential could not be adjusted to change the $\langle f_{v_2}\rangle$ value. Since the H–O–H′ angle is near the equilibrium position of H_2O at the transition state for the HO + H′Br potential (and for most other reactions), the change in this angle from transition state to products seems not to be an important mechanism for release of energy to bending motion for thermal reaction conditions. This also seems true for the unimolecular reactions, because the H′–OH angle in the transition state for the ethanol reaction was just slightly larger than the equilibrium angle of water, yet $\langle f_{v_2}\rangle$ is larger than $\langle f_{v_3}\rangle$. Inspection of the OH + HBr trajectories [32] suggested that one mechanism for acquiring bending excitation was the transfer of energy from the newly formed bond to bending excitation during traversal of the exit channel. Since a two-for-one near resonance exists between bend and stretch modes, repulsive interaction between H_2O and Br in the exit channel seem to convert stretch energy to bending energy. In fact, the calculated results for the OH + HBr potential surface actually do match the bend-to-stretch ratio and $\langle f_v(H_2O)\rangle$ for the reactions of OH with hydrocarbons. Excluding cases with possible adduct formation in the entrance channel, the trend of increasing $\langle f_{v_2}\rangle$ in the first three categories seems to correlate with increasing attractive interactions between the R fragment and H_2O. These attractive interactions could enhance the intrinsic tendency for flow of energy from the stretch mode to the bending mode during secondary encounters, which are common in the dynamics of **H′–L–H** cases. The attractive interactions can be between the polar H atoms of water and an electron pair on an atom in the R acting as a base or between a polar H atom in R and the oxygen atom of H_2O. Quasi-classical trajectory calculations on potential surfaces in which the strength of such interactions could be varied systematically and their effects observed on the bend-to-stretch ratio would be very helpful for testing this idea. Other questions are whether the couplings between the bend and stretch modes were adequately represented by the H_2O part of Clary's potential and whether quasi-classical treatments are adequate for this highly quantized vibrational level structure with large zero-point energy. Nevertheless, searches for correlation in the bending and stretching distributions with properties of the exit channel potential would be useful before more rigorous quantum scattering treatments [39–41] are pursed. The category with the highest bend-to-stretch ratio for OH + HR reactions involves truly bound intermediates, for example HO–IH or HO–$SHCH_3$. The trajectory calculations for OH + 3-hexanone [129] in which a seven-membered ring adduct assists the abstraction process suggest that the movement of the O atom toward the H atom to be abstracted is quite different from the dynamics of direct abstraction. Thus, the high $\langle f_{v_2}\rangle$ values from unimolecular decomposition of ethanol and the OH + HI, GeH_4 or CH_3SH reactions probably have other explanations than stretch-bend exit-channel couplings.

6. Summary

The IRCL spectra from water molecules formed by bimolecular abstraction of hydrogen atoms from 30 R–H molecules by OH (OD) radicals at 298 K have been analysed by computer simulation to obtain vibrational distributions. By combining data drom H_2O and HOD products, the vibrational energy in the bending and stretch modes of water can be assigned separately. The OD + DR reactions can provide support to the results from the OH (OD) + HR reactions, and provide better data for measuring product branching ratios if two types of H/D sites are in the reagent molecule because the HOD and D_2O emission bands are not overlapped. The results from the bimolecular water-forming reactions are compared with the vibrational distributions from the unimolecular elimination of water molecules from ethanol and acetic acid. The unimolecular reactions release a small fraction of the available energy as vibrational energy of water, $\langle f_v(H_2O)\rangle = 0.15$–$0.20$, in a distribution that declines with increasing stretch vibrational energy, and the energy in the bending mode exceeds the energy in the stretch modes by a ratio of ~ 1.2. In contrast, the bimolecular, direct hydrogen atom abstraction reactions by OH radicals have a much higher release of vibrational energy to water, $\langle f_v(H_2O)\rangle = 0.6$–$0.5$, with inverted distributions in the stretch modes and with low, but variable, bend-to-stretch ratios of 0.25–0.50. Several nominally hydrogen atom abstraction reactions have lower $\langle f_v(H_2O)\rangle$ values of 0.45–0.35 with higher bend-to-stretch ratios of 0.7–1.5. This pattern of energy disposal identifies an indirect mechanism in which various types of bound OH–RH intermediates participate in the reaction mechanisms. The vibrational energy distributions of the water product can augment more conventional kinetic information to delineate between direct abstraction reactions vs. those proceeding by hydrogen-bonding interaction in the entrance channel [159]. For reactions proceeding by direct hydrogen atom abstraction, the total $\langle f_v(H_2O)\rangle$ is quite similar to the $\langle f_v(HF)\rangle$ for F atoms reacting with each reagent. This general feature and the results from quasi-classical trajectory calculations show that most of the vibrational energy is initially released to the new O–H bond in direct abstraction reactions. The old OH bond is nearly a spectator, as would be expected for **H**–**L**–**H**′ dynamics [160]. Variable amounts of the energy, depending on the potential surface of the given reaction, subsequently leak to the bending mode as H_2O and R traverse the exit valley. The potential surface used to represent the OH + HBr reaction gave too small a ratio for the bend-to-stretch excitation in quasi-classical trajectory calculations and stronger interactions between H_2O and BR (or R) are needed to reproduce the experimental results. Developing models that can illustrate the dynamics associated with the variable degree of bending excitation in water-forming reactions is a goal for future research.

Leone and co-workers [161] have studied the $NH_2 + NO$ reaction by observing the time-resolved infrared emission of the water product. The induction period for the emission from water is associated with vibrational relaxation of NH_2, formed by 193 nm photolysis of NH_3. Only vibrationally and electronically relaxed NH_2 radicals react with NO to give vibrationally excited water as a product. The $OH + CH_3C(O)CH_3$ reaction has been investigated both experimentally [162] and theoretically [163] in attempts to resolve the questions of addition to the carbonyl site vs abstraction and the role of hydrogen bonding. The 1-methylvinoxy radical was monitored by laser-induced fluorescence [162] to demonstrate that the branching fraction from hydrogen abstraction is less than 0.95 but greater than 0.8. High level *ab-initio* calculations [163] find that the transition state for addition is 4.1 kcal mol^{-1}

above that for abstraction from acetone. These results are in accord with our infrared emission measurement of HOD from $OD + CH_3C(O)CH_3$. Although the barrier to abstraction is 4 kcal mol^{-1}, hydrogen bonding does alter the geometry of the transition state relative to that expected for direct hydrogen abstraction. In principle, this reaction would be a good case for testing the influence of such a transition state on the vibrational distributions of water. Unfortunately our water emission spectrum from $OH + CH_3C(O)CH_3$ was too weak for assignment of the bending distribution and this remains a project for future work. New *ab initio* molecular orbital calculations [164] have confirmed the essential properties of the four-centered H_2O-elimination transition state [15] for the unimolecular decomposition of ethanol. The authors discuss the H_2O-elimination and the bond rupture dissociation channels for the thermal decomposition of ethanol.

References

[1] Polyani, J. C., 1987, *Angew. Chem., Int. Ed. Engl.*, **26**, 952.
[2] Sloan, J. J., 1988, *J. phys. Chem.*, **92**, 18.
[3] Tamagake, K., Setser, D. W., and Sung, J. P., 1980, *J. chem. Phys.*, **73**, 2203.
[4] Moore, C. B., and Smith, I. W. M., 1996, *J. phys. Chem.*, **100**, 12848.
[5] Agrawalla, B. S., and Setser, D. W., 1987, *J. chem. Phys.*, **86**, 5421.
[6] Wategaonkar, S., and Setser, D. W., 1989, *J. chem. Phys.*, **90**, 251, 6223.
[7] Arunan, E., Wategaonkar, S., and Setser, D. W., 1991, *J. phys. Chem.*, **95**, 1539.
[8] Arunan, E., Manke II, G., and Setser, D. W., 1993, *Chem. Phys. Lett.*, **207**, 81.
[9] Manke II, G., and Setser, D. W., 2000, *J. phys. Chem.*, **104**, 11013.
[10] Butkovskaya, N. I., Muravyov, A. A., and Setser, D. W., 1997, *Chem. Phys. Lett.*, **266**, 223.
[11] Butkovskaya, N. I., Zhao, Y., and Setser, D. W., 1994, *J. phys. Chem.*, **98**, 10779.
[12] Butkovskaya, N. I., and Setser, D. W., 1996, *J. phys. Chem.*, **100**, 4853.
[13] Butkovskaya, N. I., and Setser, D. W., 1996, *J. chem. Phys.*, **105**, 8064.
[14] Butkovskaya, N. I., Manke II, G., and Setser, D. W., 1995, *J. phys. Chem.*, **99**, 1115.
[15] Butkovskaya, N. I., and Setser, D. W., 1997, *J. chem. Phys.*, **106**, 5028.
[16] Butkovskaya, N. I., and Setser, D. W., 1998, *J. chem. Phys.*, **108**, 2434.
[17] Butkovskaya, N. I., and Setser, D. W., 1998, *J. phys. Chem. A*, **102**, 6395.
[18] Butkovskaya, N. I., and Setser, D. W., 1998, *J. phys. Chem. A.*, **102**, 9715.
[19] Butkovskaya, N. I., and Setser, D. W., 1999, *Chem. Phys. Lett.*, **312,** 37.
[20] Butkovskaya, N. I., and Setser, D. W., 1999, *J. Phys. Chem.* A, **103**, 6921; the $S_v^0(100,D_2O)$ value in the appendix should read 0.47×10^{-18} cm^{-1}/molecule^{-1}cm^2.
[21] Butkovskaya, N. I., and Setser, D. W., 2000, *J. phys. Chem.* A, **104**, 9428.
[22] Crutzen, P. J., Leelieveld, J., and Bruhl, C., 1994, *Environmental Oxidants*, edited by O. Nriagu and M. S. Simmons (New York: Wiley).
[23] Warnatz, J., 1984, *Combustion Chemistry*, edited by W. C. Gardiner Jr. (Berlin: Springer).
[24] Atkinson, R., 1985, *Chem. Rev.*, **85**, 69.
[25] Atkinson, R., 1997, *J. phys. chem. Ref. Data*, **26**, 215 (1994).
[26] Atkinson, R., Baulch, D. L., Cox, R. A., Hampson, Jr., R. F., Kerr, J. A., and Troe, J., 1992, *J. phys. chem. Ref. Data*, **21**, 1125.
[27] Aliagas, I., and Gronert, S., 1998, *J. phys. Chem. A*, **102**, 2609.
[28] González-Lafont, A., Lluch, J. M., and Espinosa–Garcia, J., 2001, *J. phys. Chem.* A, **105**, 10553.
[29] Schwartz, M., Marshall, P., Berry, R. J., Ehlers, C. J., and Peterson, G. A., 1998, *J. phys. Chem.* A, **102**, 10074.
[30] Hu, W.-P., Rossi, I., Corchado, J. C., and Truhlar, G., 1997, *J. phys. Chem.* A, **101**, 6911.
[31] Sekuvak, S., Liedl, K. R., Rode, B. M., and Sabliji, A., 1997, *J. phys. Chem.* A, **101**, 4245.

[32] Nizamov, B., Setser, D. W., Wang, H., Peslherbe, G. H., and Hase, W. L., 1996, *J. chem. Phys.*, **105**, 9897.
[33] Levine, R. D., and Bernstein, R. B., 1987, *Molecular Reaction, Dynamics and Chemical Reactivity* (Oxford: Oxford University Press).
[34] Holmes, B. E., and Setser, D. W., 1980, *Physical Chemistry of Fast Reactions*, Vol. 2, edited by I. W. M. Smith (New York: Plenum), p. 83.
[35] Agrawalla, B. S., and Setser, D. W., 1985, *Gas Phase Chemiluminescence and Chemi-ionization*, edited by A. Fontijn (Amsterdam: Elsevier), p. 157.
[36] McKendrick, K. G., Rakestraw, D. J., Zhang, R., and Zare, R. N., 1988, *J. phys. Chem.*, **92**, 5530.
[37] Brouard, M., and Vallance, C., 2001, *Phys. Chem. chem. Phys.*, **3**, 3602.
[38] Harper, W. W., Nizkorodov, S. A., and Nesbitt, D. J., 2000, *J. chem. Phys.*, **113**, 3670.
[39] Nyman, G., and Clary, D. C., 1994, *J. chem. Phys.*, **101**, 5756.
[40] Clary, D. C., Nyman, G., and Hernandez, R., 1994, *J. chem. Phys.*, **101**, 3704.
[41] Nyman, G., 1996, *J. chem. Phys.*, **104**, 6154.
[42] Neuhauser, D., 1994, *J. chem. Phys.*, **100**, 9272.
[43] Schatz, G. C., 1995, *J. phys. Chem.*, **99**, 516.
[44] Bernstein, R. B., and Levine, R. D., 1975, *Advances in Atomic and Molecular Physics*, Vol. 11, edited by R. D. Bates (New York: Academic).
[45] Rengarajan, R., Setser, D. W., and Desmarteau, D., 1994, *J. phys. Chem.*, **98**, 10568.
[46] Tsang, W., and Hampson, R. F. , 1986, *J. phys. chem. Ref. Data*, **15**, 1087.
[47] Park, J.-Y., and Gutman, D., 1983, *J. phys. Chem.*, **87**, 1844.
[48] Finzi, J., Hovis, F. E., Panfilov, V. N., Hess, P., and Moore, C. B., 1977, *J. chem. Phys.*, **67**, 4053.
[49] Zittel, P. F., and Masturzo, D. E., 1989, *J. chem. Phys.*, **90**, 977.
[50] Zittel, P. F., and Masturzo, D. E., 1991, *J. chem. Phys.*, **95**, 8005.
[51] Hovis, F. E., and Moore, C. B., 1980, *J. chem. Phys.*, **72**, 2397.
[52] Herzberg, H., 1960, *Molecular Spectra and Molecular Structure*, Vol. I, *Spectra of Diatomic Molecules*, and Vol. II, *Infrared and Raman Spectra* (New York: Van Nostrand).
[53] Rothman, L. S., Gamache, R. R., Tipping, R. H., Rinsland, C. P., Smith, M. A. H., Benner, D. C., Devi, V. M., Flaud, J.-M., Camy-Peyret, C., Perrin, A., Goldman, A., Massie, S. T., Brown, L. R., and Toth, R. A., 1992, *J. Quant. Spectrosc. Radiat. Transfer*, **48**, 469.
[54] Toth, R. A., 1999, *J. mol. Spectrosc.*, **195**, 78, 98.
[55] Benedict, W. S., Gailar, N., and Plyler, E. K., 1956, *J. chem. Phys.*, **24**, 1139.
[56] Maricq, M. M., Smith, M. A., Simpson, C. J. S. M., and Ellison, G. B., 1981, *J. chem. Phys.*, **74**, 6154.
[57] Rothman, L. S., 1978, *Applied Optics*, **17**, 3517.
[58] Halonen, L., and Carrington, Jr., T., 1988, *J. chem. Phys.*, **88**, 4171.
[59] Kauppi, E., 1994, *Chem. Phys. Lett.*, **229**, 661.
[60] Polyansky, O. L., Zobov, N. F., Vitti, S., Tennyson, J., Bernath, P. F., and Wallace, L., 1997, *Astrophys. J. Lett.*, **489**, L205.
[61] Kwan, Y. Y., 1978, *J. mol. Spectrosc.*, **71**, 260.
[62] Braslawsky, J., and Ben-Aryen, Y., 1969, *J. chem. Phys.*, **51**, 2233.
[63] Linnik, Yu. V., 1961, *Method of Least Squares and Principles of the Theory of Observations*, edited by N. L. Johnson (Oxford: Pergamon) pp. 135–171.
[64] Bykov, A. D., Kapitanov, V. A., Naumenko, O. V., Petrova, T. M., Serdyukov, V. I., and Sinitsa, L. D., 1992, *J. mol. Spectrosc.*, **153**, 197.
[65] Naumenko, O. V., Bertseva, E., and Camparque, A., 1999, *J. mol. Spectrosc.*, **197**, 122.
[66] Child, M. S., 1985, *Acc. chem. Res.*, **18**, 45.
[67] Papineau, N., Flaud, J. M., Camy-Peyret, C., and Guelachvili, G., 1981, *J. mol. Spectrosc.*, **87**, 219.
[68] Flaud, J. M., and Camy-Peyret, C. 1975, *J. mol. Spectrosc.*, **55**, 278.

[69] Bykov, A. D., Lopasov, V. P., Makushnkin, Yu, S., Sinitsa, L. N., Ulenikov, O. N., and Zuev, V. E., 1982, *J. mol. Spectrosc.*, **94**, 1; Bykov, A. D., Makarov, V. S., Moskalenko, N. I., Naumenko, O. V., Ulenikov, O. N., and Zotov, O. V., 1987, *J. mol. Spectrosc.*, **123**, 126; Ormsby, P. S., Rao, K. N., Winnewisser, M., Winnewisser, B. P., Naumenko, O. V., Bykov, A. D., and Sinitsa, L. N., 1993, *J. mol. Spectrosc.*, **158**, 109; Bykov, A. D., Naumenko, O. V., Sinitsa, L. N., Winnewisser, B. P., Winnewisser, M., Ormsby, P. S., and Rao, K. N., 1994, *J. mol. Spectrosc.*, **166**, 169.
[70] Csaszar, A, G., and Mills, I. M., 1997, *Spectrochim. Acta* A, **53**, 1101.
[71] Sims, I. R., Smith, I. W. M., Clary, D. C., Bocherel, P., and Rowe, B. R., 1994, *J. chem. Phys.*, **101**, 1748.
[72] Jaramillo, V. I., and Smith, M. A. 2001, *J. phys. Chem.* A., **105**, 5854.
[73] Berkowitz, J., Ellison, G. B., and Gutman, D., 1994, *J. phys. Chem.*, **98**, 2744.
[74] McMillen, D. F., and Golden, D. M., 1982, *Annu. Rev. phys. Chem.*, **33**, 493.
[75] Stein, S. E., and Rabinovitch, B. S., 1975, *J. phys. Chem.*, **79**, 191.
[76] Fujisaki, N., Ruf, A., and Gaumann, T., 1985, *J. Am. Chem. Soc.*, **107**, 1605.
[77] Seetula, J. A., and Slagle, I. R., 1997, *J. Chem. Soc., Faraday Trans.*, **93**, 1709.
[78] Cohen, H., 1991, *Int. J. chem. Kinet.*, **23**, 397.
[79] Mellouki, A., Téton, S., and Le Bras, G., 1995, *Int. J. chem. Kinet.*, **27**, 791.
[80] Arif, M., Dellinger, B., and Taylor, P. H., 1997, *J. phys. Chem.* A, **101**, 2436.
[81] Cruickshank, F. R., and Benson, S. W., 1969, *Int. J. chem. Kinet.*, **1**, 381.
[82] Wallington, T. J., Liu, R., Dagaut, P., and Kurylo, M. J., 1988, *Int. J. chem. Kinet.*, **20**, 41.
[83] Kondo, O., and Benson, S. W., 1984, *Int. J. chem. Kinet.*, **16**, 949.
[84] Porter, E., Wenger, J., Treacy, J., Sidebottom, H., Mellouki, A., Téton, S., and Le Bras, G., 1997, *J. phys. Chem.* A, **101**, 5770.
[85] Le Calvé, S., Hitier, D., Le Bras, G., and Mellouki, A., 1998, *J. phys. Chem.* A, **102**, 4579.
[86] Atkinson, R., and Aschmann, S. M., 1988, *J. phys. Chem.*, **92**, 4008.
[87] Wallington, T. J., and Kurylo, M. J., 1987, *J. phys. Chem.*, **91**, 5050.
[88] Becerra, R., Carpenter, I. W., and Walsh, R., 1997, *J. phys. Chem.* A, **101**, 4185.
[89] Wine, P. H., Kreutter, N. M., Gump, C. A., and Ravishankara, A. R., 1981, *J. phys. Chem.*, **85**, 2660.
[90] Jefferson, A., Nicovich, J. M., and Wine, P. H., 1994, *J. phys. Chem.*, **98**, 7128.
[91] Ekwenchi, M. M., Safarik, I., and Strausz, O. P., 1981, *Can. J. Chem.*, **59**, 3226.
[92] Bedjanian, Y., Riffault, V., Lebras, G., and Poulet, G., 1994, *J. Photochem. Photobiol.* A., **128**, 15.
[93] Lafage, C., Pauwels, J. F., Carlier, M., and Devolder, P., 1983, *J. Chem. Soc., Faraday Trans. 2*, **83**, 731.
[94] Westenberg, A. A., and de Haas, N., 1973, *J. chem. Phys.*, **59**, 6685.
[95] Agrawalla, B. S., and Setser, D. W., 1986, *J. phys. Chem.*, **90**, 2450.
[96] Wilson, C., and Hirst, D. M., 1994, *J. Chem. Soc., Faraday Trans.*, **90**, 3051.
[97] Battin-Leclerc, F., Kim, I. K., Talukdar, R. K., Portmann, R. W., Ravishankara, A. R., Steckler, R., and Brown, D. 1999, *J. Phys. Chem.* A, **103**, 3237.
[98] Corchado, J. C., Espinosa-Garcia, J., Hu, W.-P., Rossi, I., and Truhlar, D. G., *J. phys. Chem.*, **99**, 687.
[99] Kwok, E. S. C., and Atkinson, R., 1995, *Atmos. Environ.*, **29**, 1685.
[100] Exner, K., and Raqué Schleyer, P., 2001, *J. phys. Chem.*, **105**, 3407.
[101] Melissas, V. S., and Truhlar, D. G., 1994, *J. phys. Chem.*, **98**, 875.
[102] Meier, U., Grotheer, H. H., Riekert, G., and Just, T., 1985, *Ber. Bunsenges. phys. Chem.*, **89**, 325.
[103] McCaulley, J. A., Kelly, N., Golde, M. F., and Kaufman, F., 1989, *J. phys. Chem.*, **93**, 1014.
[104] Picquet, B., Heroux, S., Chebbi, A., Doussin, J.-F., Durand-Jolibois, R., Monod, A., Loirat, H., and Carlier, P., 1998, *Int. J. chem. Kinet.*, **30**, 839.
[105] Nelson, L., Rattigan, O., Neavyn, R., Sidebottom, H., Treacy, J., and Nielsen, O. J., 1990, *Int. J. chem. Kinet.*, **22**, 1111.

[106] Jodkowski, J. T., Rayez, M.-T., Rayez, J.-C., Bérces, T., and Dóbé, S., 1999, *J. phys. Chem.* A, **103**, 3750.
[107] Dóbé, S., Bérces, T., Turányi, T., Márta, R., Grossdorf, J., Temps, F., and Wagner, H. G., 1996, *J. phys. Chem.*, **100**, 19864.
[108] Atadinç, Fe., Selçuki, G., Sari, L., and Aviyente, V., 2002, *Phys. Chem. Chem. Phys.*, **4**, 1797.
[109] Stemmler, K., Kinnison, D. J., and Kerr, J. A., 1996, *J. phys. Chem.*, **100**, 2114.
[110] Good, D. A., and Francisco, J. S., 1997, *Chem. Phys. Lett.*, **266**, 512.
[111] Holmes, J. L., and Lossing, F. P., 1984, *Inst. J. Mass Spectrom. Ion Proccess.*, **58**, 113.
[112] Frank, I., Parrinello, M., and Klamt, A., 1998, *J. phys. Chem.* A, **102**, 3614.
[113] Dagaut, P., Wallington, T. J., Liu, R., and Kurylo, M. J., 1998, *J. phys. Chem.*, **92**, 4375.
[114] Sauer, C., Barnes, I., and Becker, K.-H., 1999, *Proceedings of the Air Pollution Research Report 67*, EUR 18765, edited by K. Becker and G. Angeletti (Luxemburg), p. 289.
[115] Takahashi, H., Hori, T., Wakabayashi, T., and Nitta, T., 2001, *J. phys. Chem.* A, **105**, 4351.
[116] Lovas, F. J., and Lugez, C. L., 1996, *J. mol. Spectrosc.*, **179**, 320.
[117] González, L., Mó, O., and Yáñez, M., 1998, *J. chem. Phys.*, **109**, 139.
[118] Caminati, W., Moreschini, P., Rossi, I., and Favero, P. G., 1998, *J. Am. Chem. Soc.*, **120**, 11144.
[119] Watanabe, H., and Iwata, S., 1996, *J. chem. Phys.*, **105**, 420.
[120] Tyndall, G. S., Orlando, J. J., Wallington, T. J., Hurley, M. D., Goto, M., and Kawasaki, M., 2002, *Phys. Chem. Chem. Phys.*, **4**, 2189.
[121] Hynes, A. J., Wine, P. H., and Semmes, D. H., 1986, *J. phys. Chem.*, **90**, 4148; Wine, P. H., Thompson, R. J., and Semmes, D. H., 1984, *Int. J. chem. Kinet.*, **16,** 1623.
[122] Barone, S. B., Turnipseed, A., and Ravishankara, A. R., 1996, *J. phys. Chem.*, **100**, 14694, 14703.
[123] Hynes, A. J., Stoker, R. B., Pounds, A. J., McKay, T., Bradshaw, J. D., Nicovich, J. M., and Wine, P. H., 1995, *J. phys. Chem.*, **99**, 16967.
[124] Stickel, R. E., Zhao, Z., and Wine, P. H., 1993, *Chem. Phys. Lett.*, **212**, 312.
[125] Butkovskaya, N. I., and Barnes, I., 2003, to be published.
[126] Wilstons, C., and Hirst, D. M., 1995, *J. Chem. Soc., Faraday Trans.*, **91**, 3783.
[127] Muiño, P. L., 2002, *Phys. Chem. chem. Phys.*, submitted.
[128] McKee, M. L., 1993, *J. phys. Chem.*, **97**, 10971.
[129] Turecek, F., 1984, *J. phys. Chem.*, **98,** 3701.
[130] Danen, W., 1979, *J. Am. Chem. Soc.*, **101**, 1187.
[131] Bernath, P. F., 2000, *Annu. Rep. Prog. Chem.* C, **96**, 177.
[132] Arunan, E., Raybone, D., and Setser, D. W., 1992, *J. chem. Phys.*, **97**, 6348.
[133] Neil, W. S., Li, J.-Y., and Sloan, J. J., 1997, *J. chem. Phys.*, **107**, 4537.
[134] Nizkorodov, S. A., Harper, W. W., Chapman, W. B., Blackmon, B. W., and Nesbitt, D. I., 1999, *J. chem. Phys.*, **111**, 8404.
[135] Arunan, E., Liu, C. P., Setser, D. W., Gilbert, J. V., and Coombe, R. D., 1994, *J. phys. Chem.*, **98**, 494.
[136] Arunan, E., Rengarajan, R., and Setser, D. W., 1994, *Can. J. Chem.*, **72**, 568.
[137] Seakins, P. W., Woodbridge, E. L., and Leone, S. R., 1993, *J. phys. Chem.*, **97**, 5633.
[138] Butkovskaya, N. I., and Setser, D. W., 1999, *Chem. Phys. Lett.*, **312**, 37.
[139] Butkovskaya, N. I., and Setser, D. W., 2003, *J. Phys. Chem. Chem. A.*, to be submitted.
[140] Wategaonkar, S. J., and Setser, D. W., 1988, *J. phys. Chem.*, **92**, 1.
[141] Bogan, D. J., Setser, D. W., and Sung, J. P., 1979, *J. phys. Chem.*, **80**, 888.
[142] Wategaonkar, S. J., and Setser, D. W., 1987, *J. chem. Phys.*, **86**, 4477.
[143] Alagia, M., Balucani, N., Casavecchia, P., Stranges, D., and Volpi, G. G., 1995, *J. Chem. Soc. Faraday Trans.*, **91**, 575.
[144] Baer, M., Faubel, M., Martinez-Haya, B., Rusin, L., Tappe, U., and Toennies, J. P., 1998, *J. chem. Phys.*, **108**, 9694, and many other studies mentioned in this paper.

[145] Lee, S.-H., and Liu, K., 1999, *J. chem. Phys.*, **111**, 6253.
[146] Anderson, D. T., Todd, M. W., and Lester, M. J., 1999, *J. chem. Phys.*, **110**, 1117.
[147] Rakitzis, T. P., Kandel, J. A., Lev-On, T., and Zare, R. N., 1997, *J. chem. Phys.*, **107**, 9392.
[148] Bronikowski, M. J., Simpson, W. R., and Zare, R. N., 1993, *J. phys. Chem.*, **97**, 2194, 2204.
[149] Metz, R. B., Thoemke, J. D., Pfeiffer, J. M., and Crim, F. F., 1993, *J. chem. Phys.*, **99**, 1744.
[150] Thoemke, J. D., Pfeiffer, J. M., Metz, R. B., and Crim, F. F., 1995, *J. phys. Chem.*, **99**, 13748.
[151] Sinha, A., Thoemke, J. D., and Crim, F. F., 1992, *J. chem. Phys.*, **96**, 372.
[152] Hawthorne, G., Sharkey, P., and Smith, I. W. M., 1998, *J. chem. Phys.*, **108**, 4693.
[153] Longfellow, C. A., and Lee, Y. T., 1995, *J. phys. Chem.*, **99**, 15532.
[154] Sudbo, A. S., Schulz, P. A., Shen, Y. R., and Lee, Y. T., 1975, *J. chem. Phys.*, **69**, 2312.
[155] Rajakumar, B., Reddy, K. P. J., and Arunan, E., 2002, *J. phys. Chem.* A, **106**, 8346, **107**, submitted.
[156] Broida, M., and Persky, A., 1989, *Chem. Phys.*, **133**, 405.
[157] Persky, A., and Kornweitz, H., 1989, *Chem. Phys.*, **133**, 415.
[158] Urban, J., and Staemmler, V., 1993, *Chem. Phys.*, **178**, 279.
[159] Smith, I. W. M., and Ravishankara, A. R., 2002, *J. phys. Chem.* A, **106**, 4798.
[160] Akagi, H., Fujimara, Y., and Kajimoto, O., 1999, *J. chem. Phys.*, **111**, 115; **110**, 7264.
[161] Marcy, T. P., Heard, D. E., and Leone, S. R., 2002, *J. Phys. Chem.* A, **106**, 8249.
[162] Turpin, E., Fittschen, C., Tomas, A., and Devolder, R., 2002, *J. Atmos. Chem.*, submitted.
[163] Henon, E., Canneau, S., Bohr, F., and Dóbé, S., 2002, *Phys. Chem. Chem. Phys.*, submitted.
[164] Park, J., Zhu, R. S., and Lin, M. C., 2002, *J. Chem. Phys.*, **117**, 3224.